ENVIRONMENTAL AND SUBSTRATE EFFECT ON THE SURFACE PROPERTIES OF GRAPHENE AND GRAPHITE

by

Zhiting Li

B.S., Nankai University, 2010

Submitted to the Graduate Faculty of

The Dietrich School of Arts and Sciences in partial fulfillment

of the requirements for the degree of

Doctor of Philosophy

University of Pittsburgh

2015

UNIVERSITY OF PITTSBURGH

THE DIETRICH SCHOOL OF ARTS AND SCIENCES

This dissertation was presented

by

Zhiting Li

It was defended on

Oct.26th, 2015

and approved by

Dr. Alexander Star, Professor, Department of Chemistry

Dr. Geoffrey R. Hutchison, Associate Professor, Department of Chemistry

Dr. Lei Li, Assistant Professor, Department of Chemical and Petroleum Engineering

Dissertation Advisor: Dr. Haitao Liu, Assistant Professor, Department of Chemistry

ENVIRONMENTAL AND SUBSTRATE EFFECT ON THE SURFACE PROPERTIES OF GRAPHENE AND GRAPHITE

Zhiting Li, PhD

University of Pittsburgh, 2015

This dissertation is focused on understanding and controlling of surface properties of graphene and graphite. Four specific topics are presented: 1) study the intrinsic wettability of graphene; 2) minimize the airborne hydrocarbon contamination on graphitic surface during storage; 3) investigate the anti-corrosion performance of graphene during a long-term ambient oxidation process at room temperature; 4) study the catalytic effect of copper substrate during the atmospheric oxidation of graphene at high temperature. All the results have important implications for the characterization, processing, and storage of graphene (graphite) samples and related devices.

Specifically, chapter 2 reports the intrinsic wettability of graphene and the effect of airborne hydrocarbon contamination during its storage. This work overturned the long-held view that graphitic surfaces (including graphene and graphite) are hydrophobic. In chapter 3, efforts have been made to minimize the airborne hydrocarbon adsorption during the storage of graphitic surfaces, this work aimed at maintaining the intrinsic property of graphene and graphite surfaces over a long period of air exposure. Chapter 4 and 5 aimed to elucidate the mutual interactions between graphene and copper substrate during ambient air exposure as well as atmospheric oxidation at high temperature. This work is closely related to the potential application of graphene as an anti-corrosion film for metallic substrates.

TABLE OF CONTENTS

LIST OF TABLES

LIST OF FIGURES

PREFACE

Foremost, I would like to express my sincere gratitude to my research advisor, Professor Haitao Liu, for his supporting me over the past five years. I am grateful for all his contribution of time, funding, and instructions to make my Ph.D experience rewarding and productive. As a great mentor, he always showed me that doing research is a cumulative process, which includes both accomplishments as well as blocks and delays in progress. Nevertheless, patience, diligence, and painstaking attention to details are always the most important qualities to make an excellent researcher.

I am also grateful to Prof. Lei Li for providing the opportunity of doing some of my research in his lab for almost 4 years. He recommended many good papers and books to me, which deepens my understanding of various surface characterization techniques in an engineer's perspective.

I would like to express my appreciation to my thesis committee members Prof. Alexander Star, Prof. Geoffrey Hutchison, for their time and suggestions on my comprehensive exam and thesis writing. I would also thank Prof. Shigeru Amemiya for guiding me through the proposal writing.

I would also give my full gratitude to all of my colleague members and collaborators. Special thanks go to Dr. Sumedh Surwade for all his generous assistance when I first started my research; to Andrew Kozbial for training me on all the instruments in Lei's lab; to Feng Zhou for his helpful suggestions on my research and assistance in my TA work; to Ganesh Shenoy and David Parobek for doing research with me as a small team for almost 3 years. There are also other individuals that

I would like to thank cordially, including Yongjin Wang, Karen Ricardo, Prof. Shichao Zhao, Anqing Xu, Kim Hyojeong, Muhammad Salim, Mike Novak, Dr. Xiao Gong, Dong Wang, Mina Kim, Dr. Cheng Tian, Patrick Muldoon, Dr. Guolei Xiang, Alyssa Kunkel, Brittni Morganstein, Patrick Ireland. It is my great pleasure to work with all of you and I wish you all the best.

I would like to thank Dr. Joel Gillespie and Prof. Richard Butera for building up great XPS facilities and recommending good reference to analyze my XPS results accordingly. I am also grateful to Dr. Michael Golde, Dr. Stan Paul and Prof. Lillian Chong for giving me helpful suggestions on my TA work and inviting me to many important events to share my teaching experience with new TAs and lecturers.

Lastly and above all, I would like to express my great gratitude to my parents, who supported me in the past 25 years and provide me comfortable life and endless love with sufficient space for all my choices. In a sense this dissertation is also a gift to myself and I strongly hold the belief that “the greatest thing a man can do is to make the most possible out of the stuff that has been given to him” and hopefully I’m on the way.

1.0 INTRODUCTION

1.1 OVERVIEW

The growing interest in graphitic materials has been greatly fueled by the rapid development within graphene community, which has seen a phenomenal increase in both published research articles and filed patents since 2004. As a single atomic layer of carbon, graphene shows many exciting properties including efficient thermal and electrical conductivity, transparency and high flexibility. With a huge array of potential applications, graphene attracts continuous interests from both academic and industry. For example, the number of research articles published on graphene has increased from less than 100 to over 9000 in the decade between 2004 and 2013.

In spite of the great progress on graphene in the past 10 years, a systematic study on its intrinsic surface properties is still urgently needed nowadays. It is known that most chemical and physical processes occur at the surface of a material, such as gas-solid interaction, adsorption, corrosion and chemical reaction, etc. Due to the atomic layer structure, all carbon atoms on graphene contribute to its intrinsic surface properties. Therefore, the environmental exposure and underlying substrate may strongly affect its surface properties during the manufacturing, characterization, processing, and storage of graphene-based devices. In this regard, understanding and controlling the intrinsic properties of graphene is critically important for their fundamental

study and practical application in general.

1.1.1 What is graphene

Graphene is a two-dimensional monolayer form of sp^2-hybridized carbon.[1] The extended honeycomb network has a carbon-carbon bond length of 0.142 nm and lattice constant of 0.246 nm (a) (shown in Figure 1-1). These values are the same for graphite. For a multi-layer graphene, the interlayer distance is found to be 0.35 nm (c) based on Raman spectroscopy and atomic force microscopy (AFM).[2-3] The exceptional electronic and mechanical properties of graphene make it a rising star in the study of fundamental physics, materials science as well as device manufacture. For example, the electrons in graphene behave as massless particles which result in remarkably high electron mobility.[4] The resistivity of graphene could be as low as 10^{-6} Ω·cm at room temperature, even less than that of silver.[5] The thermal conductivity of graphene was measured to between (4.84 ± 0.44) x 10^3 to (5.30 ± 0.48) x 10^3 $Wm^{-1}K^{-1}$ near room temperature, which is higher than that of carbon nanotubes and diamond.[6] Graphene also demonstrates very good mechanical properties. With a tensile modulus of 1 TPa, graphene has a breaking strength 200 times greater than that of steel.[7] All these intrinsic properties could lead graphene to some potential applications such as pressure sensor and resonator.[8-12]

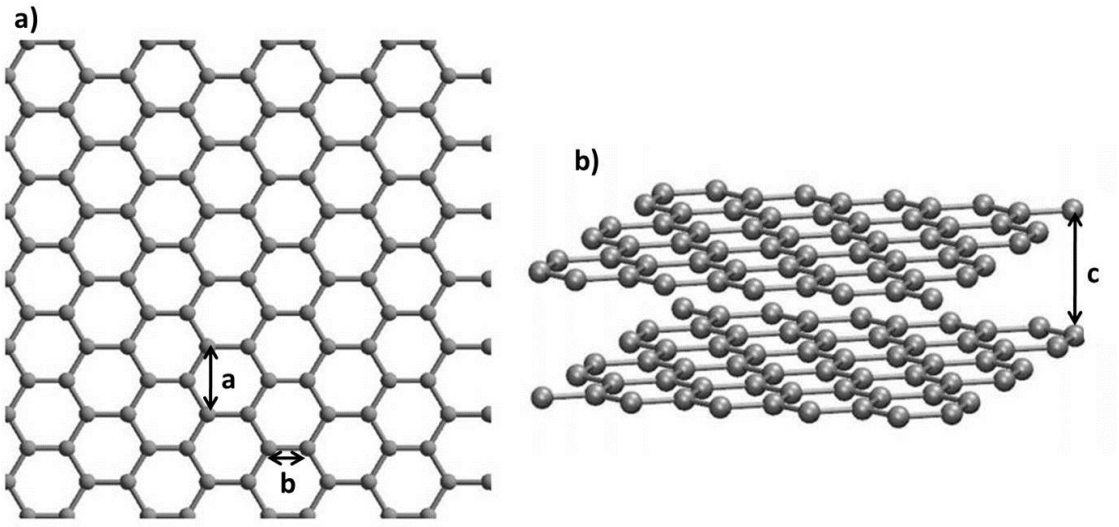

Figure 1-1 Structural images of (a) single-layer graphene and (b) bilayer graphene.

1.1.2 Synthesis of graphene

The first experimental preparation of graphene was through the micromechanical cleavage of graphite.[2] This method produces the highest quality graphene in terms of structural integrity. However, the size of graphene obtained with this method is limited to a few tens of micrometers, neither the location nor the thickness of the flakes is controllable or scalable. To overcome these disadvantages, several other synthesis methods have been developed including reduction of graphite oxide (GO),[13] epitaxial growth on single crystalline SiC substrate[14] and chemical vapor deposition (CVD) on metal catalyst substrates.[15-16]

One approach is to produce high density exfoliate graphene is by chemical reduction of exfoliated graphite oxide (GO) layers.[17-19] This exfoliation process requires extensive modification

of the graphite followed by a separation of multi-layer graphite oxide sheet into a colloidal suspension to complete the exfoliation.

Another synthesis method is the graphitization of single crystal SiC developed by De Heer and coworkers.[14, 20] When a SiC wafer is heated to 1000^{o}C in ultrahigh vacuum, Si will undergo sublimation which leaves behind small islands of graphene in high quality. The graphene sample prepared using this technique demonstrates excellent electrical property (up to 100GHz switching speed[21]). Although the price of the SiC wafer is high, this technique is still attractive to radio and THz frequency electronics industry where the excellent performance of the devices makes the cost less a concern.

Chemical vapor deposition (CVD) of graphene on transition metal films provides another approach to prepare high quality monolayer and multilayer graphene. The formation of few layered graphene grown on transition metal have been discovered 50 years ago.[22] In 2009, Ruoff and coworkers[15] pioneered an copper-based CVD synthesis which has allowed access to high quality large area single layered graphene on a copper foil. The growing process is relatively straightforward[23] and is illustrated in Figure 1.2. First, a copper foil is annealed in a hydrogen atmosphere to remove the native copper oxide on the surface. In the second stage, graphene islands start to nucleate on the pre-treated copper foil under a CH_4/H_2 flow. Dubon's group reported that the graphene islands nucleate heterogeneously with a four-lobed shape, each lobe is an individual graphene crystal differently oriented on the Cu grain.[24] The growing direction of the graphene lobe is most-often aligned along Cu <001> direction but significant variations still exist. As the growth time increases, the graphene domains increase in size and eventually coalesce into a continuous graphene film as shown in the third stage.

Compared to many other synthetic methods, copper foil based CVD method can produce

a uniform single layered graphene over a large area. It has been reported that the size of graphene prepared by this technique can be as large as 30-inches and the single layer graphene coverage is over 95% while the remaining graphene is 2-3 layers thick.[15] These features as well as the low price of copper foil, make the CVD process the most inexpensive, promising and readily accessible approach for high quality graphene. Moreover, such graphene can be transferred to any desired substrate since copper can be easily etched with chemicals.[25] The single-layer graphene used in our studies is synthesized using this method.

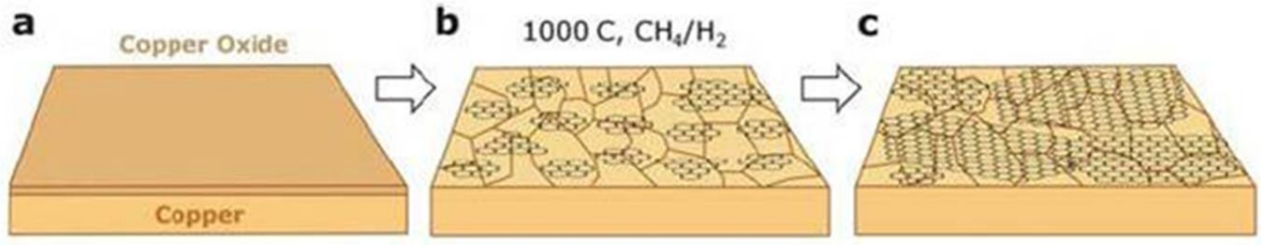

Figure 1-2 Three main stages of graphene growth on copper by CVD. Reprinted with permission from reference 24. Copyright 2015 © Royal Society of Chemistry.

1.2 CHARACTERIZATION OF GRAPHENE

In my experiments, some microscopic and spectroscopic techniques are frequently used to characterize freshly prepared graphene samples. These techniques include optical microscopy, Raman spectroscopy, ellipsometry, water contact angle (WCA), and X-ray photoelectron spectroscopy (XPS). Here, we briefly discuss their operation principles and data interpretations related to graphene characterizations.

1.2.1 Optical microscopy

The copper/graphene used in my study was grown by low-pressure CVD on a copper foil substrate at 1000°C using methane as the carbon source.[26] To minimize contamination of graphene surface, we used high purity gases in the synthesis and the CVD setup was constructed with only metal and quartz components. Fluoropolymer endcaps were also applied outside the tube furnace (see 2.3.1

for experimental details). The CVD synthesis produced a graphene film covering the entire surface of the copper substrate. For characterization purpose, a graphene film was transferred to a silicon wafer using poly-methyl methacrylate (PMMA) as the transferring agent. Figure 1.3 (a) shows an optical image of graphene transferred on silicon substrate. We surveyed an area of 1 cm × 2 cm (Figure 1.3 (b)) and determined that the overall surface coverage of single layer graphene on silicon wafer was > 99.9%, which set the minimum surface coverage of single layer graphene on the copper substrate before the transfer. Among the < 0.1% of area not covered by single layer graphene were 75 pin holes (average area: *ca.* 100 μm^2) and 100 bilayer graphene patches (average area: *ca.* 25 μm^2).

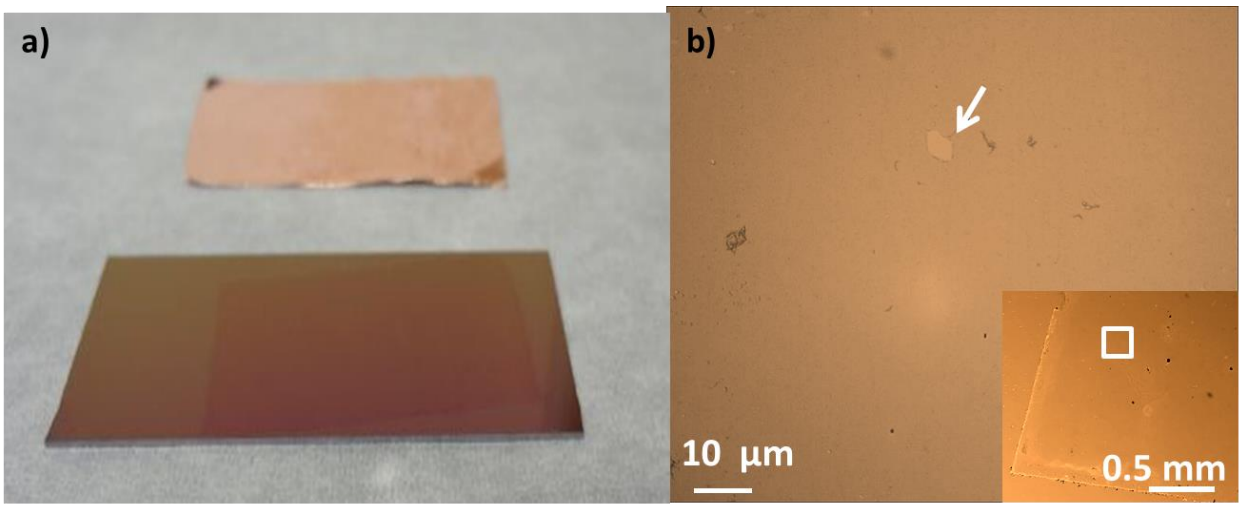

Figure 1-3 (a) Photograph of graphene films on both Cu foil and SiO_2/Si substrate; (b) optical micrograph of graphene film transferred onto a SiO_2/Si substrate. The arrow indicates a pin hole. The inset in (b) shows a lower magnification image of the same sample with the white rectangle indicating the location of (b). The overall surface coverage of single-layer graphene is > 99.9%. The image contrast and color was adjusted to enhance the visibility of graphene and pin holes. Reprinted with permission from reference 54. Copyright 2013 © Nature Publishing Group.

1.2.2 Raman Spectroscopy

Raman spectrometry is a light-scattering process in which a laser beam interacts with the target species to result in both elastic and inelastic photon scattering. The scattered light from the sample is detected and analyzed for frequency shifts. Most photons are elastically scattered by the sample at the same frequency as that of incident laser source, such process is known as Rayleigh scattering. On the other hand, a small proportion of the incident laser photons are scattered at a frequency that is shifted from the original energy level. For example, Stokes-Raman transition happens if electron

initiates from the ground state and eventually relaxes to the first excited vibrational level, releasing photons with lower energy (longer wavelength). In comparison, for those molecules that are initially in an excited vibrational state, the Raman process initiates from their excited vibrational level, relaxes to the ground state and produces photons with energy higher than those elastically scattered (Figure 1.4 (a)). This type of scattering is called anti-Stokes Raman scattering.

The vibrational states probed by Raman spectroscopy are similar to those involved in infrared spectroscopy. Therefore, these two vibrational spectroscopy techniques are always used as complementary techniques.[27-28] For example, those vibrations involving strong dipole moments are usually strong in an infrared spectrum but weak in a Raman spectrum. However, vibrations induced by non-polar functional group could show very strong Raman bands but weak infrared activity.

There are three characteristic peaks in Raman spectra of monolayer graphene (Figure 1.4 (b)): the D band (~1350 cm^{-1}), G band (~1580 cm^{-1}) and 2D band (~2700 cm^{-1}).[29] The G band is the only band coming from a first order Raman scattering process in graphene.[30] As shown in Figure 1.4(c), after absorbing a photon from the laser radiation, the electron on graphene surface undergoes an inelastic scattering and releases a G band phonon. Then such electron will shift back to the ground state and emit a photon which can be detected as G band. On the other hand, the D band and 2D band originate from a second order process, involving one iTO (in-plane transverse optical) phonon (one of the six phonon dispersion modes of graphene, corresponding to different vibrations of the sublattice A and B[31]) and one defect for the D band or two iTO phonons in the case of 2D band. The 2D band is approximately twice the D band frequency and does not require any kind of defect for its activation. In addition, the D band production involves two scattering processes: one elastic scattering induced by intrinsic crystalline defects and one inelastic scattering

through emitting a phonon, as shown in Figure 1.4(c). Unlike D band which needs intrinsic defect for its activation, 2D band consists of two inelastic scattering processes and results in two phonons formation.

Although the G band frequency is sensitive to many external factors, such as doping level[32] or strain[33], its integrated intensity I_G is more resistant to these environmental factors and often remains constant under the same laser excitation frequency.[34-35] Due to this robustness, I_G is often used as a reference to which intensities of other peaks (like D band) are compared. For example, we use the I_D/I_G ratio to evaluate the defect density on graphene surface during the thermal oxidation process.

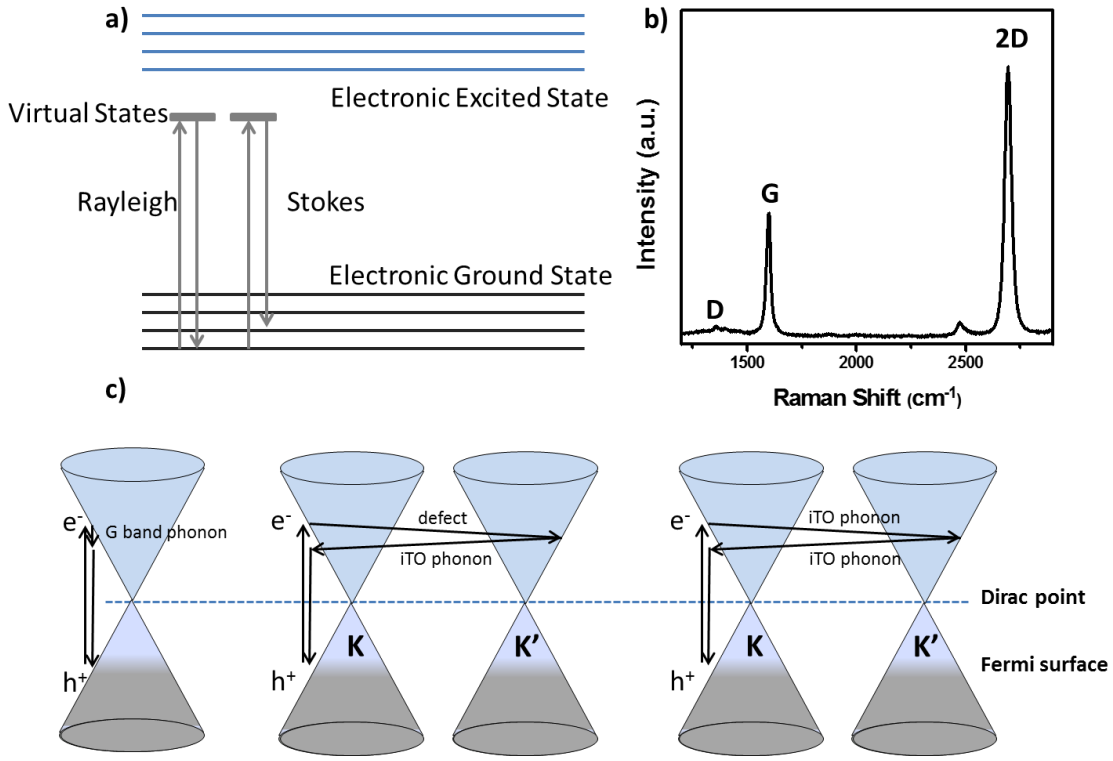

Figure 1-4 (a) Mechanism of Raman scattering; (b) Micro-Raman spectrum of graphene film on SiO_2/Si substrate; (c) Raman scattering processes for different bands. (Left) First-order G band process and (Center) one-phonon second order resonance process for D band and (Right) two-phonon second order resonance for 2D band.

1.2.3 Spectroscopic ellipsometry

Spectroscopic ellipsometry is a well-established optical technique for the determination of optical constants and thickness of surface adsorbed thin films. It is based on the polarization state change of light upon reflection from a sample surface. Due to its surface sensitive and non-destructive properties, this technique has been widely used in many application fields such as semiconductor, photovoltaics, optoelectronics, biotechnology and surface coatings, etc.[36]

In this technique, two parameters, Ψ and Δ, are measured which reflect the polarization state change of light upon reflection from a sample. Specifically, Δ refers to the phase difference between parallel (p) and perpendicular (s) polarized light, and Ψ to the amplitude ratio of p- and s-polarized components. The schematic image of the working mechanism of ellipsometry is shown in Figure 1.5(a-b). For a classic substrate/film/ambient three-phase system, both Ψ and Δ values are directly detected by ellipsometer and can be affected by the instrumental set-up, ambient phase, substrate/film property and film thickness as follows[37]:

$$\Psi = f(\Theta, n_{amb}, \lambda, d_{film}, n_{film}, k_{film}, n_{sub}, k_{sub}) \quad (1)$$

$$\Delta = g(\Theta, n_{amb}, \lambda, d_{film}, n_{film}, k_{film}, n_{sub}, k_{sub}) \quad (2)$$

Where (i) Θ and λ are the incidence angle and wavelength of the probing radiation; (ii) n_{amb} is the refractive index of ambient atmosphere; (iii) n_{sub} and k_{sub} are the refractive and extinction index of the substrate, and (iv) n_{film} and k_{film} are that of adsorbate film and d_{film} is the adsorbate film thickness. Among these parameters, Θ, λ, and n_{amb} are usually known, the substrate constant n_{sub} and k_{sub} can be obtained via blank substrate measurement. The k_{film} is usually considered as 0 for a transparent film. Therefore, the two remaining unknown parameters (d_{film} and n_{film}) can be determined using equation system (1 - 2) and measured Ψ and Δ values. According to previous studies, ellipsometry demonstrates high sensitivity to temporal surface changes even in the ultrathin film regime ($d_{film} < 10$ nm) with a high precision (standard deviation (*s.d.*) $< \pm 0.1$ nm).[38]

In our experiment, ellipsometry is applied to detect the surface adsorption of airborne hydrocarbons, which is usually in the range of 0.1 – 5 nm in thickness. Figure 1.5(c) shows the evolution of both airborne hydrocarbon (blue) and 1-octadecene (red) adsorption on freshly cleaved highly oriented pyrolytic graphite (HOPG) surface. This technique enables a non-destructive, efficient and highly sensitive detecting over a long term scale.[38]

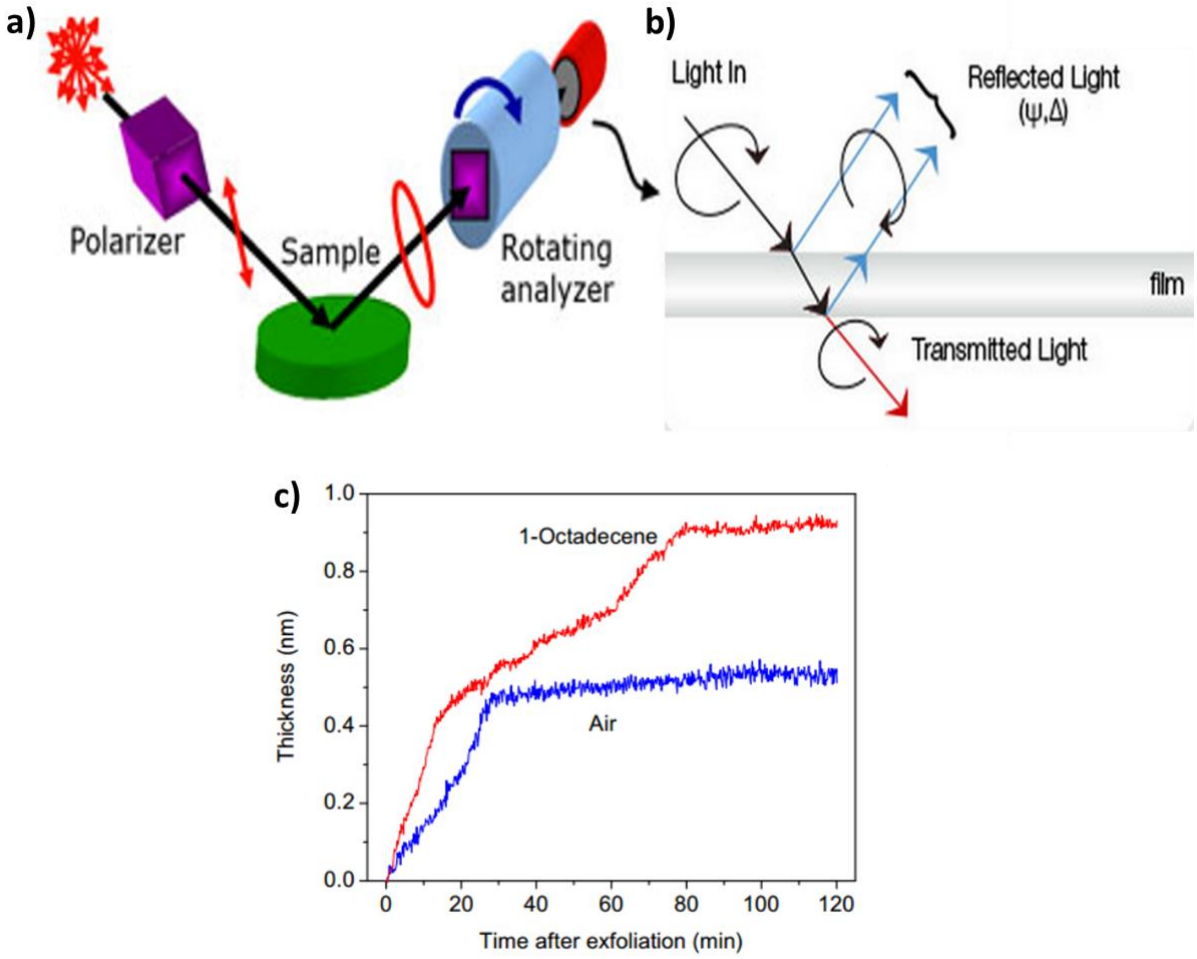

Figure 1-5 (a-b) Schematic of ellipsometer configuration with a polarizer to define the incoming polarization and a rotating analyzer after light reflection. Reprinted with permission from reference 36. Copyright 2007 © WILEY-VCH. (c) Spectroscopic-ellipsometry of hydrocarbon deposition on HOPG surface during exposure to ambient air (blue) and 1-octadecene (red), respectively. Reprinted with permission from reference 38. Copyright 2014 © American Chemical Society.

1.2.4 Water contact angle

To study the surface wettability of graphitic surface, water contact angle measurement is applied to describe a surface as hydrophilic or hydrophobic (Figure 1.6(a)). Generally speaking, when a liquid droplet is placed onto a solid surface, its behavior depends on the adhesive forces between the liquid and the surface. For a hydrophilic surface, the adhesive forces are attractive so that the liquid drop is pulled toward the surface and spreads out to increase the contact, resulting in a small water contact angle ($< 90^{o}$). In contrast, a hydrophobic surface usually shows repellent forces towards the water drop, which beads up ($> 90^{o}$) in order to minimize its contact with the solid surface.

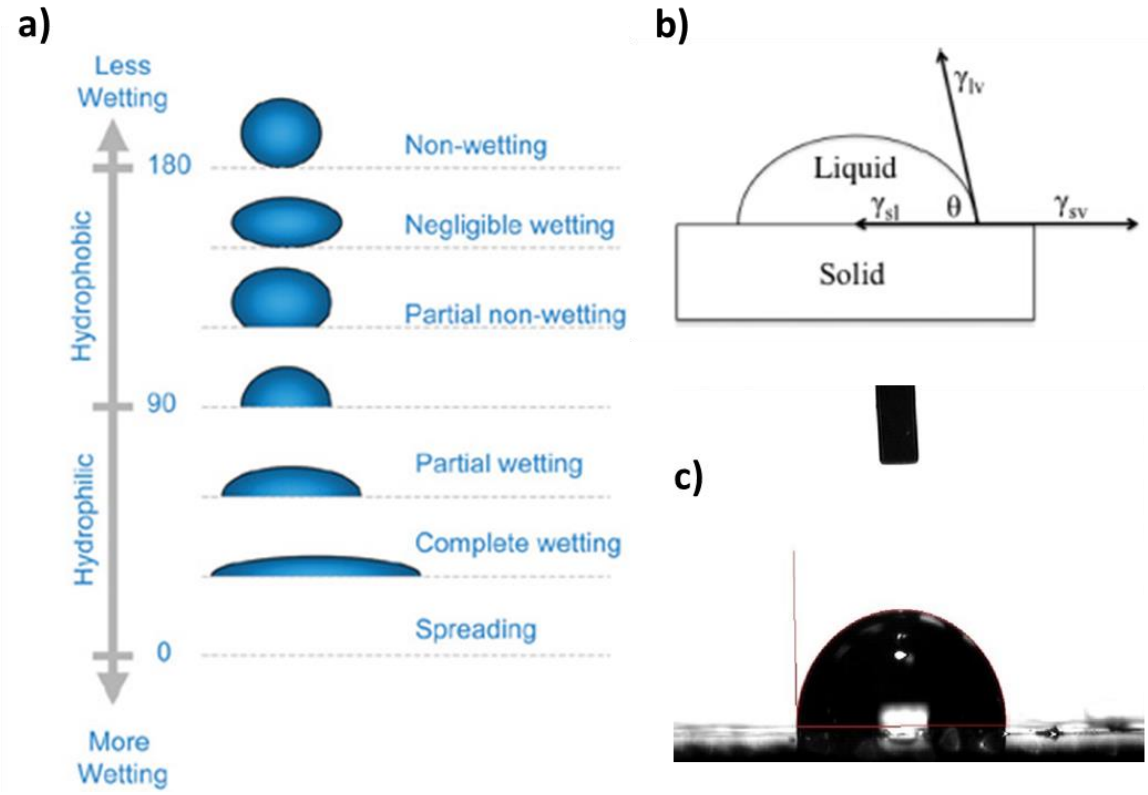

Figure 1-6 (a) Schematic of water contact angle test and its correlation with surface hydrophilicity and hydrophobicity. Reprinted with permission from reference 49. Copyright 1997 © Global Specialty Lens Symposium; (b) Schematic depicting the interface of a liquid droplet on a solid surface. Reprinted with permission from reference 158. Copyright 2014 © American Chemical Society; (c) Water contact angle measured on a copper/graphene surface that has been stored in air for 2 days.

The Young's equation is usually used to determine the static equilibrium of a liquid-vapor interface. As shown in Figure 1.6(b), the equilibrium contact angle θ is given by (3):

$\gamma SG - \gamma SL - \gamma LG * \cos\theta = 0$ (3)

Where γSG is the solid-vapor interface energy, γSL is the solid-liquid interface energy, γLG is the liquid-vapor interface energy.

In the modified Young-Dupré equation, the contact angle can be directly related to the surface tension of liquid drop as follows:

$\gamma^*(1+\cos\theta) = \Delta W_{SLV}$ (4)

Where γ is the surface tension of the liquid drop and W_{SLV} is the solid-liquid adhesion energy per unit area in the medium V.

Wettability of graphitic surface Figure 1.6(c) shows the water contact angle on a copper/graphene surface which was stored in ambient air for 2 days. The angle was measured to be 91° and is generally regarded as hydrophobic. In fact, since experiments by Fowkes and Harkins in 1940,[39] extensive studies have concluded that graphitic surfaces are hydrophobic with WCA within the 75° - 95° range.[39-51] Early experiments were conducted on natural graphite and later experiments utilized HOPG. Fowkes and Harkins tested Ceylon graphite and reported WCA of 85.3° – 85.9° using the tilting plate method.[39] Morcos reported WCA of 84.2° on exfoliated graphite determined by the indirect meniscus height method where the sample was partially immersed in water.[44] Morcos also reported WCA of 83.9° on highly oriented graphite by advancing meniscus method.[45] More recently, WCAs determined by static sessile drop were reported as 91°,[48] 79°,[50] and 75°[51] on exfoliated HOPG, 98.3° on graphite,[43] and 91.0° on HOPG aged in air for days.[46] Adamson and Gast reported advancing WCA of 86° on graphite.[49] Raj *et al.* recently reported advancing WCA on HOPG to be *ca.* 91°.[47] Hydrophobicity has also been observed on other graphitic materials. Aligned carbon nanotubes have shown superhydrophobic behavior where WCAs of 163.4° and 158.5° were observed.[52-53] Additionally, as-grown carbon nanotube

forests exhibit WCA of 161°.[41] Raj *et al.* reported advancing WCA of monolayer graphene on SiO_2 substrate of *ca.* 90°, similar to that of graphite.[47]

Despite the dominant view that graphite (graphene) is hydrophobic, a few studies have reported evidence of a much more hydrophilic surface with WCA of 35 - 65°.[54-59] In 1975, Schrader reported that WCA of exfoliated graphite was 35 ± 4° under an ultrahigh vacuum (UHV) environment and ion bombardment of the surface decreased the WCA to 0°.[55] Subsequent experiments indicated that ion bombardment damaged the graphite surface; however, the 35° WCA was determined on a surface exposed only to bakeout temperature up to 750°C under UHV and the surface was verified by low energy electron diffraction to be clean and not damaged.[55-56] Schrader[60] proposed that the "hydrophobicity" reported is due to the airborne hydrocarbon contamination. Additionally, Tadros *et al.* used the captive bubble method and reported advancing WCA of 63 - 65° on pyrolytic high-density isotropic carbon.[57] Luna *et al.* also found WCA of *ca.* 30° on graphite utilizing scanning force microscopy techniques.[59] Heath and coworkers discovered that water on HOPG adsorbs as nanodroplets with WCA of less than 10° under microscopic conditions.[58]

The idea that graphite is (mildly) hydrophilic has not been generally accepted by the scientific community; one of the reasons is likely due to the issues of earlier experimental procedures.[17] For example, a report has directly challenged the validity of Schrader's results [61] since Schrader determined WCA in an UHV environment,[55] which is known to result in lower WCA due to water evaporation.[62-63]

1.2.5 XPS

XPS identifies surface element by exciting electrons from the irradiated material into higher energy states using an incident X-ray (Figure 1.7(a)). Then it measures the kinetic energy and number of electrons escaping from the top 1-10 nm of the material surface. A typical XPS spectrum is a plot of number of detected electrons (Y-axis) versus the binding energy of the detected electrons (X-axis). Each element (except hydrogen) owes a characteristic set of XPS peaks corresponding to related characteristic binding energy values, which can be used to directly identify each element exists on the surface of analyzed material. The peak intensity is proportional to the amount of element within the X-ray irradiated area (volume).

In our experiment, we applied XPS to identify the species on copper/graphene and other graphitic surfaces. As shown in Figure 1.7(b), copper (Cu2p: 933.0 - 934.7 eV) and carbon (C1s: 284.2 – 288.6 eV) are the dominant species on freshly synthesized copper/graphene surface. In an XPS spectrum, the peak shift usually associates with the chemical state in which the element exists. For example, the C1s peak can be decomposed into 5 components: sp^2 C=C (284.4 eV), sp^3 C-C (284.8 eV), sp^3 C-H (285.2 eV), C-O-C (286.4 eV), and O=C-O peaks (288.9 eV).[64] Among these components, sp^2 C=C peak is the dominant species which is assigned to the sp^2 carbon framework of graphene. The sp^3 C-C and sp^3 C-H peaks demonstrate slightly higher binding energy than that of the sp^2 C=C peak. These two peaks are attributed to physisorbed hydrocarbons as well as some surface modifications such as alkyl chain containing groups.[65] The C-O-C and O=C-O peaks are associated with ether, ester and carboxylic groups, thus indicating the degree of oxidation on graphene surface as well as oxygen containing adsorbents.[66-67]

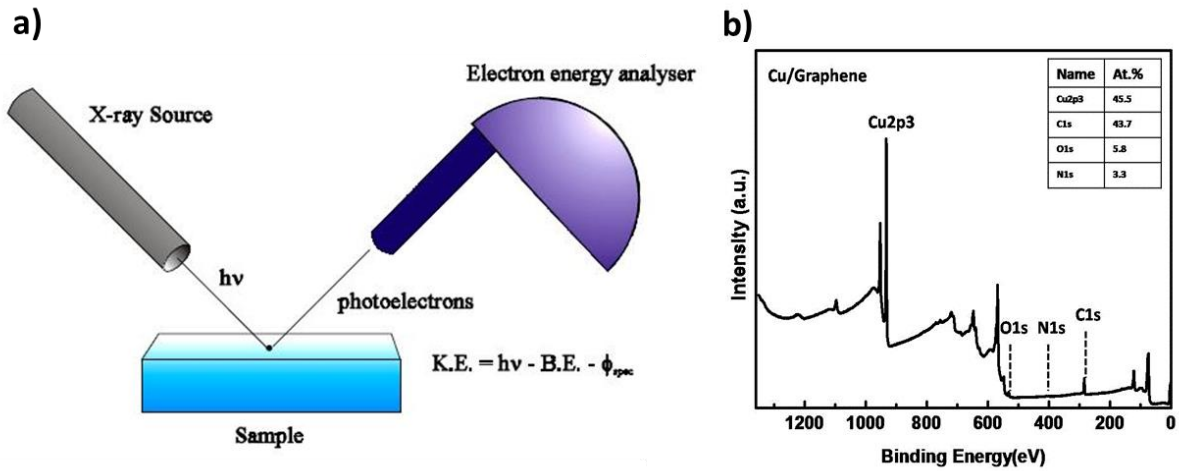

Figure 1-7 (a) Schematic of X-ray photoelectron spectroscopy. Reprinted with permission from reference 171. Copyright 1992 © Springer. (b) XPS spectrum of copper/graphene, the insert column is the atomic percentage of each element within the detected area.

Why study surface property?

Due to its exceptional electrical, optical, mechanical and chemical properties and the availability of samples in both micron and large scale, graphene is particularly suited in many applications such as high performance transistors, gas sensors, transparent conductor, anti-corrosion coating, etc.[68-71] Due to the atomic layer thickness, all the carbon atoms are either directly contacted with the underlying substrate or exposed to the environment. It is known that any molecule attached to the graphene surface could potentially impact its electrical and optical properties,[72] in this regard, understanding the intrinsic surface properties of graphene and its interaction with environment is highly desirable in the integration of graphene into real-life devices.

The environmental and substrate effects on graphene surface have been extensively

investigated by many research groups.[68, 71, 73-78] Figure 1.8 shows the application of graphene in both heat transfer coating and field-effect transistor (FET) devices. In Figure 1.8(a), coating the condenser surface (copper) with a layer of graphene significantly improves its heat transfer efficiency by a factor of 4 compared to conventional polymer coatings.[79] However, the condensation of steam on graphene surface also promotes the formation of a water film, which drastically reduces its heat transfer efficiency for a long time use. In microscale applications, Figure 1.8(b) shows a failed attempt in depositing Au electrode on the top of graphene. Due to the poor interaction between graphene and gold, part of the electrode on the graphene has been peeled off during the lift-off process, results in an unsuccessful manufacture process.[48]

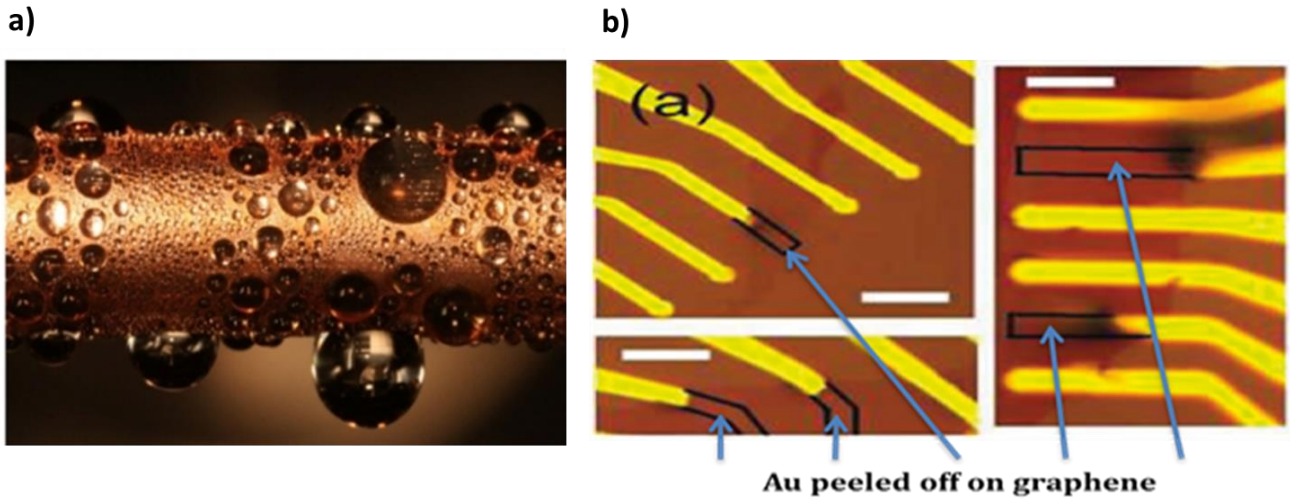

Figure 1-8 (a) Photograph of a copper condenser tube coated with graphene. When exposed to water vapor at 100°C, the film shows a dropwise condensation; Reprinted with permission from reference 79. Copyright 2015 © American Chemical Society; (b) Optical microscopy of a FET device with Au peeled off on graphene. Reprinted with permission from reference 48. Copyright 2010 © American Chemical Society.

Moreover, it has been reported that even ambient air exposure can significantly affect the intrinsic surface property (*e.g.*, electroactivity) of many graphitic surfaces.[80-82] For example, Figure 1.9 shows the cyclic voltammogram (CV) of freshly exfoliated HOPG as a function of ambient exposure time. HOPG was applied as an electrode in this experiment and a rapid deterioration in the CV response was clearly observed during the 3 hours ambient exposure, indicating a substantial decrease of electrochemical activity on HOPG surface due to the adsorption of airborne impurities.[82-83]

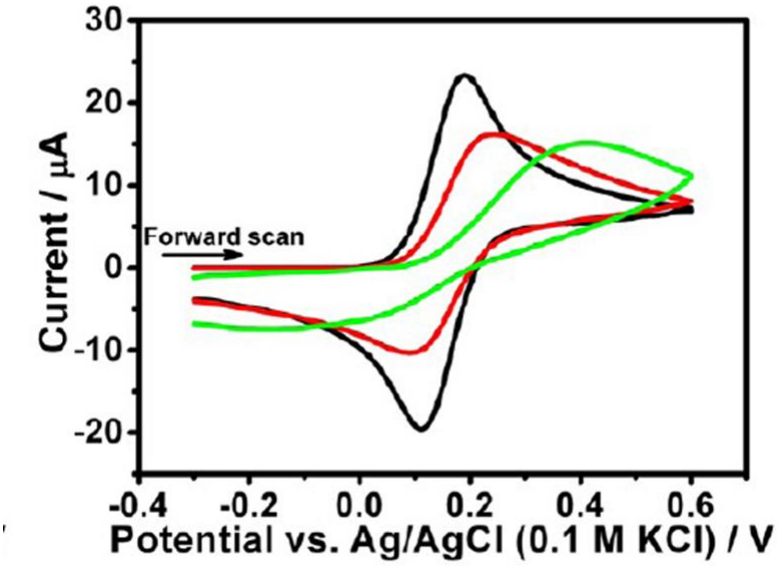

Figure 1.9 CVs for the oxidation of 1 mM $Fe(CN)_6^{4-}$ in 1.0 M KCl at 0.1 V s^{-1} : on freshly exfoliated HOPG exposed in air at room temperature for 0 h (black), 1 h (red), 3 h (green). All CVs run on HOPG (SPI-1). Reprinted with permission from reference 82. Copyright 2012 © American Chemical Society.

1.3 ENVIRONMENTAL AND SUBSTRATE EFFECT ON GRAPHENE SURFACE

In my research, we mainly focused on CVD-grown copper/graphene sample to study its surface properties, including surface wettability and oxidation activity. Specifically, my dissertation mainly discusses the effect of airborne hydrocarbons, water and oxygen on its surface properties as well as the mutual interaction between graphene and the underlying copper substrate.

1.3.1 Airborne hydrocarbon effect

According to literature studies, the airborne hydrocarbon contaminants (AHC) are mostly composed of anthropogenic alkanes, alkenes, alcohols and aromatic species, which are associated with plant growth, fuel combustion, and chemical industry.[84-88] Although the concentrations of such AHC usually range from parts-per-trillion (ppt) to parts-per-million (ppm) level,[89] they still demonstrate a profound impact on the surface wettability of graphitic materials.

Moreover, such AHC induced effect has been put into a rather broad perspective by correlating it with many other controversial topics in graphite community. For example, there have been contradictory reports on the effect of substrate on the wettability of single layer graphene, *i.e.,* (non)wetting transparency;[47, 90-91] water has been shown to spontaneously wet the inside of carbon nanotubes, which were traditionally known as hydrophobic;[92-94] even the debate about the intrinsic electrochemical activity of graphite basal plane was related to the surface cleanliness of graphite.[82-83, 95]. In regard to all these anomalies, it is highly possible that the intrinsic property of a graphitic surface has been obscured by the unwanted hydrocarbon contaminants, which has been rarely considered in all these studies. Therefore, an overall investigation on AHC-free graphitic surface is critically desirable for rationalizing these discrepancies and more importantly, promoting a more effective fabrication of graphitic materials.

1.3.2 Water adsorption

It is generally accepted that water adsorption usually initiates from a chemisorption of 1-2 layers of water film that tightly bound to a surface in well-ordered structure, followed by a subsequent physisorption of water layer with a more liquid-like character.[96] The thickness of such physisorbed

water layer ranges from nanometer to micrometer scale depending on the temperature, humidity and substrate. In a thermodynamic view, the condensation of water onto most hydrophilic surfaces is exothermic at all coverages. Besides, water condensation shows much lower enthalpy change (ΔH) and entropy (S) during the first 1-2 layers adsorption, indicating a more ordered adlayer arrangement with much stronger bonding to the surface.[97]

In particular, water adsorption on graphitic surface (*e.g.*, HOPG) is generally believed to initiate from the defect sites (or step edge).[39, 48, 49] For example, Cao *et al* reported the use of graphene templating to visualize the microscopic structure of adsorbed water on HOPG surface.[58] By employing atomic force microscopy (AFM), lateral growth of water nanodroplets along the step edge (or defect sites) were observed with 5 - 15 nm in height while most of the basal plane area were still water free. It should be noted that the water contact angle on their HOPG sample was measured to be 90^{o}, indicating an aged surface with a certain degree of hydrocarbon contamination. Interestingly, in their follow-up experiments conducted on a modified mica surface with a water contact angle *ca.* 40^{o}, a much more uniform distribution of water nanodroplets were observed with 0.5-1.5 nm in height. In another work reported by Chakarov *et al.*,[98] they studied the water adsorption on a freshly cleaved HOPG in UHV via a temperature-programmed desorption (TPD) process. Though still initiated from the defect sites as the first layer, such water film on fresh HOPG surface can grow two-dimensionally as the adsorption continues and eventually coalesced at a certain high coverage. In fact, the lattice parameter of sp^2 C-C in graphite closely matches the 2D unit cell of the basal plane of type I ice,[98] that is, the graphite crystalline surface can serve as a good template for the growth of ice-like water layers at low temperature. Indeed, a "square ice" structure was recently observed to exist between two graphene sheets.[99]

1.3.3 Atmospheric oxidation

Theoretically, due to the lack of dangling bonds and defect sites, graphene with perfect hexagonal lattice structure is highly resistant to atmospheric oxidation below 700-800ºC. [100-101] However, CVD-grown graphene usually shows relatively higher reactivity, which can readily react with oxygen molecules at low temperature (<400ºC).[102] This can be explained that many active sites (*e.g.*, defect sites, wrinkles, crystalline boundaries, etc.) can be produced during a vapor deposition process, which shows significantly lower activation energy when reacting with oxygen.[103]

In addition, oxidation of graphene has received extensive studies owing to its fundamental importance and potential applications. Firstly, to realize many technological applications of graphene requires the tailoring of its physical, chemical properties by chemical reactions. Although graphene is known to be a chemically inert material, controllable oxidation can be a versatile tool to selectively functionalize the surface of graphene and manipulate its properties. For example, by changing the oxidation level and the relative composition of epoxy and hydroxyl groups on graphene surface, the energy band gap can be tuned in a range of 0 - 4.0 eV,[104] indicating a controllable band gap tuning through oxidation process. It has also been found that defects on graphene surface induced by oxidation also have significant effects on the electrical,[105] transport,[106] thermal conductive and chemical properties[107] of graphene.

1.3.4 Substrate effect

Graphene has drawn significant attention due to its unusual physical properties and promising applications in electronic devices.[108] In practice, many of the predicted properties (*e.g.,* high electron mobility) of graphene can be obscured or altered by its interactions with an underlying

substrate.[109-114] For example, it was observed that the thermal conductivity of supported graphene is considerably lower than that of the suspended graphene due to phonons leaking across the graphene-support interface.[115] As another example, charges trapped at the graphene-substrate interface[116-117] could act as external scattering centers and degrade transport properties in single-layer graphene whose atoms are all exposed directly to extrinsic impurities.[118-119]

Given the importance of studying the substrate effect on graphene surface, it should be noted that such effect varies from substrate to substrate. For example, graphene shows different degrees of local morphology and charge disorder when deposited on different substrates.[120-122] On atomically flat mica substrate, the morphology of graphene has been observed to be free of ripples[123] while a step-like graphene flask was shown on step-bunched sapphire substrate.[124] Among the many studies of graphene-substrate interaction, a substantial portion was devoted to understand the effect of copper surface during the CVD growth of single layer graphene. Many of these studies were motivated by the need to grow high quality, defect-free graphene samples.[125-128] For example, Yan *et al.* decreased the graphene nucleus density through electrochemical polishing and high pressure annealing copper surface.[125] Lyding and coworkers explored the effects of copper crystal structure on graphene synthesis, they observed that the copper (111) facet, having a hexagonal crystalline structure and the best match to that of graphene, facilitates graphene growth in the highest quality.[129] More recently, Hao *et al.* reported that oxygen-rich copper surface enabled the growth of single-crystal graphene in centimeter scale.[130]

2.0 EFFECT OF AIRBORNE CONTAMINANTS ON THE WETTABILITY OF SUPPORTED GRAPHENE AND GRAPHITE

2.1 CHAPTER PREFACE

Materials contained in this chapter were published as a research article in *Nature Materials*; figures used in this chapter have been reprinted with permission from: *Nat. Mater*. **2013**, *12*, 925-931 (listed as reference 54 in the bibliography section).

List of Authors: Zhiting Li*, Yongjin Wang*, Andrew Kozbial, Ganesh Shenoy, Feng Zhou, Rebecca McGinley, Patrick Ireland, Brittni Morganstein, Alyssa Kunkel, Sumedh P. Surwade, Lei Li and Haitao Liu.

(*): equal contribution

Author Contributions: H.L. and L.L. designed and directed the experiments. Z. L., A.K., Y.W., G.S., F. Z., R.M., P.I., B.M., A.K., and S.S. conducted the experiments. All authors discussed the results. H.L., Z.L., and L.L. wrote the manuscript.

2.2 INTRODUCTION

In graphene community, it is a long-held view that a pristine graphene surface is hydrophobic and its wetting property is similar to that of graphite.[39-51] For example, Shin *et al.* conducted WCA measurement on epitaxial graphene grown on a SiC substrate and reported that the WCA of their graphene sample is 92º and is independent of its thickness.[131] For graphene film grown by CVD and subsequently transferred to a SiO_2 substrate, Kim *et al.* reported WCA of 90.4º and 93.8º for Ni-grown (multi-layer) and Cu-grown (single-layer) graphene samples, respectively.[132] This dominant view has guided many follow-up studies both theoretically and experimentally, such as the computational model set-up of graphite-water interface,[133] graphitic surface modification for efficient device fabrication,[37] etc.

Though supported by the mainstream community, the intrinsic hydrophobicity still met problems in explaining many hydrophilic behaviors of graphitic surface. For example, water is known to not only wet but also transport inside a single-walled carbon nanotube at very high speed, implying a hydrophilic interior surface for such small-diameter carbon nanotubes.[134-136] Very recently, two groups claimed that monolayer graphene is either completely or partially wetting transparent, indicating the surface wettability of graphene is to some extent dictated by its underlying substrate.[47, 90-91] All these studies raised questions about the intrinsic wetting behavior of graphitic surface.

Being a surface property, it is widely accepted that water wettability is highly sensitive to

surface contamination. Among the many molecular to nanoscale contaminants, airborne hydrocarbons trigger special interests in materials science communities since they have a profound impact on surface wettability, which is one of the most important surface properties and also affects adhesion,[137] adsorption,[138] carrier mobility[139] and charge doping[140]. Many surfaces are known to adsorb hydrocarbon from ambient air, including metal,[141] TiO_2,[142] SiO_2,[143-144] and hexagonal BN.[145] Such hydrocarbon adsorption decreases the surface energy of the substrate and increases its hydrophobicity, which is reflected as an increase of their WCA.[141-146] This airborne hydrocarbon has not been previously considered to affect the wettability of graphene, presumably because graphite has long been regarded as a low energy surface and therefore should have a weak tendency to adsorb hydrocarbon. However, this assumption has never been validated experimentally.

Herein we report a study that probes the intrinsic water wettability of graphene. We show that exposure to ambient air has a drastic impact on the water wettability of CVD-grown copper/graphene surface. Both Infrared (IR) spectroscopy and XPS indicated that the increase of WCA is linked to the adsorption of airborne hydrocarbon onto the graphene surface. Similar observations were also made on single layer graphene films deposited on SiO_2, glass, and gold substrates as well as multi-layer graphene film grown on a Ni substrate, suggesting that the wettability of all graphene surfaces are affected by ambient air exposure. Our findings show that graphene is more hydrophilic than previously thought and suggest that the reported hydrophobic nature of graphene is due to unintentional hydrocarbon contamination from ambient air.

2.3 EXPERIMENTAL SECTION

2.3.1 Synthesis of single-layer graphene on copper foil (copper/graphene)

The typical synthesis process is reported by Li *et al.*[126] Typically, a ~ 4 cm^2 copper foil (Alfa Aesar, 99.8%, 25 μm thick) was placed at the center of a 1-inch-diameter fused quartz tube. The furnace tube was evacuated and heated to 1000ºC under a 2.0 standard cubic centimeters per minute (SCCM). H_2 gas flow with a pressure of 100~110 mTorr for 30 min, followed by CH_4 (carbon source) gas flow of 20 SCCM at 1000ºC for another 30 min at a total pressure of 500 mTorr. Then the copper foil was cooled to room temperature under H_2 and CH_4 gas flow and taken out from the tube furnace.

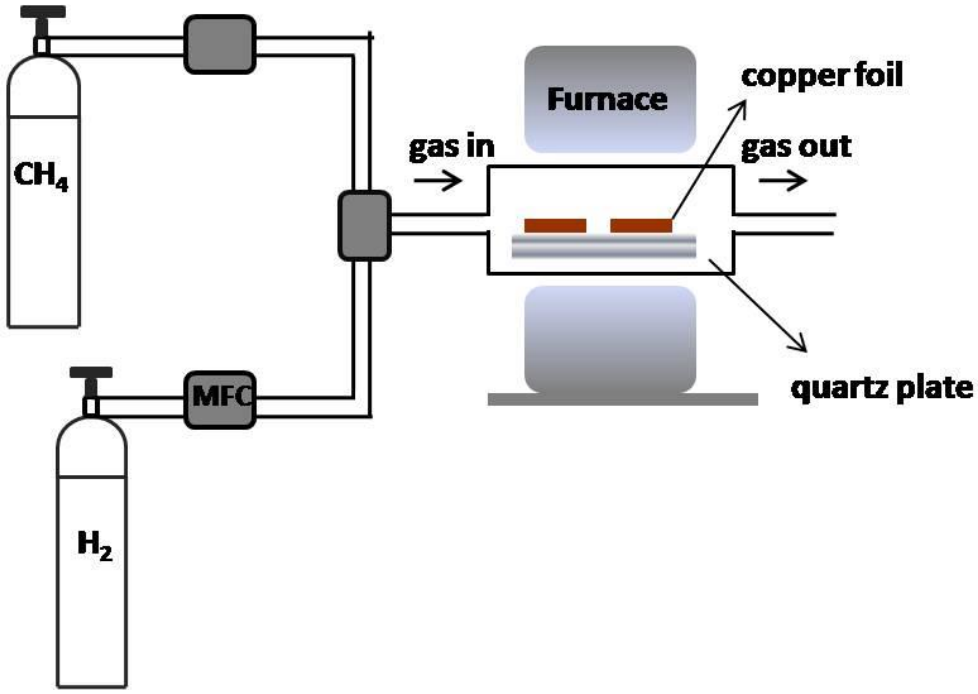

Figure 2-1 Experimental setup for low-pressure CVD synthesis of graphene using Cu as substrate. MFC: mass flow controller.

2.3.2 Synthesis of multi-layer graphene on Ni foil (nickel/graphene)

The CVD synthesis was conducted on a Ni film vacuum deposited on a silicon wafer. Briefly, on a silicon wafer was deposited a Ti layer at 0.4 nm/s for a total of 5 nm followed by a Ni layer at 0.1 nm/s for a total of 300 nm. The deposition was carried out on a Thermionics VE-180 e-beam evaporator at a pressure of 2 x 10^{-6} Torr.

The CVD synthesis of multilayer graphene is almost the same as the case of single layer

graphene, except the reaction temperature was 800 °C. The sample was determined to be 2-3 layers of graphene-based on its Raman spectrum.

2.3.3 Graphene transferred onto different substrates

Substrate preparation: Gold substrate preparation: a Si wafer/Ti (5 nm)/Au (300 nm) substrate was prepared by first depositing a Ti layer on to a Si wafer at a rate of 0.4 nm/s for a total of 5 nm followed by depositing an Au layer at a rate of 0.1 nm/s for a total of 300 nm. The deposition pressure was 2 x 10^{-6} Torr. Before its use, the Au substrate was rinsed with acetone and deionized (DI) water and blown dry with nitrogen.

Si wafer with a 300 nm of SiO_2 (University Wafers) and glass substrate were soaked in piranha solution (70% concentrated sulphuric acid + 30% hydrogen peroxide (30%)) for 1 hr, followed by a thorough rinse of DI water and then blown dry with dry nitrogen before use. *Caution: piranha solution reacts violently with organic compounds. Wear proper personal protection equipment and perform all experiments in a fume hood.*

Transfer procedures: The graphene film grown on a copper foil was transferred onto different substrates following the procedures reported by Li *et al*.[147] The transfer process began with spin-coating poly methyl-methacrylate (PMMA (Aldrich, M_w 996000)) layer on one side of the copper/graphene surface, followed by etching Cu foil in 1 M $FeCl_3$ (Sigma-Aldrich, 97%) /3.5 M HCl (Fisher Scientific, 37.1%)) aqueous solution for 20min. After the copper foil being completely etched, PMMA/graphene film was transferred to a DI water bath for cleaning and then carefully collected onto different substrates. The PMMA film was then dissolved in acetone for 8h followed by immersion in a dichloromethane bath for another 8h. To further remove the surface

contamination, the graphene covered substrate was then annealed in Ar atmosphere at 400 ºC for 30 min.

2.3.4 WCA

The WCA measurement was conducted with a VCA optima XE contact angle system at 24°C and 48% relative humidity. Each water droplet has a volume of ~ 2 μL and was carefully touched to the copper/graphene surface. A charge-coupled device (CCD) camera was used to take images of water droplets, which was followed by an automatic calculation of the static contact angle by the vendor supplied software. Each static WCA measurement was repeated three times and the average value was reported.

2.3.5 Attenuated total reflectance Fourier-transform infrared spectroscopy (ATR-FTIR)

ATR-FTIR spectra were collected with a Bruker VERTEX-70LS FTIR and a Bruker Hyperion 2000 FTIR microscope in reflectance mode utilizing a germanium 20x ATR objective and a liquid nitrogen cooled mid-band MCT A detector (7000 - 600 cm^{-1} spectral range). Before measurements, the system was purged for 20 minutes with nitrogen gas and a background spectrum was collected without having the ATR crystal contacting the sample. Each sample spectrum was collected for 150 scans with a resolution of 4 cm^{-1} and a total acquisition time of 2.5 min. The ATR crystal was lifted off the sample to provide air exposure (17.5 min) before the next spectrum was taken. The spectra were processed by the vendor supplied software to correct for the atmospheric H_2O and CO_2 peaks and perform integration of the C-H peaks.

2.3.6 XPS

XPS measurements were carried out on a custom built multi-technique surface analysis instrument operating at a base pressure of less than $1x10^{-10}$ torr. Spectra were collected using the Al-Kα X-ray line and a Leybold-Heraeus EA-10 hemispherical energy analyzer typically operating with a bandpass of 50 eV for both survey scans (1.0 eV/step) and detailed scans (0.1 eV/step).

2.3.7 Raman spectroscopy

Room temperature micro-Raman spectra were conducted on a custom-built setup using 532 nm single-longitudinal mode solid-state laser with a spot size less than 1 μm. A 40x objective (NA: 0.60) was used in all the micro-Raman experiments. Laser power was kept less than 1 mW at the entrance aperture to avoid laser induced thermal effect on graphene. Raman spectra were shifted on the y-axis for clarity.

2.3.8 UV/O_3 treatment of copper/graphene sample

UV/O_3 treatment was carried out with a PSD Pro Series Digital UV Ozone System at room temperature. The treatment time was indicated in the main text.

2.3.9 Thermal annealing of copper/graphene sample

After CVD synthesis, a copper/graphene sample was taken out of the CVD chamber and exposed to air for 2 hr. The sample was then put back to the CVD chamber under flowing Ar (99.999%) at 500 mTorr for 30 min to flush out air in the chamber. The sample was then heated to 550 °C for 1 hr and followed by a fast cooling under Ar to room temperature. The sample was taken out of the CVD chamber to measure its WCA and Raman spectrum.

2.4 RESULTS AND DISCUSSION

2.4.1 Intrinsic wettability of graphene and graphite

We found that an as-prepared graphene sample is hydrophilic and becomes hydrophobic when exposed to ambient air. Shown in Figure 2.2(a), within 10 s of taking a graphene/copper sample out of the CVD chamber, its WCA was found to be only 44°. The WCA quickly reached *ca.* 60° within 20 minutes, after which the rate of increase drastically slowed down. The WCA eventually plateaued at 80° after 1 day. The overall trend of the WCA increase was highly reproducible (Figure 2.2(b)). However, the initial WCA can be somewhat variable, ranging from 37° to 56°; the WCA after 1 day of exposure showed a much smaller variation, ranging from 80° to 90° (Figure 2.2(c)). Both the initial WCA and the rate of WCA increase are sensitive to the local environment, such as location of sample storage and type of container (*vide infra*). The previously reported WCA for a graphene/copper sample is 86°,[148] similar to the result we obtained on samples after 1 day of air exposure.

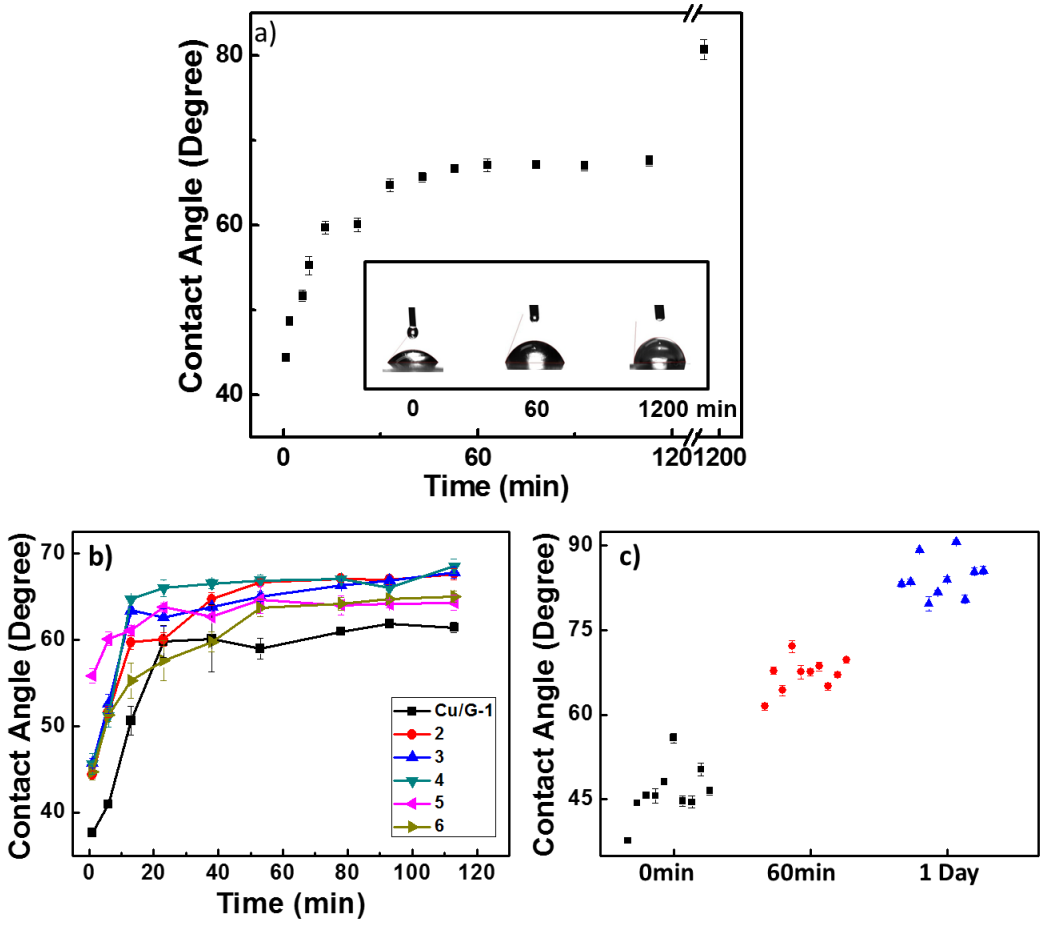

Figure 2-2 (a) Temporal evolution of the WCA measured on a graphene/copper sample. The sample was taken out of the CVD chamber at time 0. The three photographs show the water drops captured at 1 min, 60 min, and 1200 min; (b) Temporal evolution of WCA for 6 graphene/copper samples upon their exposure to air. The samples were taken out of the CVD chamber at time 0; (c) WCA of 10 graphene/copper samples after *ca.* 1 min (black), 60 min (red), and 1 day (blue) of air exposure. The data points are shifted in the time axis for clarity.

In addition to copper/graphene, nickel/graphene and HOPG samples also show a more hydrophilic surface wetting behavior right after CVD synthesis (exfoliation). Note that our CVD process allows *ca.* 2-3 layers of graphene grown on nickel substrate. As shown in Figure 2.3, the WCA measured on a freshly cleaved HOPG was 64.4º and for a freshly prepared nickel/graphene samples the corresponding value was 59.6º. Upon extended exposure to ambient air, both samples showed a significant increase of WCA to 91º (HOPG) and 94.6º (nickel/graphene). Given that the generally accepted WCA in the literature for HOPG is 86º,[148-149] we believe their data are very similar to the value we observed for aged HOPG.

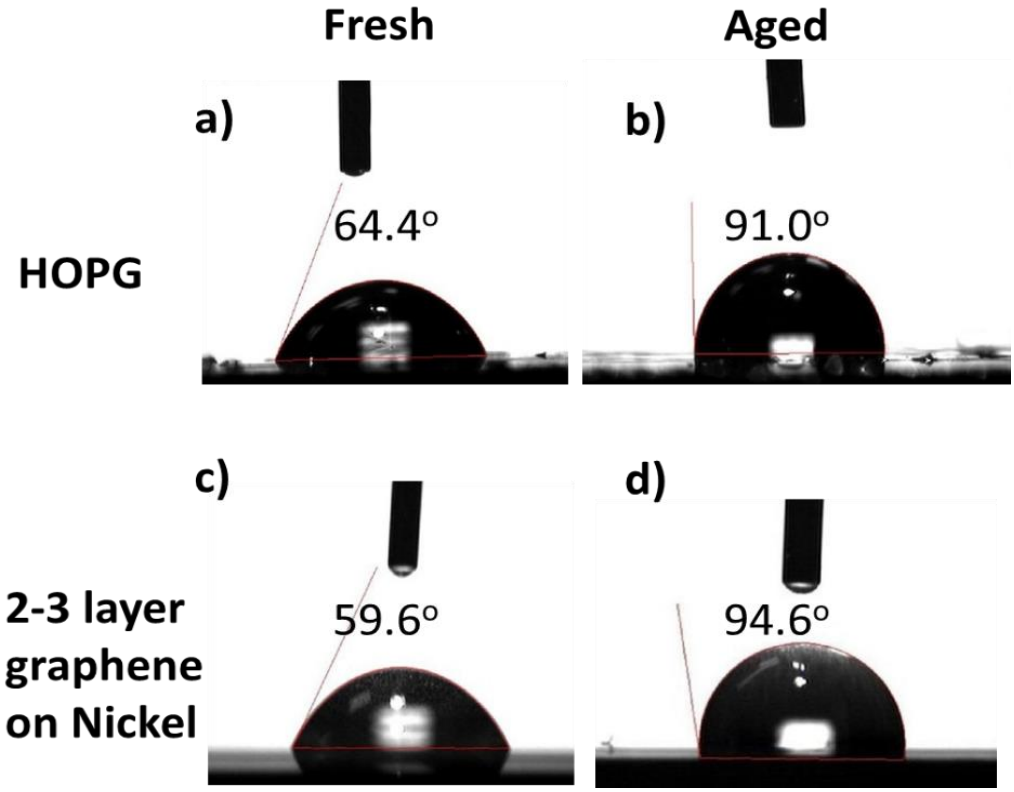

Figure 2-3 (a-b) WCA of HOPG and (c,d) WCA of CVD grown multilayer graphene on a nickel substrate. 'Fresh' samples were measured within 1 min of exfoliation (HOPG) or taken out of CVD chamber (graphene/nickel). Aged samples have been exposed to ambient air for 2 days.

2.4.2 Effect of airborne hydrocarbon contamination

We attributed the time-dependent WCA increase to the adsorption of airborne hydrocarbon on graphitic surface upon ambient air exposure. This hypothesis was firstly supported by ATR-FTIR.

Shown in Figure 2.4(a) are the ATR-FTIR spectra taken on the same location of a copper/graphene sample as a function of its exposure time in ambient air. Two major peaks were observed at 2850 cm^{-1} and 2930 cm^{-1}, which can be assigned to the symmetric and asymmetric stretching of methylene group ($-CH_2-$), respectively.[143] Both peaks showed a monotonic increase with increasing air exposure (Figure 2.4(b)). At longer times, a much weaker peak can be observed at 2950 cm^{-1} that can be assigned to the asymmetric stretching of $-CH_3$ group.[143]

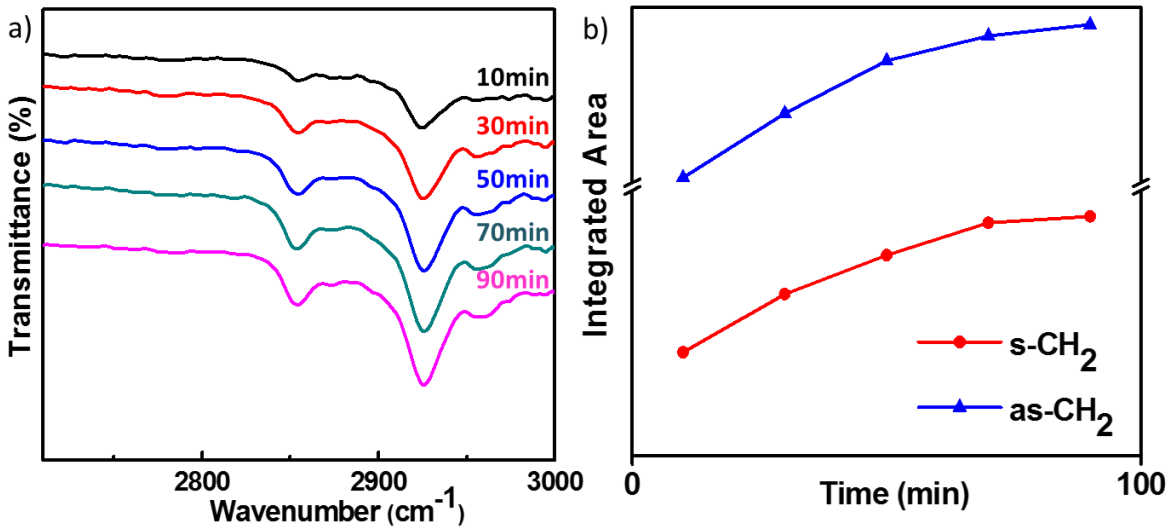

Figure 2-4 (a) ATR-FTIR spectrum of a graphene/copper sample. The spectra were shift vertically for clarity. The sample was taken out of the CVD chamber at time 0. (b) The integrated peak area vs time for the peaks at 2930 cm^{-1} (asymmetric CH_2 stretching, blue) and 2850 cm^{-1} (symmetric CH_2 stretching, red).

The same hydrocarbon accumulation on graphene was also observed with XPS. In Figure 2.5, we compare two C1s XPS spectra of the same copper/graphene sample, one collected within 10 minutes after taking out of the CVD chamber and the other after 2 weeks of storage in air. The difference spectrum showed a positive peak near 285.7 eV with a shoulder at 287.6 eV. This peak is consistent with the adsorption of hydrocarbon onto graphene; its integrated peak area was 19% of the total C1s peak area of the freshly prepared sample. Although some of the adsorbed hydrocarbons will desorb when subject to the high vacuum (10^{-10} torr) of the XPS chamber and as

a result the XPS measurement will not quantitatively correlate with that of the ATR-FTIR, both characterization methods clearly showed that the adsorption of airborne hydrocarbon occurred on the graphene surface. Our XPS data indicates that the surface coverage of hydrocarbon is at least 19% after 2 weeks of air exposure.

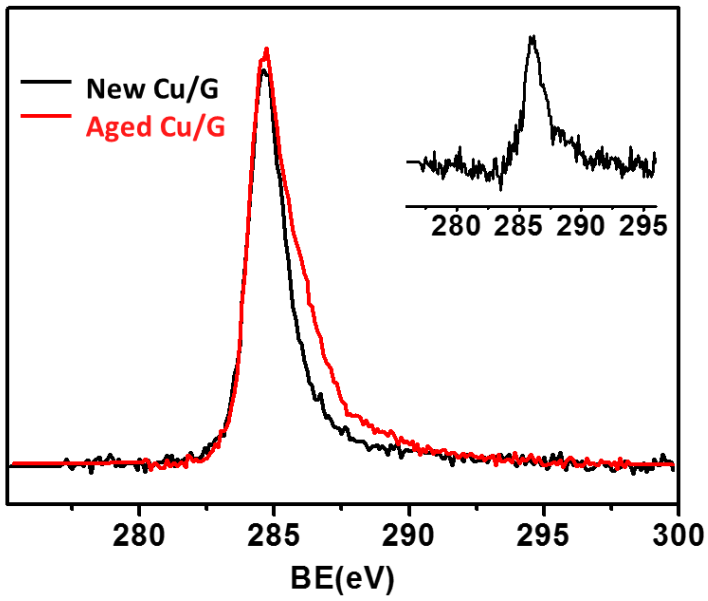

Figure 2-5 Carbon 1s XPS peak of an as-prepared copper/graphene sample and the same sample after exposed to air for 2 weeks. Inset: difference between new and aged copper/graphene (Cu/G) sample, BE: binding energy.

It is noted that the adsorption of airborne hydrocarbon and its effect on WCA have been documented for a number of metal and ionic surfaces, such as gold,[150] SiO_2,[143] and TiO_2.[142] Moreover, a recent study also investigated the hydrocarbon adsorption on hexagonal boron nitride, which is topologically similar to graphene but has a much more polar surface.[145] For all these surfaces, adsorption of airborne hydrocarbon leads to a concurrent increase of their WCA, similar to what we observed for graphene.

In all, the WCA, ATR-FTIR, and XPS results suggest that a clean copper/graphene sample is

intrinsically hydrophilic and becomes hydrophobic only after absorbing hydrocarbon from ambient air. The fact that we never observed a decrease of WCA suggests that the contaminants are mostly hydrophobic molecules. Although graphitic surfaces have long been regarded as a low energy surface, our results clearly showed that a copper/graphene surface can be rapidly contaminated by airborne hydrocarbon, leading to a significant increase of its WCA.

The uncertainty in our conclusion arises principally from another assumption that other gas molecules (*e.g.*, O_2, CO_2, water, etc.) can also adsorb on graphitic surface and induce WCA increase. To exclude this hypothesis, we conducted two additional control experiments to confirm that it is indeed the hydrocarbon contamination that caused the increase of WCA of graphene. In one experiment, we exposed a freshly prepared copper/graphene sample to 1-octadecene (b.p.: 315°C) vapor at 50°C for 30 min and observed an increase of WCA to 80° (Figure 2.6(a)). In comparison, the WCA of a copper/graphene sample only increased to *ca.* 65° in the absence of 1-octadecene vapor but under otherwise the same conditions. Exposing this "contaminated" graphene to UV/O_3 restored its hydrophilic nature without introducing significant damage to graphene. In another experiment, we found that a copper/graphene sample kept in a polystyrene petri dish showed consistently higher WCA than another sample kept in a carefully cleaned glass container (Figure 2.6(b)). To understand this result, we note that plastics emit volatile organic compounds (VOC), in particular plasticizers, even at room temperature.[143, 151-152] The emitted VOC is an additional source of hydrocarbon and can reach a steady state concentration up to the parts-per-billion (ppb) level,[151] which is similar to the typical hydrocarbon concentration in air.[153] Both experiments clearly showed the correlation between hydrocarbon adsorption and the WCA increase on graphene surface.

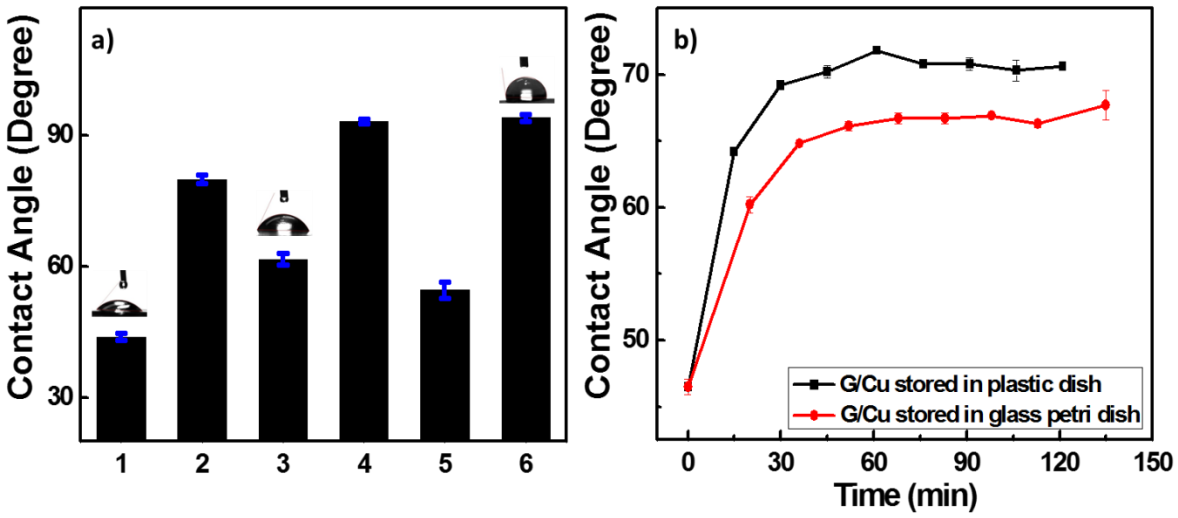

Figure 2-6 (a) Effect of intentional exposure to organic vapor on the WCA of a copper/graphene sample. Keys: (1) as-prepared; (2), (4), and (6): after exposure to 1-octadecene vapor for 30 min; (3) and (5) after 2 min of UV/O_3 treatment. (b) Effect of volatile organic compound emission from a plastic petri dish on the WCA of a copper/graphene sample.

2.4.3 Conventional techniques to remove AHC

Both thermal annealing and UV/O_3 treatment could remove the hydrocarbon contaminants and at the same time decrease the WCA of graphene. It is known that thermal annealing was frequently used to remove polymer residues (*e.g.*, PMMA) on graphene.[154] In our experiment, we found that annealing an "air-contaminated" copper/graphene sample in Ar at 550 ºC decreased its WCA to as

low as 55º (Figure 2.7(a)). When exposed to air, the annealed copper/graphene sample showed a rapid increase of WCA, similar to the behavior observed for an as-prepared sample. To confirm the decrease of hydrocarbon contamination on graphene surface during thermal annealing, Figure 2.9(a) showed the ATR-FTIR measurement before and after thermal annealing in Ar. The C-H peak intensity decreased by at least 50% after the annealing while Raman spectroscopy (Figure 2.9(b)) showed no apparent damage in annealed graphene.

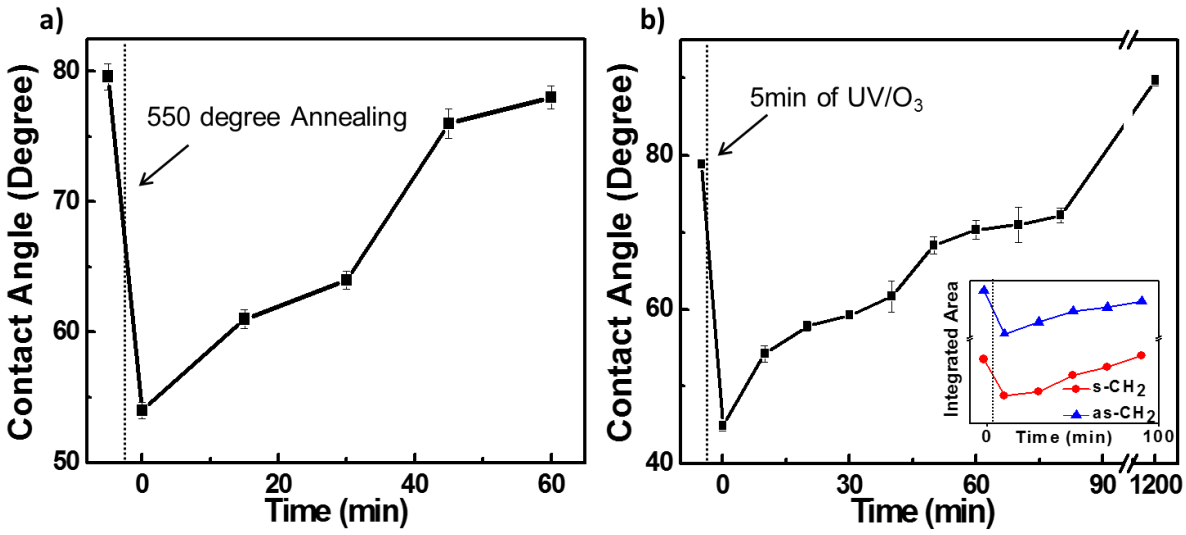

Figure 2-7 Effect of (a) thermal annealing in Ar at 550°C and (b) UV/O_3 treatment on the wettability of a copper/graphene sample. The inset in (b) shows the integrated peak area vs time for the ATR-FTIR peaks at 2930 cm^{-1} (asymmetric CH_2 stretching, blue) and 2850 cm^{-1} (symmetric CH_2 stretching, red). The thermal annealing and UV/O_3 treatment ended at time 0.

In addition, we also transferred CVD-grown single layer graphene to gold, glass, and SiO_2 substrates and observed a decrease of WCA after thermal annealing. These transferred graphene samples and their substrates are all contaminated by hydrocarbon because their preparation necessitates their long exposure in air and contact with organic solvent and polymer. The WCA of the transferred single layer graphene samples range from 76° to 85° after the transferring process. We then annealed these single layer graphene samples as well as an 'air-contaminated' multi-layer Ni/graphene sample under Ar at 600°C. We observed a decrease in their WCAs immediately after the thermal treatment. The WCAs measured right after the annealing ranged from 65° to 75° with

an average decrease of 17° (Figure 2.8). We note that the annealing is unlikely to remove all the hydrocarbons and as a result, the WCA we measured after the annealing will depend on the degree of hydrocarbon removal, which could be affected by the underlying substrate. As such, these values should be regarded as the higher bound of the intrinsic WCA of these samples.

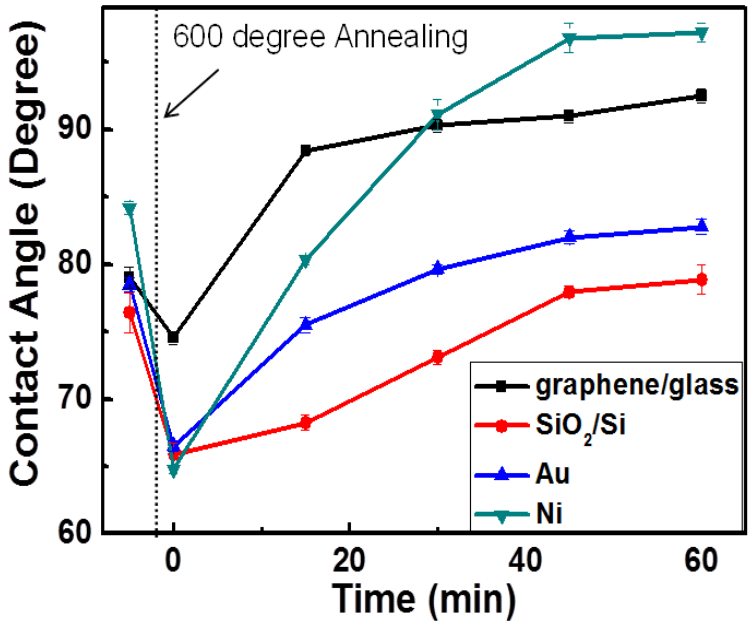

Figure 2-8 Effect of thermal annealing (Ar, 600ºC, 60 min) on the WCA of single layer graphene deposited on Si/SiO_2, glass, and Au substrates as well as multi-layer graphene grown on a Ni substrate. The samples were taken out of the annealing chamber at time 0.

UV/O_3 treatment was applied as an alternative method to decrease the surface hydrocarbon contamination on graphene surface. As shown in Figure 2.7(b), we also found that a brief UV/O_3 treatment could effectively remove the hydrocarbon contaminants without damaging graphene. The ATR-FTIR spectrum of the UV/O_3 treated graphene sample (Figure 2.7(b) inset) showed a 62% reduction in the peak intensity at 2930 cm^{-1} while the XPS showed a decrease in the C-H species (Figure 2.10(a)). In addition, the Raman spectrum of UV/O_3 treated sample showed a very weak D peak (Figure 2.10(b)), indicating that the removal of hydrocarbon was achieved without

introducing significant amount of structural damage to graphene. Similar to the case of thermal annealing, the UV/O_3 treatment also resulted in a decrease of WCA. We attribute this decrease to the removal of hydrocarbon although we cannot rule out the possible contribution from partially oxidized hydrocarbon species. Upon exposure to ambient air, the C-H peaks in the ATR-FTIR spectrum increased in intensity and fully recovered after approximately 80 min (Figure 2.7(b)).

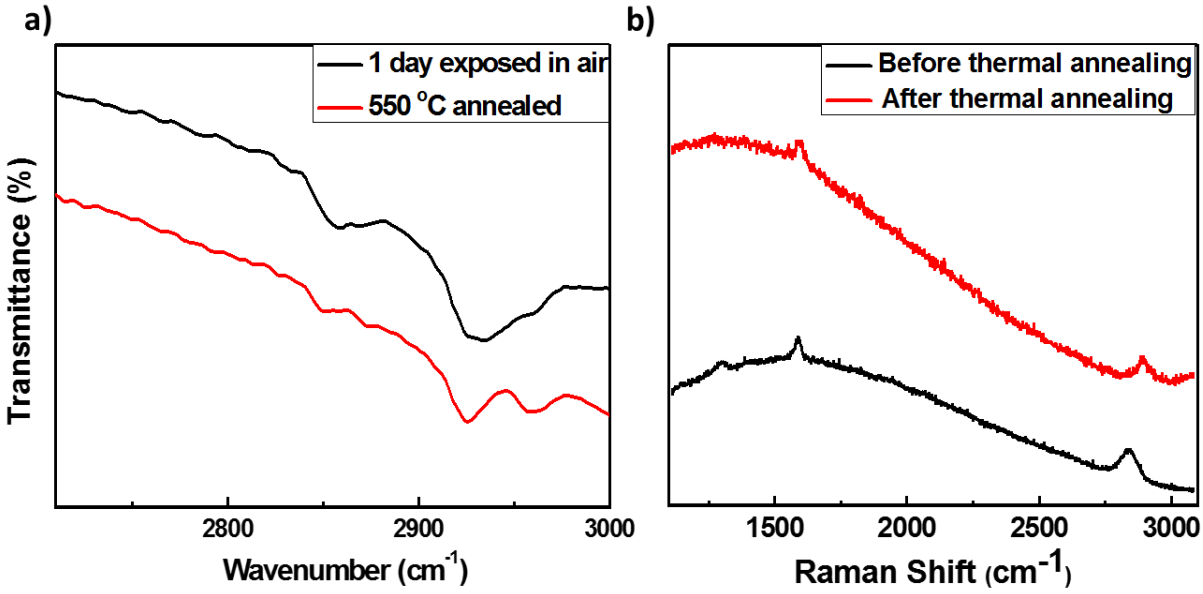

Figure 2-9 (a) ATR-FTIR spectrum of a graphene/copper sample before (black) and after (red) thermal annealing in Ar at 550ºC for 1h. (b) Raman spectra of a graphene/copper sample before and after thermal annealing in Ar at 550ºC. The D peak was very weak, indicating that the thermal annealing introduced minimal structural damage to graphene. The large background is typical for graphene/copper samples.

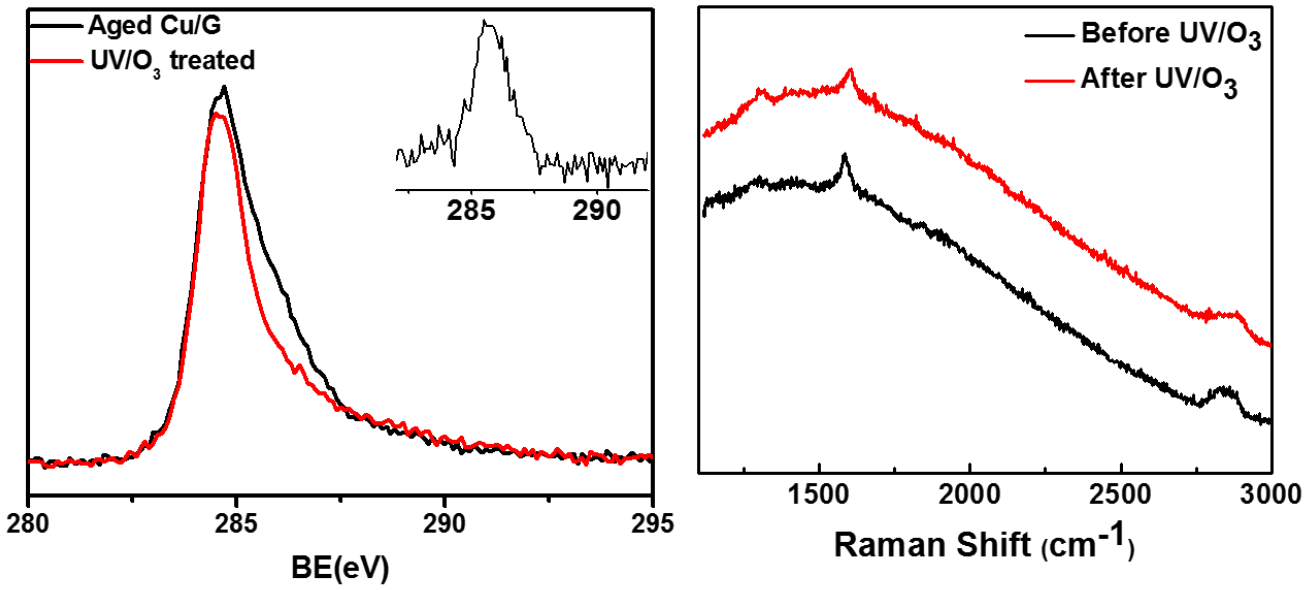

Figure 2-10 (a) Carbon 1s XPS spectrum of an aged graphene sample (black) and the same sample after UV/O_3 treatment (red). The inset shows the difference of the two spectra. (b) Raman spectra of a graphene/copper sample before and after 4 min of UV/Ozone treatment. The D peak was weak, indicating that the UV/Ozone exposure introduced minimal structural damage to graphene. The large background is typical for copper/graphene samples.

2.5 CONCLUSION

In conclusion, our study showed that a clean graphene surface is in fact mildly hydrophilic as opposite to hydrophobic, and the previously observed hydrophobicity is actually due to contamination from airborne hydrocarbon. For a graphene/copper sample, the WCA can be as low as 37° for a clean surface and increases to *ca.* 80° for a hydrocarbon-contaminated one. Similar observations were also made on single layer graphene deposited on SiO_2, glass, and gold substrates as well as multi-layer graphene grown on a Ni substrate, suggesting that this hydrocarbon contamination may affect the wettability of all graphene surfaces. In addition, significant hydrocarbon contamination could occur within several minutes of air exposure and as a result, this effect could be easily overlooked if the WCA measurement was not done immediately after the synthesis of graphene. Given that wettability is an essential concept in interpreting and predicting many surface phenomena and even used to calibrate force fields for molecular dynamic simulations.[155] Our result suggests that water – graphene interaction is stronger than previously believed[156] and calls for a revisit of the wetting models developed for graphitic surfaces.

3.0 WATER PROTECTS GRAPHITIC SURFACE FROM AIRBORNE HYDROCARBON CONTAMINATION

3.1 CHAPTER PREFACE

Materials contained in this chapter were submitted as a research article to *ACS Nano*.

List of Authors: Zhiting Li*, Andrew Kozbial*, Nikoloz Nioradze, David Parobek, Ganesh J. Shenoy, Muhammad Salim, Shigeru Amemiya, Lei Li and Haitao Liu.

Author Contributions: Z.L., H.L., and L.L. designed and directed the experiments. Z.L., A.K., N.N., D.P., G.S., M.S conducted the experiments. All authors discussed the results. Z.L. and H.L. co-wrote the manuscript with input from all authors.

3.2 BACKGROUND

We and others have reported that many graphitic surfaces, such as graphene and graphite, are mildly hydrophilic and the previously observed hydrophobicity is actually due to contamination from airborne hydrocarbons.[38, 157-162] Given that wettability is one of the most fundamental surface properties, it directly impacts many other surface properties, such as adhesion,[137] adsorption,[138] carrier mobility[139] and charge doping[140]. In this regard, it is highly expected to revisit those surface properties on airborne hydrocarbon contaminants (AHC) free graphitic surface.

However, a thorough and systematical investigation on the hydrocarbon-free graphitic surface has been restricted by rapid hydrocarbon adsorption onto the pristine surface. For example, our recent studies demonstrated the kinetics of airborne hydrocarbon adsorption on HOPG surface, which becomes saturated within 10 - 15 minutes upon air exposure after exfoliation.[38] Such a short timescale inevitably limits further characterization targeting the intrinsic properties of graphitic surface. Maintaining a clean graphitic surface will require either a hydrocarbon-free environment, methods to clean the surface, or ways to protect the surface from contamination.

It is extremely difficult to maintain a hydrocarbon-free environment because even parts-per-trillion (ppt) level of hydrocarbon is detrimental. Although it is possible to remove hydrocarbons from air by passing contaminated air through cryogenically cooled activated charcoal,[163] such an approach requires the experimental setup to be isolated from ambient air, making it impractical for most experiments and large scale applications. We also note that glovebox and clean room do not provide a hydrocarbon free environment; in fact, both contain

high levels of hydrocarbon due to emission from plastics (*e.g.*, gloves, wafer storage containers, etc.).

Conventional surface cleaning techniques are not effective in cleaning graphitic surface.[164] For instance, solvent washing is able to remove the surface contaminants, but solvent residue can easily become trapped on graphitic surface due to the existence of step edges (*i.e.*, defect sites);[165] cleaning methods based on thermal desorption or UV photocatalysis removes the surface adsorbed airborne hydrocarbon at the expense of producing additional defect sites on the basal plane;[166-167] high-speed air jet requires a pressure drop about 10^5 Pa along the centerline of gas flow,[168] which can easily blow off graphene (graphite) layers from the underlying substrate.[169] All things considered, a strategy that simply protects a fresh graphitic surface from airborne hydrocarbon is expected to be suitable for both fundamental study and large-scale applications of graphitic materials.

Herein, we report a convenient method to significantly inhibit hydrocarbon contamination through water coverage of graphitic carbon. This approach significantly slows down (by a factor of *ca.* 20) the airborne hydrocarbon contamination on a fresh graphitic surface, thus maintaining its intrinsic wetting behavior for many hours in air. Follow-up surface characterization shows that water condenses on graphitic surface, likely forming a 2D ice structure that persists even at room temperature. Our method provides a convenient strategy to fabricate graphitic materials with minimal hydrocarbon contamination, maintaining its intrinsic surface properties in device application. As an example, we show that water-treated graphite electrode maintained high level of electrochemical activity in air for up to one day.

3.3 EXPERIMENTAL SECTION

3.3.1 Preparation of HOPG samples

HOPG purchased from SPI Supplies. Both SPI-1 (Grade:10 x 10 x 1 mm) and SPI-2 samples (Grade: 20 x 20 x 1 mm) were used for all experiments. Exfoliation was performed by the well-established tape method where a piece of adhesive tape was placed on the sample surface and gently rubbed to ensure contact between the tape and sample.[170] The tape (Scotch® brand 1 inch) was then carefully pulled back, removing the upper surface layer, thereby exposing a fresh HOPG surface. Care was taken to ensure that a complete layer of HOPG was removed in each exfoliation. Testing was performed on the pristine surface away from flakes and surface defects.

Note:

Synthesis of single-layer graphene on copper foil: see experimental details in 2.3.1

Graphene transferred onto silicon substrate: see experimental details in 2.3.3

3.3.2 Low-temperature storage

One piece of HOPG was kept in a glass petri dish without lid covered to ensure ambient exposure. The glass petri dish was carefully cleaned (acetone wash followed by UV/Ozone cleaning for 30 min) and then surrounded by a pile of dry ice particles during the low temperature storage. Care

was taken to not directly contact the HOPG sample with dry ice. The local temperature was mearured to be -15 - -20^{o}C using a non-contact laser infrared thermometer. During the WCA measurement, sample was taken out of the petridish every 1-30 min and then immediately put back.

3.3.3 XPS

XPS measurements were carried out in a UHV chamber (base pressure ~ $1x10^{-10}$ torr) of an Escalab 250XI XPS instrument. Spectra were collected using the Al-Kα X-ray line and a CAE analyzer. The characterization was operated with a bandpass of 50 eV for both survey scans (1.0 eV/step) and detailed scans (0.1 eV/step). After raw data collection, the Thermo Scientific^{TM} Advantage Data System software was used in data analysis of background subtraction and peak fitting.

Note:

ATR-FTIR: see experimental details in 2.3.5

WCA: see experimental details in 2.3.4

3.4 RESULTS AND DISCUSSION

3.4.1 Low temperature storage effects graphitic surface wettability

We found that the intrinsic wettability of freshly prepared graphitic surface (*e.g.*, HOPG, copper/graphene) can be well preserved for many hours when stored at low temperature. Shown in Figure 3.1 is the static WCA evolution on newly exfoliated HOPG samples exposed in air at

room temperature (r.t.) and low temperature, respectively. Upon r.t. storage, the HOPG sample showed an initial WCA *ca.* 65^{o} and increased in the next 15 min to a constant value of *ca.* 90^{o}, in agreement with our previously reported WCA on freshly cleaved HOPG surface during air exposure. In comparison, HOPG stored at low temperature showed consistently lower WCA initiated from *ca.* 60^{o}, which slightly reached *ca.* 70^{o} within 15 min air exposure and plateaued without further increase. This remarkable WCA contrast over different storage methods is highly reproducible regardless of testing time and locations, whereas a small variation of WCA (60-65^{o}) exists on different HOPG samples right after exfoliation.

The consistently low WCA was also observed on other graphitic surfaces during a low temperature storage. In Figure 3.1(b), CVD-grown copper/graphene sample showed an initial WCA about 40-45^{o}, which drastically increased to 60^{o} within 20 min air exposure and plateaued at *ca.* 80^{o} overnight. When stored at low temperature, its intrinsic wettability can be effectively preserved with a constantly lower WCA about 50^{o}, indicating a minimal hydrocarbon deposition on copper/graphene surface during the 2 hours low temperature storage. We also transferred graphene onto two SiO_2 substrates and then thermally annealed them in vacuum at 500^{o}C to get rid of the surface hydrocarbons. As shown in In Figure 3.1(c), we observed a decrease in their WCAs immediately after the thermal annealing, suggesting a substantial decrease of surface hydrocarbon level. During the subsequent 1h ambient exposure, SiO_2/graphene exposed in air at r.t. showed a rapid recovery of WCA (80 – 85^{o}) due to the airborne contamination. In contrast, SiO_2/graphene stored at low temperature maintained a low WCA with a slight variation from 59^{o} to 65^{o}, indicating a reduced hydrocarbon contamination on graphitic surface at low temperature.

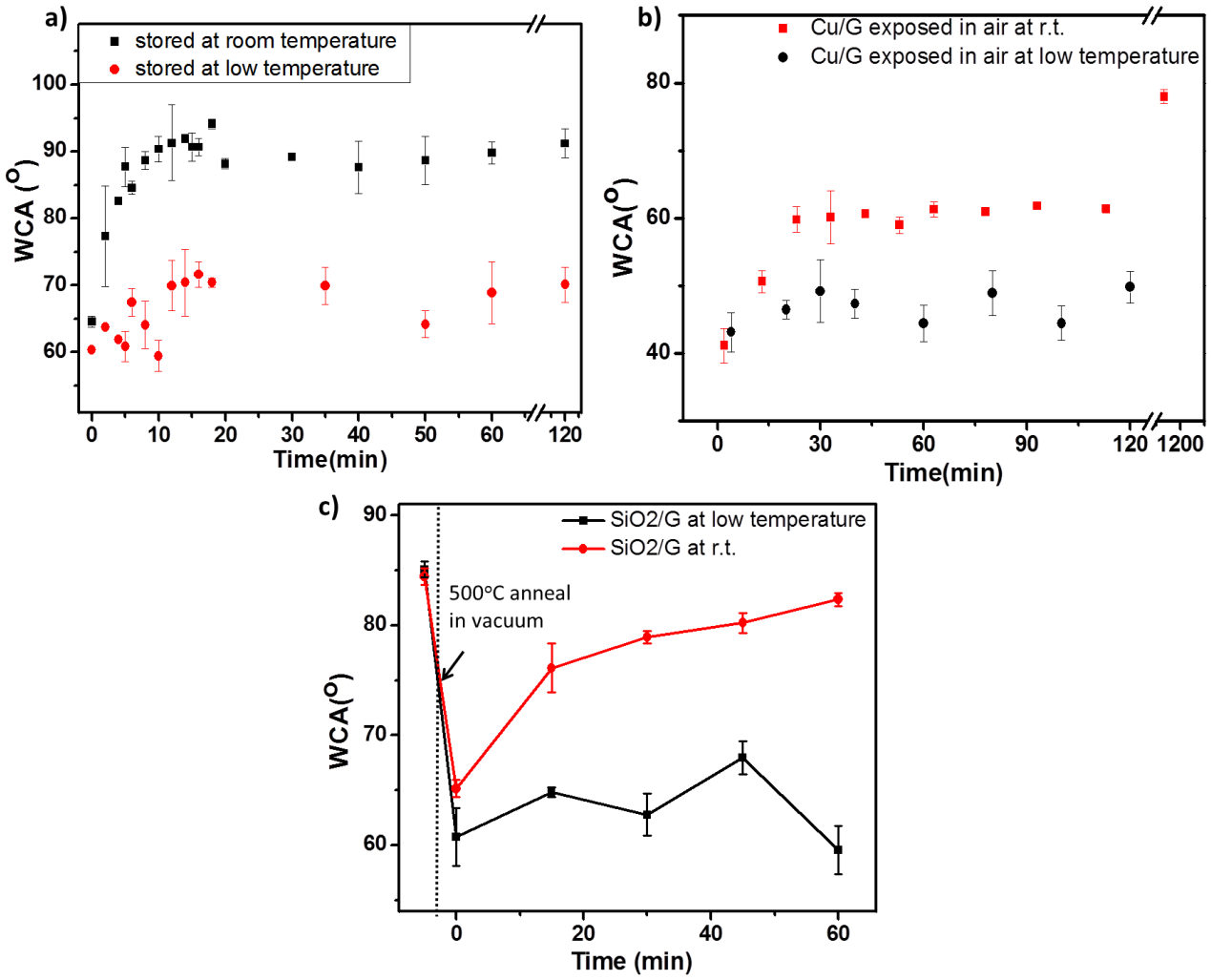

Figure 3-1 Temporal evolution of the WCA measured on (a) freshly exfoliated HOPG (b) freshly synthesized CVD-grown copper/graphene and (c) SiO_2/graphene thermal annealed in vacuum at 500°C for 1 hour. All samples are stored at room temperature (r.t.) and low temperature, respectively. For the samples stored at low temperature, they were only exposed to r.t. during the WCA measurement.

3.4.2 Inhibition of AHC adsorption

According to previous studies, such WCA increasing trend is mainly due to the adsorption of airborne hydrocarbon upon ambient exposure. The adsorbed hydrocarbon decreases the surface energy and thus converts the fresh graphitic surface from mildly hydrophilic to more hydrophobic. In our current experiments, we demonstrated that such airborne hydrocarbon adsorption on HOPG surface has been significantly inhibited during low temperature storage, as evidenced by both ATR-FTIR and XPS measurements.

Shown in Figure 3.2 are ATR-FTIR spectra of two freshly exfoliated HOPG samples stored at r.t. Figure 3.2(a) and low temperature Figure 3.2(b) for 2 days. For the r.t. stored HOPG sample, peaks at 2850 cm^{-1} and 2930 cm^{-1} can be clearly observed after 2 days of air exposure, corresponding to symmetric and asymmetric stretching of methylene group (-CH_2-), respectively. In comparison, such hydrocarbon induced peak was barely detectable on low temperature stored HOPG surface while a broad peak around 3000 cm^{-1} – 3500 cm^{-1} was observed, which can be assigned to the O-H stretching vibrations of water molecules. Interestingly, unlike liquid-phase water that always shows an IR peak centered in around 3400 cm^{-1}, HOPG stored at low temperature gives rise to a water peak locates in 3250 cm^{-1}, indicating an ice-like structure with a more restricted –OH bond stretching (*vide infra*).

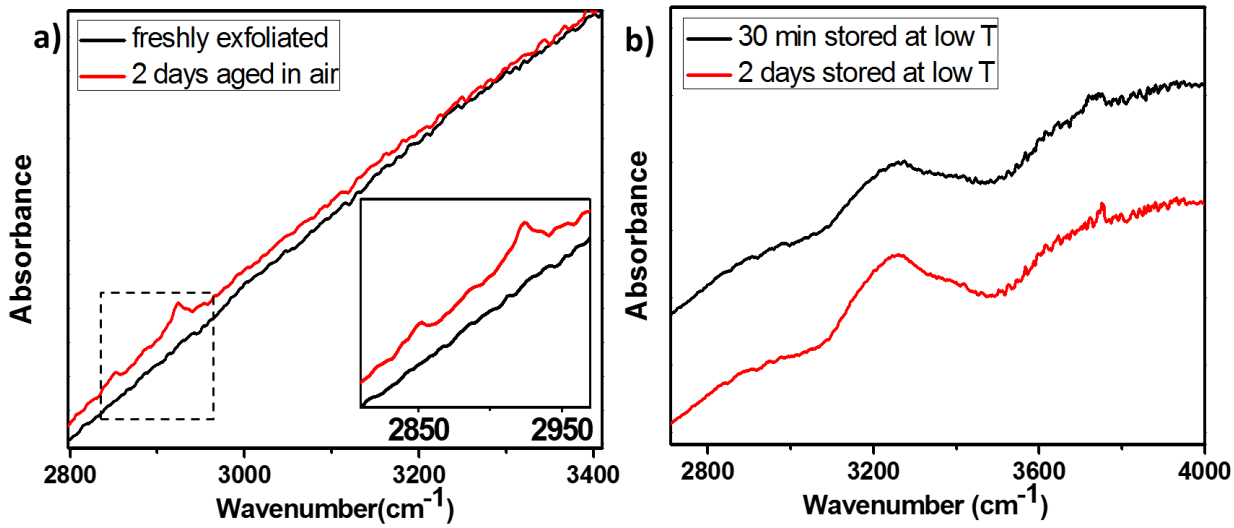

Figure 3-2 ATR-FTIR spectra of freshly exfoliated HOPG stored at (a) room temperature and (b) low temperature for 2 days. For each sample, spectra were taken right after exfoliation (30 minute low temperature storage) and after 2 days storage in ambient air, respectively. The insert shows a magnified image of the dashed area in (a). Note that the spectra are plotted in absorbance mode and vertically shifted for clarity.

The impact of storage method on the hydrocarbon accumulation on HOPG surface was also observed with XPS. As shown in Figure 3.3(a), a freshly cleaved HOPG sample was firstly analyzed to provide a benchmark, which displayed a single C1s peak at 284.5 eV corresponding to the sp^2 structured C-C (surface and bulk). Given that the C1s peak would have contribution from both surface as well as many sub-layers of graphite, we performed C1s peak analysis to calculate the contribution from the top layer of HOPG.

To estimate the contribution of the top layer of HOPG, we make the following assumptions:

1. While the x-ray penetrates into the sample, there is a limited escape depth of the ejected electrons. Based on the energy of our x-ray gun (*ca.* 1400 eV), the depth is around 10 nm,[171] corresponding to *ca.* 29 graphene layers in total.
2. According to Beer-Lambert relationship: $I_o = I / \exp(-(d_G / \cos\theta) / \lambda)$, where I_o (I) attributes to the peak intensity of top (second) graphene layer, $d_G = 3.5$ Å is the thickness of graphene layer and θ is the escape angle (45°), λ is the Inelastic Mean Free Path (IMFP) and equals 24.8 Å.[172]

With these assumptions, the contribution of the k^{th} ($k<30$) layer of graphene to the observed C1s peak will decrease to 0.819^{k-1} for each increase of layer depth. As a result, the contribution from the top layer of HOPG accounts for 18% of the observed C1s peak. Therefore, instead of a significant broadening of C1s peak as we previously distinguished on monolayer graphene, a relatively small but comparative broadness of C1s peak was observed after 6 days ambient exposure at r.t. In contrast, HOPG stored at low temperature showed a C1s peak similar to that from fresh surface, with a slight increase of FWHM by 0.003 eV, only 7 % of that occurs on r.t. aged surface. Note that although the changes are small, the FWHM are highly reproducible. Showing in Figure 3.3(a) inset are error bar derived using measurement from three different locations on the same sample surface.

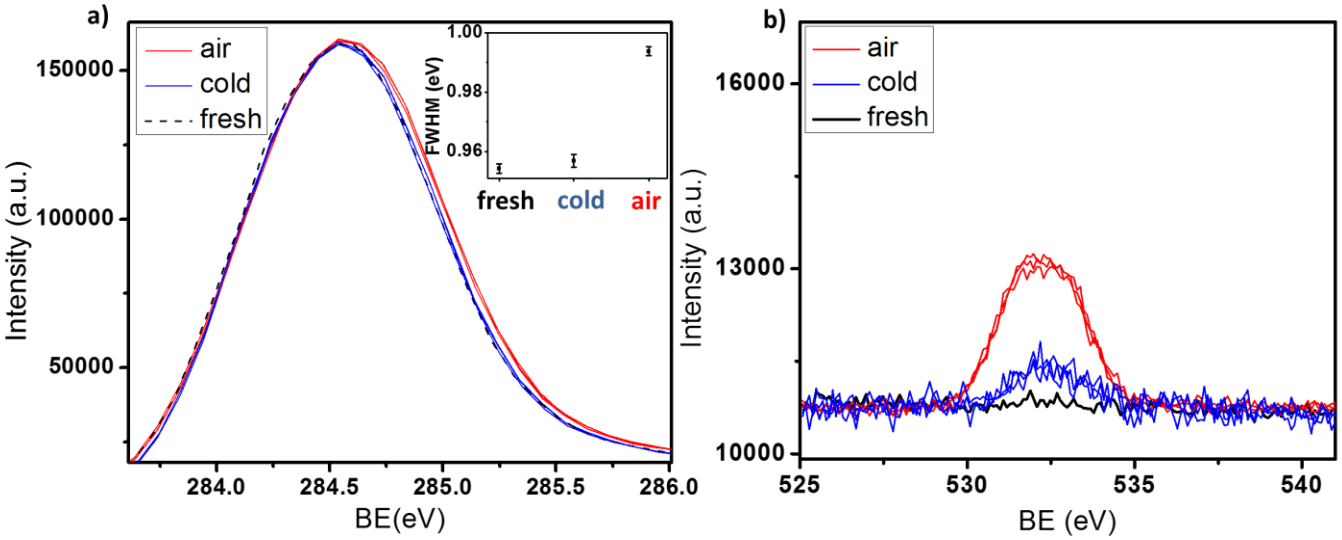

Figure 3-3 (a) Carbon 1s and (b) Oxygen 1s XPS peak of freshly exfoliated HOPG samples right after exfoliation (black), after 6 days ambient exposure at room temperature (red) and at low temperature (blue), respectively. The inset shows the FWHM of C1s peak using measurements from three different locations on the same sample surface. Note that the black and blue curves in (a) almost completely overlap.

On the other hand, oxygen species on HOPG surface displayed a much remarkable change over different storage methods. We note that unlike C1s peak, which has contributions from both surface and sub-surface layers, O1s peak presumably comes from only the HOPG surface, without interference from the bulk. As is shown in Figure 3.3(b), fresh HOPG surface showed negligible O1s peak, further corroborating that the freshly cleaved surface is dominated by sp^2 C-C species. Storage at r.t. resulted in a significant increase of oxygen peak, which is about 4 times higher than that observed on low temperature treated HOPG surface. Accordingly, we plotted the peak difference between these two aged samples (Figure 3.4(a-b)). The C1s peak clearly showed the

additional hydrocarbon species that primarily located at 286.6 eV with a shoulder peak at 288.7 eV. Besides, the integrated peak area indicated an atomic ratio of C:O about 3:1, in well accordance with the known dominant hydrocarbon contaminants reported in our previous studies.[157] We note that the O% measured by XPS only provide a lower bound of the surface oxygen species, as some of the adsorbed molecules is expected to desorb under UHV condition. Therefore, the peak area cannot be directly extrapolated to the surface coverage of hydrocarbon. In all, both the ATR-FTIR and XPS results suggest that the AHC accumulation level on HOPG surface can be efficiently minimized during low temperature storage.

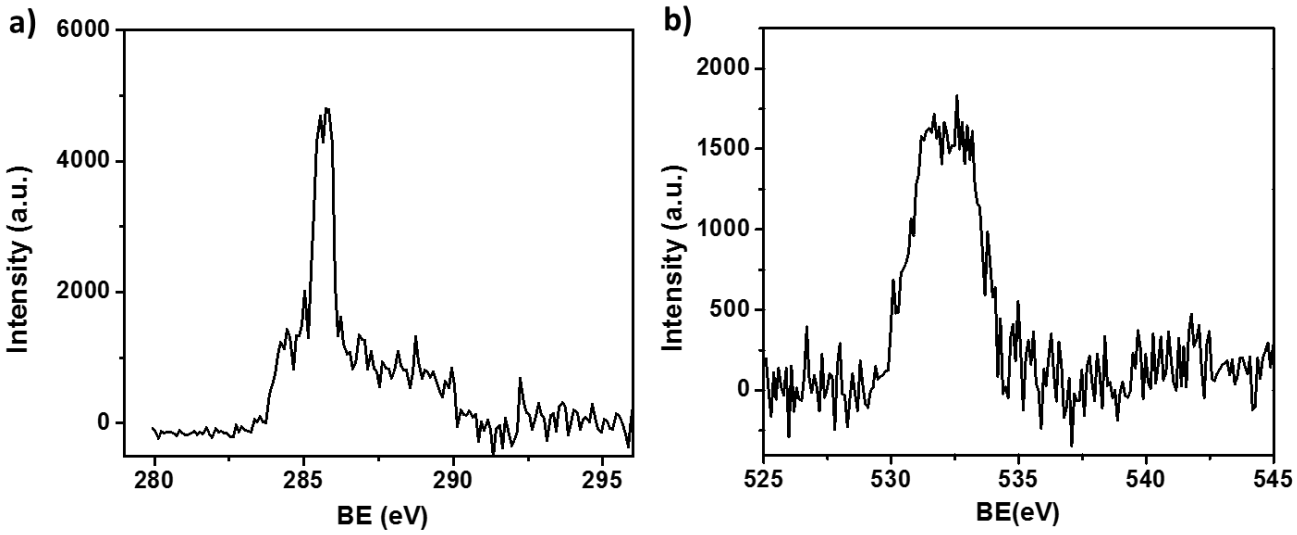

Figure 3-4 XPS differential spectrum of (a) Carbon 1s and (b) Oxygen 1s regions between two HOPG samples, one stored at room temperature and the other at low temperature, both for 6 days.

3.4.3 Long term preservation of surface wettability

In addition, it is interesting to note that HOPG also shows a much slower WCA increase even after removal from low temperature environment. In one experiment, an exfoliated HOPG was pretreated at low temperature for 30 min, followed by a subsequent ambient exposure at r.t. when the WCA measurement started. As shown in Figure 3.5, the initial WCA was 64º right after removal from low temperature, which slowly increased to *ca.* 72º within 1 hour and eventually plateaued at *ca.* 85º after 20 hours air exposure. Also, we noted that although the kinetics of WCA evolution varies at different temperatures, however, the initial and final WCA on HOPG appear to

be independent of storage methods, indicating only a temporary role played by low temperature storage in effecting its surface wetting behavior. Besides, additional WCA measurement on aged HOPG surface before and after low temperature treatment showed similar high value (85 - 90^{o}), excluding another competing mechanism that low temperature treatment may introduce additional defects on HOPG surface and thus contribute to the surface hydrophilicity.

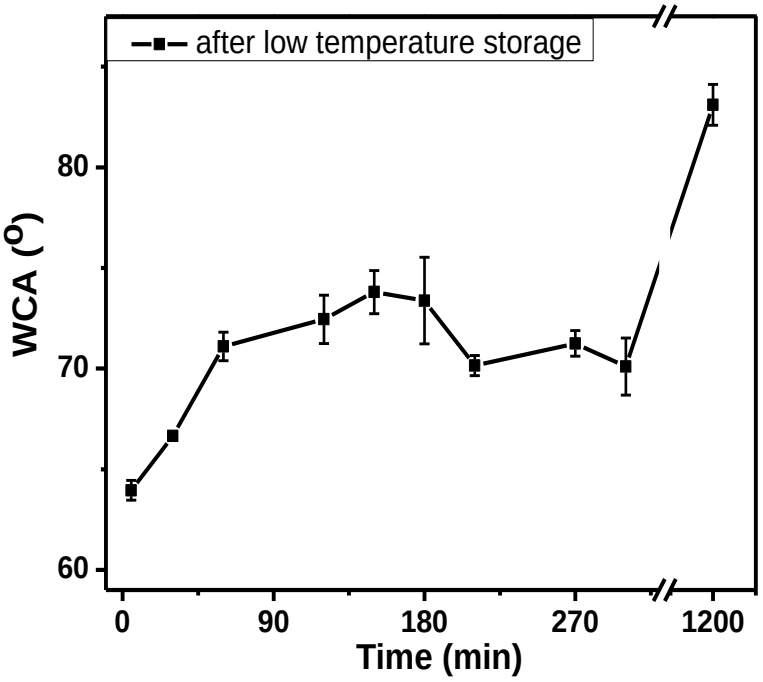

Figure 3-5 Temporal evolution of the WCA on low temperature pretreated HOPG surface. The sample was stored at -15°C for 30 minutes then removed from low temperature environment at time 0. It was kept at r.t. throughout the measurement.

The retarding of hydrocarbon adsorption on HOPG surface after low temperature treatment is further supported through spectroscopic ellipsometry, as shown in Figure 3.6(a). In one experiment, we conducted temporal monitoring on exfoliated HOPG surface exposed in ambient air at r.t. During the first 50 minutes of air exposure, a linear growth of adsorbed hydrocarbon layers occurred reaching a thickness about 0.55 nm, after which the rate of increase drastically slowed down and plateaued at 0.60 nm after 5 hours. Similar hydrocarbon adsorption kinetics have

been observed in our previous studies.[38]

In another experiment, we stored freshly exfoliated HOPG in a cold glass petri dish for 10 minutes and the local temperature was measured to be -10ºC. The first ellipsometry data point was collected right after exfoliation of HOPG and the surface assumed to be free of hydrocarbon contamination. After 10 minute low temperature treatment, the glass petri dish was removed immediately and another ellipsometry measurement was conducted on the same location for 5 hours. To analyze the data, we used a three-layer (HOPG/water/hydrocarbon) model (Figure 3.6(b)) in which both the thickness of water and hydrocarbon are determined by fitting.[38] As shown in Figure 3.6(a), the low temperature treatment produced a water film of *ca.* 0.08 nm in thickness, indicative of a submonolayer to monolayer of water film on HOPG surface. The presence of such water film significantly inhibited the follow-up hydrocarbon adsorption rate by 83%, which reached a hydrocarbon thickness *ca.* 0.40 nm after 200 minute ambient exposure.

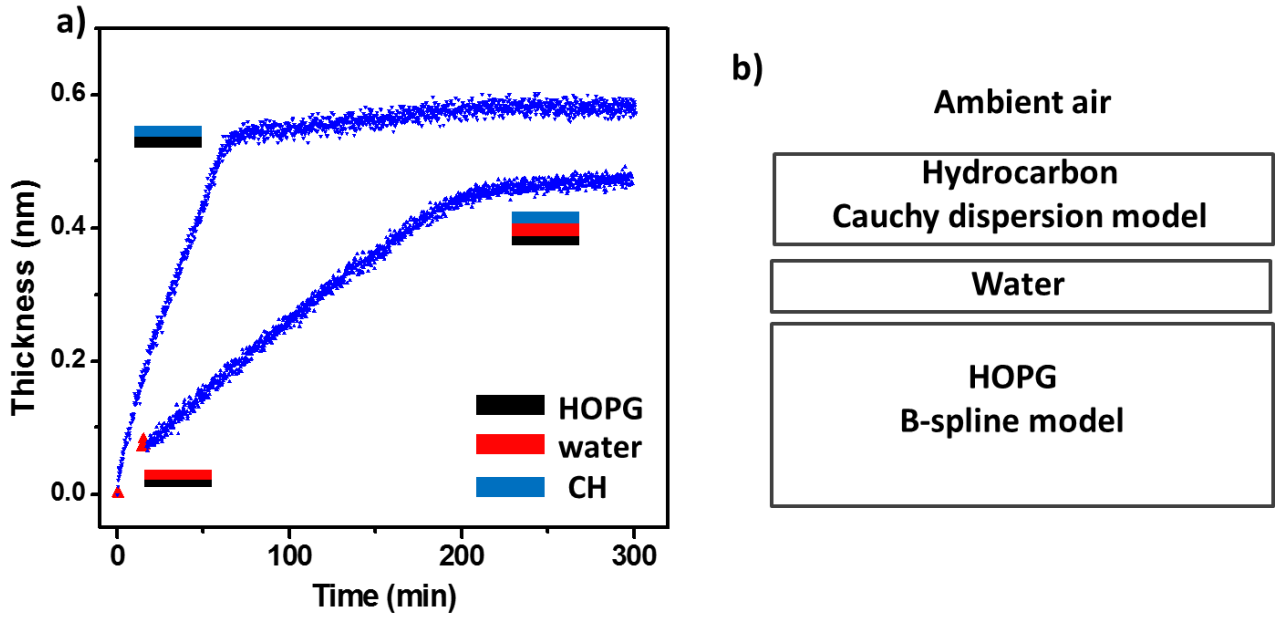

Figure 3-6 (a) Spectroscopic ellipsometry monitoring of hydrocarbon thickness on exfoliated HOPG surface exposed in ambient air with and without low temperature treatment, respectively. (b) The schematic model used for ellipsometric measurement of hydrocarbon adsorbed on low temperature treated HOPG surface.

3.4.4 Role of water in AHC adsorption

We hypothesized that the reduced hydrocarbon contamination is due to the increased adsorption of water on graphite at low temperature. To test this hypothesis, we performed two control experiments to probe the role played by water during ambient air exposure. In one experiment,

freshly exfoliated HOPG was pretreated at low temperature for 30 minutes, followed by storage in room temperature surrounded by anhydrous $CaCl_2$. $CaCl_2$ is a desiccant used to decrease the local vapor pressure of water. As shown in Figure 3.7(a), this sample showed an increase of WCA from 65^o to 80^o within 90 minutes, in contrast to the much slower WCA increase when the sample was stored without desiccant but otherwise identical conditions (Figure 3.1(a)). This result suggests that less water on graphite may promote hydrocarbon adsorption. In another experiment, both freshly exfoliated and aged HOPG samples were placed in DI-water steam for 2 minutes before storage in air at r.t. The freshly exfoliated HOPG surface showed consistently lower WCA (65^o – 70^o) compared to that on aged HOPG surface (88^o – 95^o) during the subsequent 2 hours air exposure (Figure 3.7(b)). On aged HOPG we observed similar high WCA (88^o – 95^o) before and after the steam treatment; this result shows that water in the environment, by itself, does not necessarily impact the wettability of graphite. Indeed, the effect of ambient humidity on wettability has been documented for a number of hydrocarbon-based materials, such as polyethylene terephthalate (PET), paraffin, etc. For all these surfaces, the increase of relative humidity (25% - 100%) leads to a concurrent increase of WCA by only 2 - 5^o,[21] almost an order of magnitude smaller than the WCA change induced by hydrocarbon contamination. Collectively, these results suggest that the water adsorption on the fresh HOPG surface, but not on the aged and therefore hydrocarbon-covered HOPG surface, inhibits hydrocarbon adsorption.

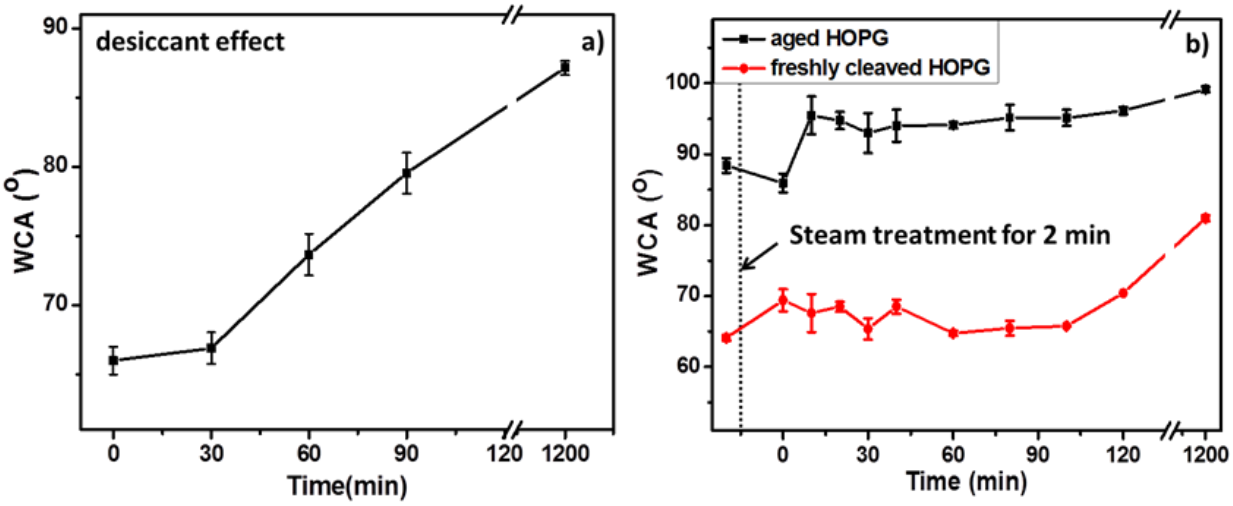

Figure 3-7 Effect of water deposition on HOPG surface. (a) Temporal evolution of the WCA measured on low temperature pretreated HOPG surface. The sample was taken out of low temperature and surrounded by $CaCl_2$ desiccant at time 0. (b) Temporal evolution of the WCA on freshly exfoliated (red) and aged (black) HOPG surface after 2 minutes steam treatment.

To further confirm our hypothesis that the water layer stays on HOPG surface for an extended period of time even at r.t., we conducted temporal ATR-FTIR experiments on freshly exfoliated HOPG that was stored at low temperature for 10 minutes. Unlike the data shown in Figure 3.2, in this experiment, after the low temperature treatment, the HOPG sample was left in air at r.t. throughout the entire experiment period. As shown in Figure 3.8(a), instead of a substantial decrease in water peak (3100 - 3800 cm^{-1}) as one would expect for liquid phase water due to the desorption at r.t. (40% RH), the water film formed on graphitic surface only showed a slight increase during the 3 hours of ambient exposure, with a 15% monotonic increase of peak

intensity. It is interesting that the main peak (center at 3250 cm^{-1}) showed a red shift compared to normal liquid-like water (center at 3400 cm^{-1}), suggesting an ice-like structure with a hydrogen bonding network.[173] Considering that this ATR-FTIR experiment has been conducted at r.t. for several hours, such orderly structure is most likely stabilized by the strong H-bonding between chemisorbed water and HOPG surface.[58, 174] Other minor peaks (center at 3650 cm^{-1} and 3740 cm^{-1}) refer to dissociated water monomers that imply a possible structural unit during the water adsorption process. For example, Wang *et al.* reported the IR spectra of a water hexamer, which shows a similar O-H stretching vibration at 3740 cm^{-1}.[175] More recently, a "square ice" structure has been observed between two graphene sheets, indicating another 2D ice structure on graphitic surface.[99] These results indicate that the stable "ice-like" structure of the adsorbed water adlayers on HOPG is the key to significantly retarding hydrocarbon adsorption in air, even at room temperature.

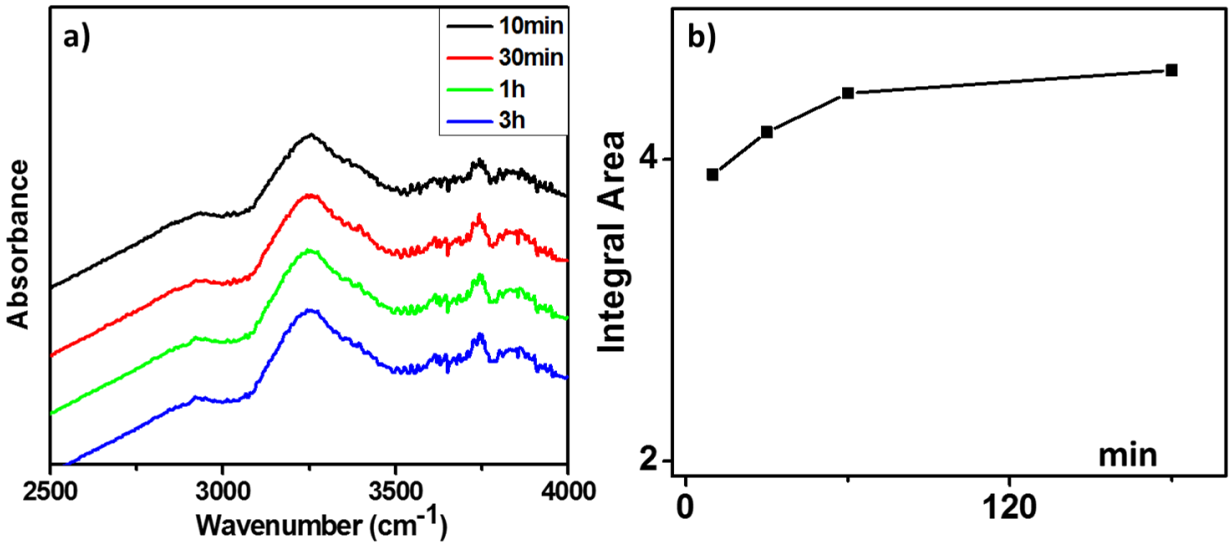

Figure 3-8 (a) ATR-FTIR spectrum of a freshly exfoliated HOPG sample after low temperature treatment. The sample was removed from low temperature at time 0; (b) The integrated peak area versus time for the peak at 3250 cm^{-1} (-OH stretching). Note that the spectra are plotted in absorbance mode and vertically shifted for clarity.

3.4.5 In-depth discussion

The study of low temperature storage of fresh graphitic surface is motivated by both fundamental and applied considerations. Although the protective role of water on metallic surface has long been proposed,[176] using this approach to protect graphitic surface from hydrocarbon contamination has not been discussed in the literature.

In the perspective of technology, although we did not expect the hydrocarbon contaminants attribute to any identifiable structure due to their complexities in species, such low temperature treatment indeed shows a universal suitability for different graphitic surfaces. Besides, a further advantage of the water-based protection is that this technique potentially generates only water as waste product, which can be easily removed via low temperature thermal annealing, UHV, or desiccant without affecting other surface properties of graphene/graphite. In contrast, other techniques targeting hydrocarbon removal (*e.g.*, high temperature thermal annealing, UV/O_3, etc.) often introduce defects onto the graphene/graphite surface.[157]

In addition, low temperature storage is also considered to be more advantageous over other alternative methodologies (*e.g.*, soaking in water) whereas graphitic surface is still covered with water. We note that direct soaking of fresh graphitic surface in liquid water will inevitably lead to secondary contamination since the solubility of typical hydrocarbons in water is still high in the context of surface contamination.[83] For example, the Nanopure water purification system (Thermo Scientific), one of the most popular purification system used in research laboratories, produces purified water with a total organic carbon (TOC) level between 5 – 10 ppb, similar to that of the hydrocarbon in ambient air. The condensation of water at low temperature makes it possible to produce a clean water film on graphitic surface. Indeed, to ensure the cleanliness of the water droplets during the WCA measurements, previous work also applied a stainless steel cold finger that was mounted vertically on the target surface for water drop condensation under a certain humidity level.[60]

In addition to being technologically relevant, it is also fundamentally important to understand the competing adsorption of water and hydrocarbon on graphitic surface. Our data shows that covering the graphitic surface with a (sub)monolayer of water can substantially reduce

the rate of hydrocarbon adsorption. The formation of this water monolayer requires a high relative humidity environment (*e.g.,* by lowering the temperature or using steam); surprisingly, once formed, the water monolayer persisted in low relative humidity environments (20-40%) for at least 2 hours.

Our ATR-FTIR data indicates that little water was adsorbed on HOPG when the sample was only exposed to lab air at room temperature (Figure 3.2(a)). As such, one would expect that the adsorbed water rapidly desorbs once the HOPG sample is removed from the low temperature environment. Surprisingly, this is not the case. According to our measurement (Figure 3.8(a)), the peak at 3250 cm^{-1}, which corresponds to surface adsorbed water, did not show any significant change in peak shape or intensity, indicating a relatively stable structure within at least a few hours. We speculate that there is a significant hysteresis in the formation and desorption of the 2D ice structure: such structure is thermodynamically unstable at r.t. and *ca.* 40% R.H.; however, once a full monolayer forms, the water molecules within the 2D ice structure are stabilized by multiple hydrogen bonds and therefore exhibits a high kinetic barrier for the desorption process.

3.4.6 Mechanism of reduced AHC adsorption.

We attribute the inhibition of the hydrocarbon adsorption on graphitic surface to water adlayers. During the low temperature storage, a much thicker water film consisting of both physisorbed and chemisorbed water molecules are expected to form on fresh graphitic surface. We also noted that a 5 nm thick water film has been reported on HOPG surface where it was exposed to ambient air at >90% relative humidity.[177-178] The presence of such water film on graphitic surface may significantly increase the van der Waals (vdW) interaction distance between hydrocarbon and

graphitic surface. The adsorption of hydrocarbon molecule on ice greatly depends on its partial pressure and the density of free surface -OH groups.[179] For a thermodynamically stable ice phase, it has been observed that the saturated coverage is within submonolayer to monolayer regime for a wide variety of small organic molecules (C2-C6 *n*-alcohols, acetone, acetic acid, etc.) between 200 – 240 K;[180-181] the surface coverage further decreases for hydrocarbons with longer alkyl chains or aromatic groups due to the lower vapor pressure and water solubility.[182-183] In all, the existence of an ice-like water film on graphitic surface will result in a drastic decrease of the overall hydrocarbon adsorption rate.

At much longer time scales, airborne hydrocarbons gradually replace the adsorbed water on the surface. This is expected because some of the airborne hydrocarbons may have much higher molecular weight than water and therefore their interaction with the surface is stronger than water. In addition, a large hydrocarbon molecule could displace several water molecules, resulting in a positive change of entropy. It has been reported by Hayashi *et al*.[184] that small molecules with low boiling point initially rapidly adsorb on the wafer surface. However, as the exposure time increases, the original surface adsorbate will be gradually replaced by competing adsorbate with much higher molecular weight and/or boiling point, an effect termed "fruit-basket phenomenon". Considering that airborne hydrocarbons have a higher boiling point than water, it is expected that the adsorbed water layer would eventually be replaced by airborne hydrocarbon. However, the existence of the adsorbed water layers significantly slows down the rate of this process, by a factor of *ca.* 4 – 6, according to our ellipsometry experiments.

3.5 CONCLUSION

Our study showed that storing freshly prepared graphitic surface at low temperature can greatly minimize hydrocarbon contamination and thus preserve its intrinsic wetting behavior. Ellipsometry and ATR-FTIR data indicates that a nanometer thick water film formed on the graphitic surface during the low temperature treatment. This thin water film remains a stable structure after a few hours of air exposure at room temperature and plays a vital role in slowing down the subsequent hydrocarbon adsorption. This new method offers a convenient solution to minimize hydrocarbon contaminants and may be useful in the surface modification of graphene and related device fabrication.

4.0 ENHANCED ROOM TEMPERATURE CORROSION OF COPPER IN THE PRESENCE OF GRAPHENE

4.1 CHAPTER PREFACE

Materials contained in this chapter were published as a research article in *ACS Nano*; figures used in this chapter have been reprinted with permission from: *ACS Nano*. **2013**, 7, 6939-6947 (listed as reference 205 in bibliography section).

List of Authors: Feng Zhou*, Zhiting Li*, Ganesh J. Shenoy, Lei Li and Haitao Liu.

Author Contributions: F.Z., Z.L., and H.L. designed and directed the experiments. F.Z., Z.L., G.S., conducted the experiments. All authors discussed the results. H.L. wrote the manuscript with input from all authors.

4.2 INTRODUCTION

Graphene has captured great interests from engineers for one of the most effective and thinnest protective layer against atmospheric corrosions.[68, 71, 73-78] Such anti-corrosion performance of graphene film is intimately related not only to the protection of microscale devices, but also to the "bottleneck" of industrial anticorrosion for all the steel-based constructions and transportations. From previous investigations, the protection behavior of graphene can be understood by its unique physical and chemical properties. That is, such two-dimensional monolayer structure can form a physical separation barrier on substrate surface, preventing further directing interaction between protected metal and ambient oxygen. For example, Ruoff, Park, and coworkers first reported that a chemical vapor deposition (CVD) grown graphene can effectively protect Cu and Cu/Ni alloys from thermal oxidation in air at 200°C for 4 hours and wet oxidation by 30% H_2O_2 within 2 min.[71] In a closely related study, Nayak *et al.* reported similar anti-corrosion effect of CVD-grown multi-layer graphene for the thermal (500°C for 3 hrs) and wet chemical (31% H_2O_2, 2 hrs) oxidation of Ni.[69]

Generally speaking, the oxidation kinetics of graphene coated surface is dominated by two factors, that is, the diffusion rate of oxidation agents (*e.g.*, O_2 and H_2O_2) and their reaction with the metal. Among the aforementioned literature, we noted that the anti-corrosion behavior of graphene were mostly observed under very harsh conditions (*e.g.*, 300^{o}C and H_2O_2 treatment) over a relatively short time scale, typically several minutes to several hours. Under these conditions, the diffusion of oxidation agents (*e.g.*, O_2 and H_2O_2) is expected to be the rate-limiting step of the overall corrosion process.[1-4]

Our study of graphene over a long-term oxidation process is motivated by both practical and fundamental considerations. For example, many technologically relevant corrosion processes (*e.g.*, steel corrosion) occur at room temperature but over a relatively long time scale, from months to years. Under such conditions, the overall corrosion kinetics could be dominated by the reaction between the metal and the oxidation agent; as a result, the slower diffusion of oxidation agent through an anti-corrosion coating may not help to slow down the overall corrosion process. More importantly, electrochemical oxidation plays a significant role for the low temperature corrosion of metals. It is very well established that the presence of impurities, including graphitic materials, on metal surface could enhance its galvanic corrosion by serving as an electrode for oxygen reduction.[185-187] Given these considerations, it is not clear if graphene can serve as an effective anti-corrosion coating for the long-term protection of metals.

In this work, we show that a CVD-grown graphene coating accelerates the room temperature, long-term oxidation of copper. By using a combination of Raman spectroscopy, XPS, and energy-dispersive X-ray spectroscopy (EDX), we show that copper is oxidized faster in the presence of a graphene coating than in its absence. Furthermore, the oxidation is not spatially homogenous; instead, it occurs in micron-sized domains surrounded by areas having minimal oxidation. Our observation suggests that graphene promotes electrochemical corrosion of copper at room temperature.

4.3 EXPERIMENTAL SECTION

4.3.1 Optical Microscopy

Optical microscope imaging of the copper surface was conducted using a Olympus BH2-UMA in reflectance mode with a Moticam 2000 2.0M Pixel camera or a Nikon Eclipse Ti – U in reflectance mode with an Ample Scientific 3.0M Pixel camera.

4.3.2 EDX

A Philips XL-30 SEM was used to carry out EDX analysis of aged copper/graphene and annealed copper samples to provide oxygen ratio under the same condition. EDX was performed with an acceleration voltage of 10 kV and a working distance of 10 mm.

A JOEL JSM6510LV SEM was used for imaging and EDX analysis shown in Figure 4.4(a). EDX was performed with an acceleration voltage of 20 kV and a working distance of 10 mm.

Note:

Synthesis of single-layer graphene on copper foil: see experimental details in 2.3.1

Annealed copper foil (without graphene coating): this sample was prepared by subjecting a copper foil to the same condition above except no CH_4 gas flow was introduced

4.4 RESULTS AND DISCUSSION

In our experiment, we studied the oxidation of copper in two types of samples over a timeframe of 6 months: a single layer graphene coated copper foil (graphene/copper sample or graphene-coated sample) and a H_2-annealed copper foil (annealed copper sample or uncoated sample).

4.4.1 Short term anti-corrosion effect of graphene.

Anti-corrosion effect of graphene by heating copper/graphene in ambient air at high temperature was reported in literature.[67] To study the short-term effect, we repeated this experiment by heating bare Cu foil and copper/graphene in air under 250^{o}C for 20min. Figure 4.1 shows the OM images of both bare Cu and copper/graphene after thermal annealing, respectively. Annealing of bare Cu led to a loss of its metallic luster and a drastic color change to grey and black, which was attributed to the formation of oxides on its surface.[71] In contrast, copper/graphene sample following the same procedure was not severely oxidized, still showing similar metallic luster as bare Cu foil. Such observations verify prior experimental results and demonstrated that graphene coating can effectively prevent atmospheric oxidation at high temperature over a short term.

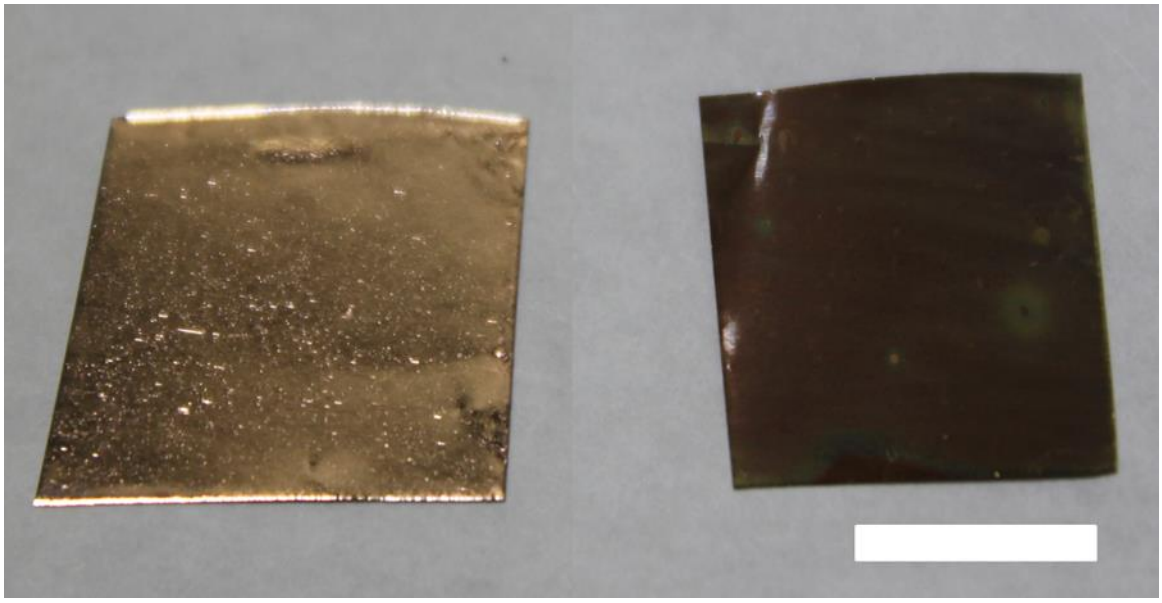

Figure 4-1 Photograph of (left) a copper/graphene sample and (right) an as-received copper foil after heating both in air at 250°C for 20 min. The scale bar represents 1 cm.

4.4.2 Long term anti-corrosion effect of graphene

During the long term atmospheric oxidation process at room temperature (*ca.* 21°C), we exposed both bare copper foil and copper/graphene film in ambient air for up to 6 months. To investigate its surface morphology change, we conducted the same OM comparison between copper and copper/graphene samples. For bare copper sample, copper foil was firstly thermal annealed in H_2 under 1000°C for 30 min to get rid of possible contaminations. As shown in Figure 4.2(a) and (d), both freshly prepared copper and copper/graphene samples (<1 day) showed a homogeneous yellow color under an optical microscope, suggesting a characteristic copper cluster color without

any visible CuO/Cu_2O induced by oxidation.

After 6 months of ambient exposure, the annealed copper showed almost no color contrast to the naked eye and the surface morphology change was hardly distinguishable under optical microscope. Under a high resolution optical image (Figure 4.2(f)), only small patches of red area can be observed and many millimeter sized patches in deep-brown color covering almost the whole copper surface. In contrast, the copper/graphene sample developed many millimeter sized patches in deep-brown, red, or yellow colors (Figure 4.2(b) inset). Under the magnified optical microscope (Figure 4.2(c)), most (~ 90%) of these patches appeared to be red when recorded on a digital camera; a small percentage (~10%) of the patches appeared to be yellow. It is noted that the color contrast on copper surface is indicative of different oxidation status of copper, *i.e.*, patches with deeper color probably has higher density of Cu oxide. In this regard, copper was oxidized faster at room temperature in the presence of graphene than in its absence.

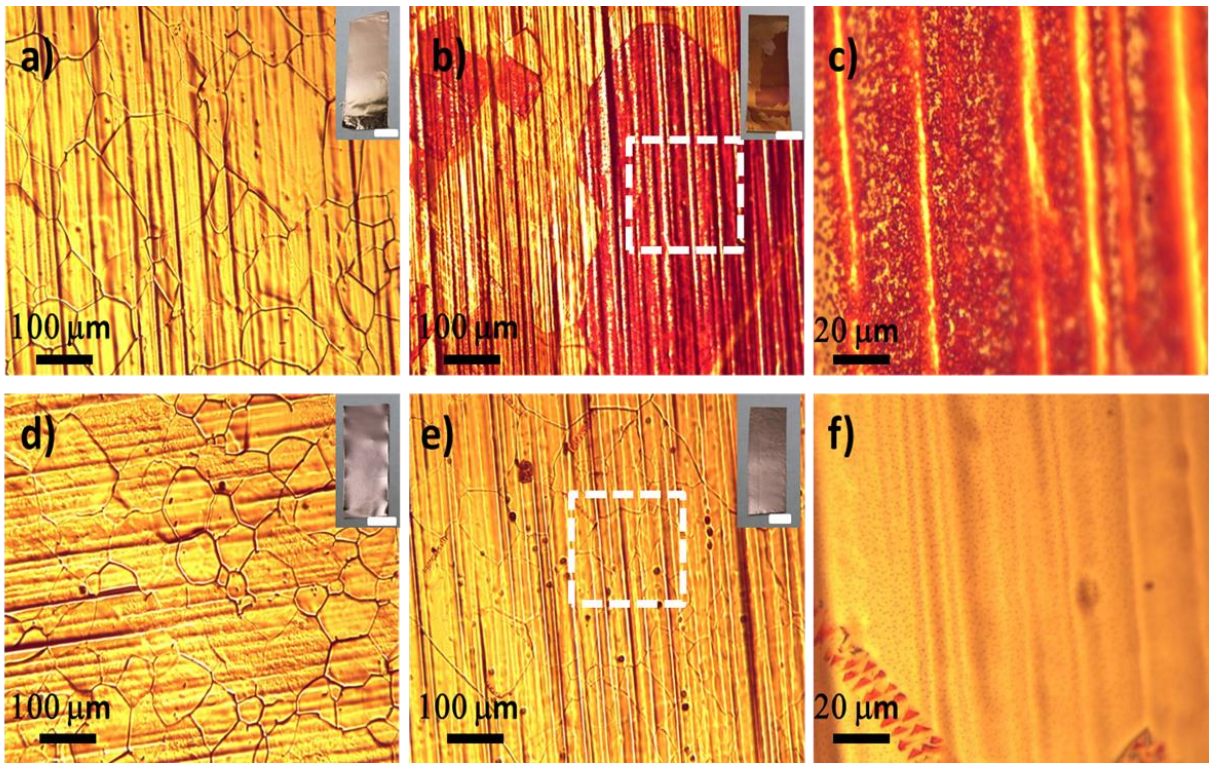

Figure 4-2 Optical micrographs of (a) an as-prepared copper/graphene sample, (b) a 6-month-aged copper/graphene sample, (d) an as-prepared annealed Cu foil, and (e) a 6-month-aged annealed Cu foil. (c) and (f) are magnified optical images of the dashed area in (b) and (e), respectively. Inset in (a), (b), (d), and (e) show the photograph of the respective samples. Scale bars in the insets represent 1 cm.

4.4.3 Quantification of oxidation degree

To quantify the degree of oxidation of the two 6-month aged samples, we carried out XPS, Raman and EDX analysis on both samples. The result confirms that graphene-coated sample indeed underwent more severe oxidation than the non-coated one.

XPS tests were conducted on both annealed copper foil and copper/graphene sample surface, respectively. Figure 4.3 shows the XPS spectra over the binding energy range 920-980 eV of thermal annealed copper and copper/graphene sample. Differentiation between CuO and Cu/Cu_2O is usually recognized by two strong shake-up satellites at ~ 6 and 8 eV higher binding energy than principal Cu $2p_{3/2}$ and $2p_{1/2}$ peaks.[188] After 6 months exposure in ambient air, annealed copper exhibiting broader $2p_{3/2}$ peak (933.6 eV) and $2p_{1/2}$ peak (953.2 eV) together with intense satellite peaks at 943.2 and 961.2 eV indicated the formation of CuO on Cu surface. The absence of shake-up satellites on aged copper/graphene sample excluded the existence of CuO as oxidative product on copper/graphene surface. Further analysis by peak deconvolution showed that the atom% of Cu(II) on the surface was 6% on the 6-month-aged coated copper foil and 37% for the uncoated one. Although XPS allows quantitative characterization of CuO and indicates a higher density of CuO on aged copper surface, such XPS results cannot provide unambiguous conclusion that annealed copper undergoes more severe oxidation in ambient air.[188-193] Firstly, the amount of Cu_2O (I), another oxidative product during ambient corrosion, can hardly be distinguished by XPS due to the similar chemical shift in Cu (2p) lines between Cu (0) and Cu (I) at 932.5 eV BE. [189] It has been reported that exposure of copper surface to oxygen at 300 K for 30 min results in a thin layer of Cu_2O as the main oxidative product.[194] Furthermore, with detecting depth limited to ~ 10 nm, XPS characterization does not always represent the full range of oxidation on Cu surface.

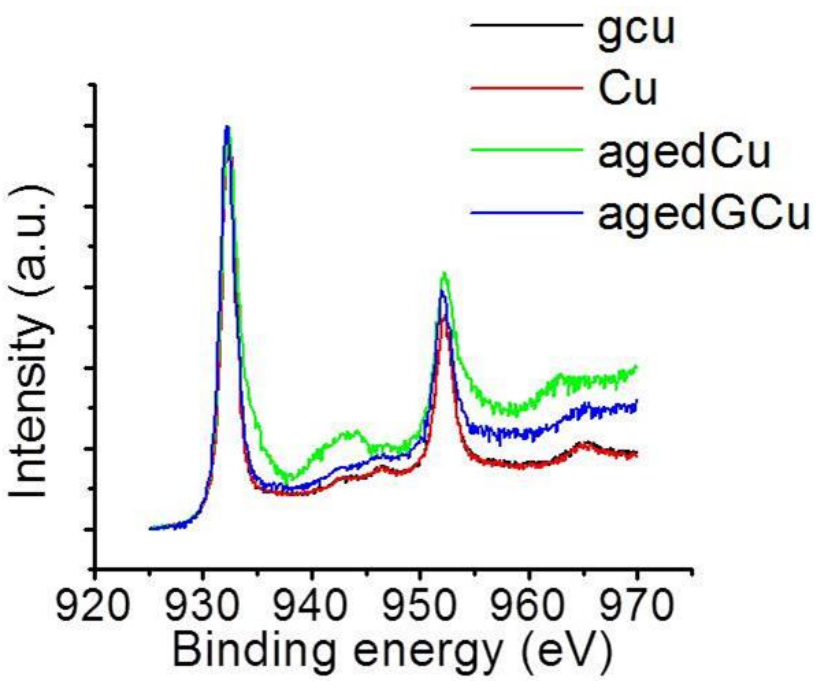

Figure 4-3 Normalized XPS spectra of fresh and 6-month-aged copper foil with and without graphene coating. Note: the spectra of two fresh samples (red and black curves) overlap.

To quantify the degree of oxidation of the two 6-month aged samples, we carried out EDX and Raman analysis on both samples. The result confirmed that graphene-coated sample indeed underwent more severe oxidation than the non-coated one. In the case of EDX analysis, we collected EDX spectrum from the red-colored regions of a 6-month-aged copper/graphene and the yellow-colored region of 6-month-aged annealed Cu sample. As shown in Figure 4.4(a), the average O : Cu atom ratio, obtained from several of such spectra, were 1 : 17 and 1 : 13 for aged annealed Cu and aged graphene/copper sample, respectively. Note that EDX probes *ca.* 1 μm thick of sample within the surface.[195] Therefore, it can probe both copper oxides on the surface and the

underneath Cu unless the thickness of oxide layer is significantly larger than 1 μm.

The Raman spectra of Cu_2O and CuO are significantly different in terms of Raman shift and allow quantitative characterization of both components. Given that the peak intensity is in proportion to the density of copper oxide, the relative density of CuO and Cu_2O can thus be determined by ratioing peak intensities at two different Raman shifts.[192, 196-198] However, there is considerable variation in the literature of the Raman shift quoted for CuO and Cu_2O which makes the comparison with a standard literature value is difficult. To account for this, we thermal annealed bare copper foil at 200ºC for 1h and then took Raman on this sample as reference. As shown in Figure 4.4(b), for bare copper after thermal annealing, 3 major peaks are observed in the range of 200 – 800 cm^{-1}, attributed to the formation of Cu_2O (210, 640 cm^{-1}) and CuO (300 cm^{-1}), respectively. In this respect, it is interesting to note that aged copper/graphene displayed strong Cu_2O peaks around 210 and 640 cm^{-1}. The broadened peak centered at 620 cm^{-1} showed signs of several Cu_2O-related sub-peaks (550, 618, 624 cm^{-1}).[192] In contrast, the Raman spectra of thermal annealed copper in the range of 200 – 800 cm^{-1} was barely detectable, indicating much less copper oxide producing during ambient corrosion. To quantify the oxidation degree based on Raman peak intensity, one can estimate the relative ratio of copper oxide between annealed copper and copper/graphene after 6 months ambient corrosion is 1:40. This verified prior OM results, which showed copper/graphene undergoes more intensive oxidation than bare copper after 2 weeks exposure in ambient air.

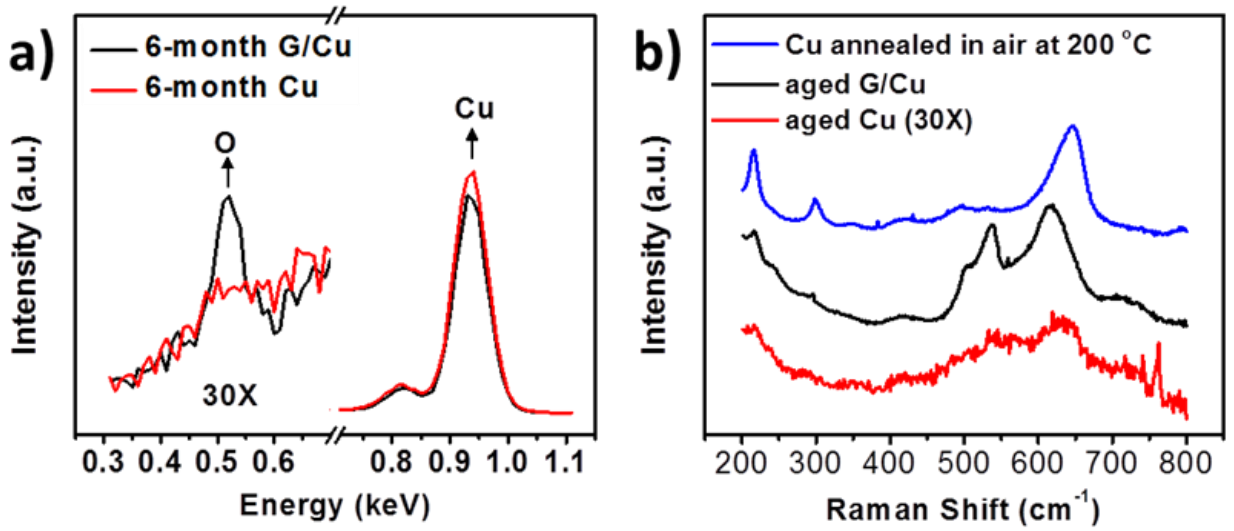

Figure 4-4 (a) Typical EDX spectra of 6-months-aged copper/graphene (black) and 6-months-aged annealed copper (red) from 0.3 to 1.1 keV. Note that the spectra from 0.3 to 0.7 keV of both samples have been magnified by 30 times. (b) Typical Raman spectra of Cu foil annealed at 220°C for 15 min, 6-months-aged copper/graphene (black) and annealed copper (red) from 200 to 800 cm^{-1}. Note that the spectrum of annealed copper has been magnified by 30 times. For both a) and b), the data were taken from red-colored area (90% of the surface) for graphene/copper sample and from yellow-colored area (99% of the surface) for annealed copper sample.

4.4.4 Effect of graphene defect and water

To explain the enhanced oxidation behavior of graphene covered copper surface, we discussed the effect of defect sites, oxygen and water during the ambient oxidation process.

Quality of graphene. We observed that the graphene film developed significant defects after 6 months of storage in air at room temperature. Shown in Figure 4.5(a), the copper/graphene sample exhibited negligible defect peak when freshly prepared. However, the Raman spectrum of the 6-month-aged sample showed a strong D peak, with an I_D/I_G ratio of 1.3. Although the formation of D peak indicates a moderate to severe damage on graphene surface during the 6 months ambient oxidation, however, it cannot be conversely concluded that the defect sites also promote the oxidation of underlying copper substrate. In fact, spectra collected from both red and yellow regions (Figure 4.5(b)) showed similar I_D/I_G ratio, suggesting that there is lack of direct correlation between graphene defect sites and copper oxidation degree. This fact suggests that atomic level defects in graphene, although could lead to enhanced oxidation of underlying copper substrate at high temperature,[77] may not necessarily do so at low temperature.

Another interesting observation was that the absolute Raman peak intensity of the yellow region is substantially lower than that of the red region, in some cases by a factor of almost 20. This difference in Raman intensity can be explained by the difference in oxide thickness in the two regions: in the absence of a thick oxide layer, the graphene film is in close contact with copper metal; as a result the graphene will experience a much reduced electric field of the incident laser beam and give a weak Raman response.[199]

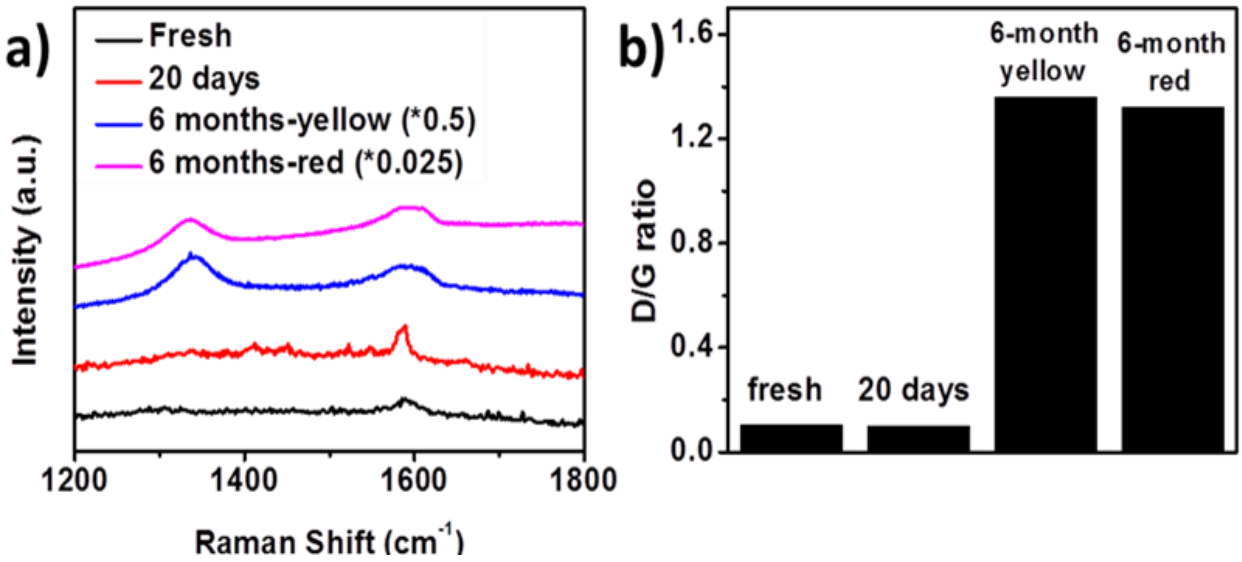

Figure 4-5 (a) Raman spectra (1200 – 1800 cm^{-1}) of copper/graphene samples at different air-exposure times: freshly prepared, 20 days exposure, and 6 months exposure. For 6-month-aged sample, the spectra were taken on both yellow and red regions; the intensity of these two spectra has been scaled by a factor of 1/2 (yellow region) or 1/40 (red region). (b) I_D/I_G ratio of spectra in (a).

Although the defect of graphene does not dominate the oxidation of copper during oxidation, conversely, the oxidation of copper strongly promotes the mechanical breakage of surface covered graphene film. In our experiment, we found that graphene developed significant mechanical damage in areas having severe Cu oxidation. Shown in Figure 4.6, we transferred the graphene from a 6-month aged copper/graphene sample to a silicon wafer using PMMA as the transferring agent. The PMMA was then removed by a thermal annealing at 410 °C under low-pressure (~ 50 mTorr) for 1 hour. The optical micrographs showed that the graphene covering the severely

oxidized copper (red region) broke into micron sized patches. In contrast, the graphene covering the less oxidized copper (yellow region) remained as a continuous film. The breakage of graphene can also be confirmed by Raman since graphene on the non-breakage area shows *ca.* 20 times stronger Raman peak intensity compared to that on breakage area (Figure 4.6(c-d)).

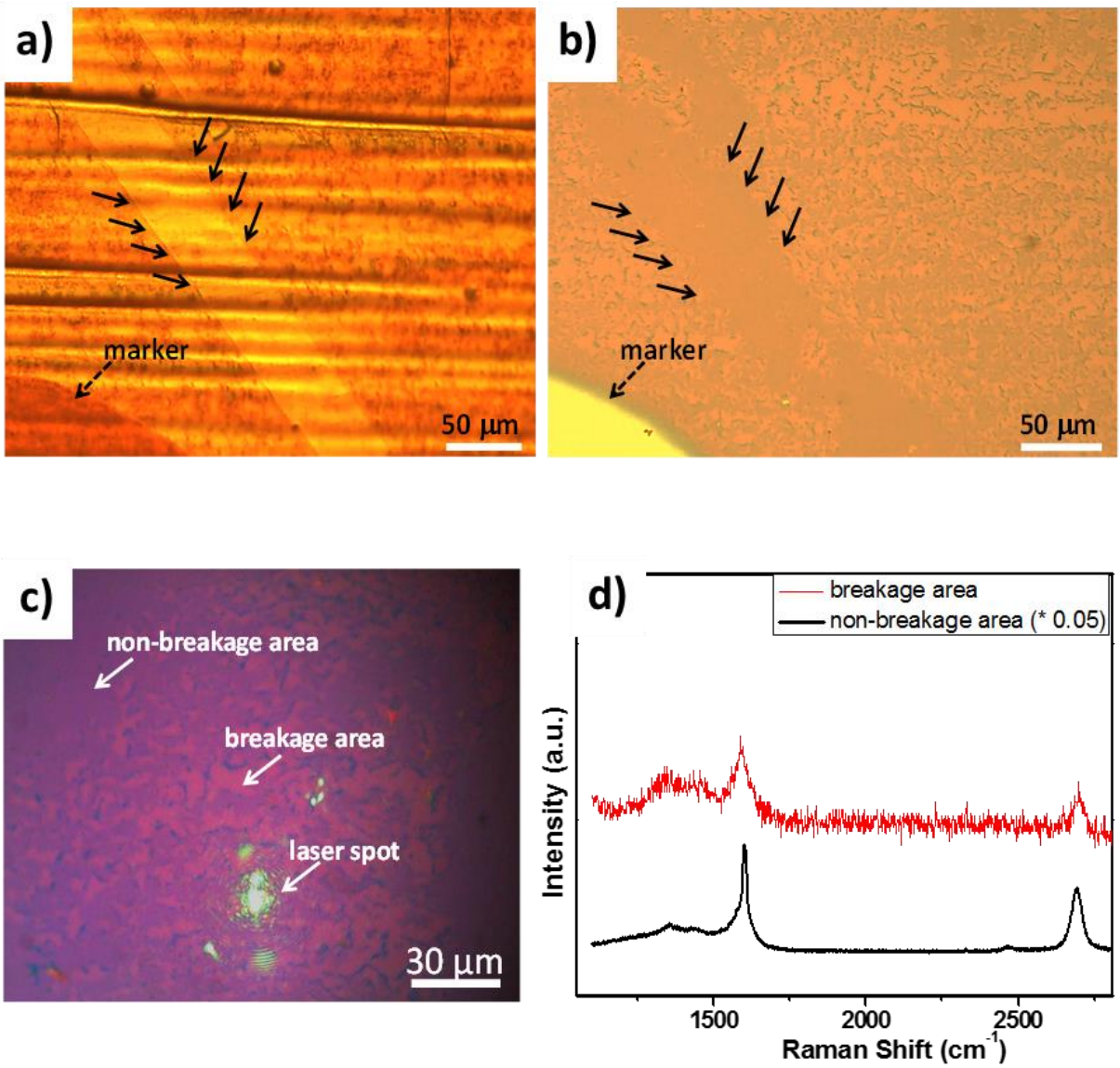

Figure 4-6 Optical micrograph of the same area of (a) a 6-months-aged copper/graphene sample and (b) after transferring the graphene to a silicon wafer. (c) Higher magnification image showing the breakage of graphene in the areas having severe Cu oxidation while no such breakage was observed in areas having minimal Cu oxidation. (d) Raman spectrum taken from the two areas of graphene shown in (c).

Water effect We also investigate the effect of humidity on the oxidation of graphene coated surface. As we mentioned above, the diffusion rate of oxygen on copper surface is on longer the dominant factor that determines the overall oxidation rate. Instead, the reaction between oxygen and copper is the rate determining step. Given that the relative humidity in our lab ranges from 40-60%, it is highly possible that water might assist the oxidation of copper during ambient exposure.

To study the effect of water, we compared the oxidation of three pieces of copper with (without) graphene coated, respectively. As shown in Figure 4.7, a copper/graphene sample stored in a closed vial inside a desiccator for 1 year showed less oxidation than a similar sample stored in air for 6 months. This observation is consistent with the well-known notion that reduced exposure to ambient moisture and salt aerosol slows down the electrochemical corrosion process.[200]

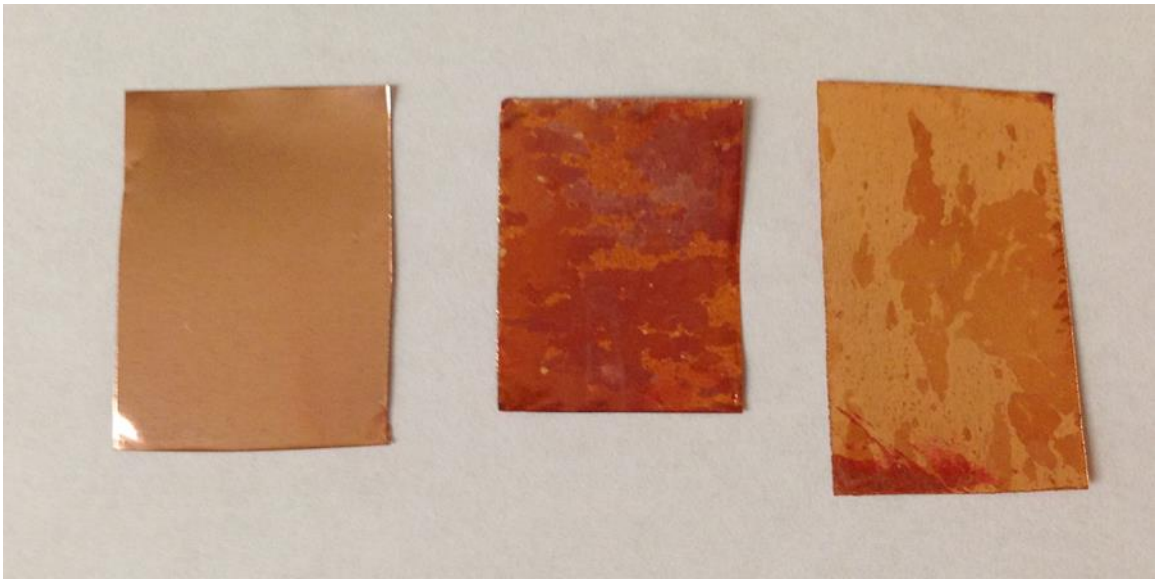

Figure 4-7 From left to right: a 6-months-aged annealed copper sample, a 6-months-aged copper/graphene sample, and a copper/graphene sample stored in a closed vial inside a desiccator for 1 year followed by 3 weeks of exposure in ambient air.

4.4.5 Proposed mechanism of corrosion-promotion effect of graphene

We attribute the corrosion-promotion effect of graphene to its high electrical conductivity. To understand this effect, we consider the following three key steps during the electrochemical corrosion of copper on a model surface that consists of a metallic copper substrate and a thin layer of native Cu_2O (Figure 4.8):

(1) Electrochemical oxidation of Cu^0 to Cu^+. This process occurs at the Cu/Cu_2O interface. The oxidation produces a free electron and a Cu^+ ion that diffuses into the Cu_2O lattice.

(2) Migration of Cu^+ and charge from Cu/Cu_2O interface to Cu_2O/air interface. The electron and Cu^+ generated in step (1) diffuse through the Cu_2O film to the Cu_2O/ air interface, driven by the charge and ion gradient within the oxide film. It was suggested that the charge and ion migration occurred though hole transfer and cation vacancy diffusion, respectively.[201]

(3) Electrochemical reduction of O_2. This process occurs at the Cu_2O/air or Cu_2O/graphene/air interface. The reduction of O_2 requires a reducing agent and produces O^{2-} as the product. The electrochemically generated O^{2-} then incorporates into the Cu_2O lattice and combines with the incoming Cu^+ ion to form Cu_2O. A reducing agent, either free electron or Cu^+, is required for the reduction of O_2.

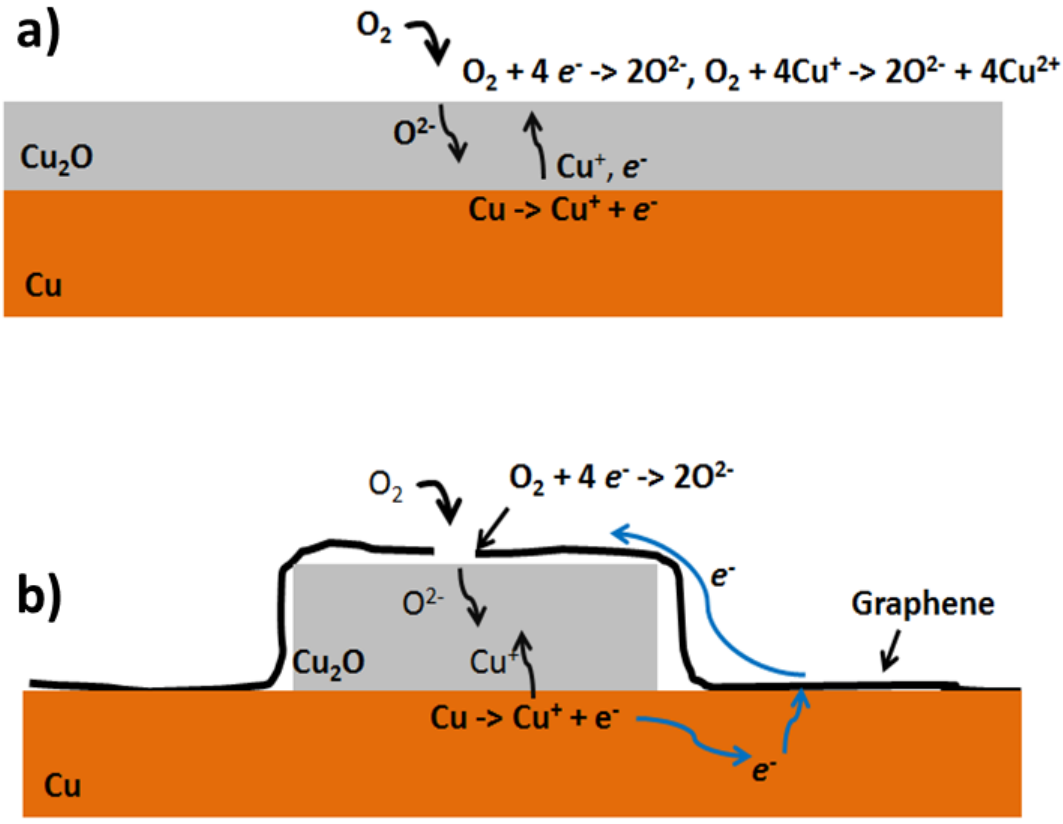

Figure 4-8 Electrochemical oxidation of copper in the (a) absence and (b) presence of a graphene film.

In the absence of a graphene coating, the electrons generated in step (1) need to migrate through the Cu_2O film to the Cu_2O/air interface. Cu_2O is a semiconductor with a band gap of *ca.* 2.0 eV[202] and its resistivity can be as high as 10^{13} Ω·m.[203] The fact that there was significant concentration (37% by atom%) of Cu^{2+} on the surface of 6-month-aged uncoated copper sample indicates that electrochemical reduction of O_2 was to some degree accompanied by the oxidation

of Cu^{+} to Cu^{2+}, implying that the charge migration of step (2) is slow relative to the electrochemical reduction of O_2.

In the presence of a graphene coating, the electrons generated in step (1) could be rapidly transported to the Cu_2O/graphene/air interface for O_2 reduction. In this case, O_2 likely diffuses through the cracks and defects in graphene to the Cu_2O surface. Because the overall copper oxidation is spatially inhomogeneous, as long as there is still some local electrical contact between graphene and copper, electrons can easily migrate from copper to graphene, therefore enhancing the corrosion. Consistent with our proposed mechanism, we note that the surface concentration (6%) of Cu^{2+} on the aged graphene-coated copper is much lower than that of the aged copper foil. This observation is consistent with the improved availability of free electrons for O_2 reduction in the presence of graphene.

4.5 CONCLUSION

Our study confirmed that graphene is a corrosion protector for short term oxidation under aggressive chemical environments. However, graphene also promotes the long-term, room temperature oxidation of copper. The corrosion enhancement effect of graphene is attributed to its conductive nature, which enhances the electrochemical corrosion process. Our study calls for a clear understanding of the mechanism of metal corrosion in the presence of graphene in order to enhance its long-term performance as an atomically-thin anti-corrosion coating.

5.0 COPPER SUBSTRATE AS A CATALYST FOR THE OXIDATION OF CHEMICAL VAPOR DEPOSITION GROWN GRAPHENE

5.1 CHAPTER PREFACE

Materials contained in this chapter were published as a research article in *Journal of Solid State Chemistry*; figures used in this chapter have been reprinted with permission from: *Journal of Solid State Chemistry* **2014**, *224*, 14-20 (listed as reference 204 in bibliography section). Copyright 2014 © Elsevier.[204]

List of Authors: Zhiting Li*, Feng Zhou*, David Parobek, Ganesh J. Shenoy, Patrick Muldoon, and Haitao Liu.

Author Contributions: Z.L., and H.L. designed and directed the experiments. Z.L., F.Z., D.P., G.S., and P.M. conducted the experiments. All authors discussed the results. Z.L. and H.L. co-wrote the manuscript with input from all authors.

5.2 INTRODUCTION

The copper-catalyzed CVD growth of graphene is considered to be most advantageous in terms of high quality, controlled thickness, easy transferability and low cost.[125-128] Given its importance, a complete understanding of the interaction between graphene and the underlying copper substrate is highly desirable for both fundamental and applicable considerations.[23, 205] Among the many aspects of copper-graphene interaction studies, a substantial portion was devoted to understand the effect of copper surface during the CVD growth of single layer graphene. However, investigations on the post-storage of as-prepared copper/graphene samples have lagged behind, mainly due to the fact that graphene grown on copper are mostly defect-free with much strong oxidation resistance even at high temperature. In this regard, simply storing copper/graphene samples in ambient oxygen has not been previously considered to affect the follow-up characterization and fabrication process, whereas this empirical behavior has never been experimentally confirmed.

Although the activation energy barrier for graphene-oxygen reaction is proved to be very high both experimentally and theoretically, one essential factor may not be ignored in this case: the underlying copper substrate may facilitate the oxidative reaction occurring on graphene surface.[206-209] In fact, several investigations have been carried out into the copper-catalyzed oxidation of graphite since 1970s. For example, McKee *et al.* reported that both the ignition temperature and activation energy for graphite-oxygen reaction decreased from 740ºC (54 kcal/mol) to 600ºC (34 kcal/mol) with very small addition of Cu (<0.3 wt.%).[208] In their experiments, a copper salt solution was used as the metal source, which produced copper oxide particles 1 - 5 μm in size during the catalytic oxidation process. These particles moved rapidly

above 600°C and cut channels on the graphite surface by reacting with graphite:

$$CuO + C \longrightarrow Cu + CO$$

These studies suggested that the underlying copper substrate may facilitate the oxidation of graphene surface. However, to the best of our knowledge, the copper catalyzed oxidation of graphene has not been systematically investigated.

Compared to the copper-catalyzed oxidation of graphite, the copper foil supported graphene is quite different in many ways. On one hand, all carbon atoms on graphene surface are in direct contact with the underlying copper substrate, which could result in a significant enhancement of the catalytic efficiency. On the other hand, unlike graphite surface, which has substantial amount of step edges acting as reactive center,[206] graphene grown on a copper foil is mostly defect-free without almost no step edge. In addition, the fact that graphene covers the copper substrate may suggest the absence of any catalytic effect of copper. Given these considerations, it is difficult to predict whether the graphene-oxygen reaction can be enhanced by the underlying copper substrate.

Herein, we report our studies on the effect of copper substrate during the thermal annealing of copper/graphene sample in high purity Ar having tracing amount of O_2. Graphene on copper substrate undergoes a complete oxidation at 600°C within 2 hours in the presence of < 3 ppm of O_2. The reaction was characterized by Raman, X-ray photoelectron spectroscopy XPS, and Auger electron spectroscopy (AES). Our results suggest that ambient oxygen can diffuse into the interlayer of copper/graphene upon air exposure, resulting in the formation of copper oxide which catalyzes the graphene-oxygen reaction at high temperature.

5.3 EXPERIMENTAL SECTION

5.3.1 Thermal annealing of copper/graphene sample.

After CVD synthesis, a copper/graphene sample was taken out of tube furnace and exposed in air for 5 hours. The sample was then put back to the tube furnace under Ar (99.999%) flow at a flow rate of 1.5 L/min for 30 min to ensure removal of air in the chamber. The sample was then annealed at 600^{o}C in Ar for 2 hours, followed by a fast cooling process to room temperature before taken out of the chamber.

5.3.2 AES.

AES was performed on a Perkin Elmer 10-155 cylindrical Auger electron optics in the same UHV chamber as XPS, operated with an electron multiplier supply under 2-kV-mode. The spectra were collected using the same HSA with a bandpass of 50 eV for multiple scans (0.5 eV/step).

Note:

Synthesis of single-layer graphene on copper foil: see experimental details in 2.3.1

Synthesis of multi-layer graphene on Ni foil: see experimental details in 2.3.2

Graphene transferred onto different substrates.: see experimental details in 2.3.3

Optical Microscopy: see experimental details in 4.3.1

Raman Spectroscopy: see experimental details in 2.3.7

XPS: see experimental details in 2.3.6

5.4 RESULTS AND DISCUSSION

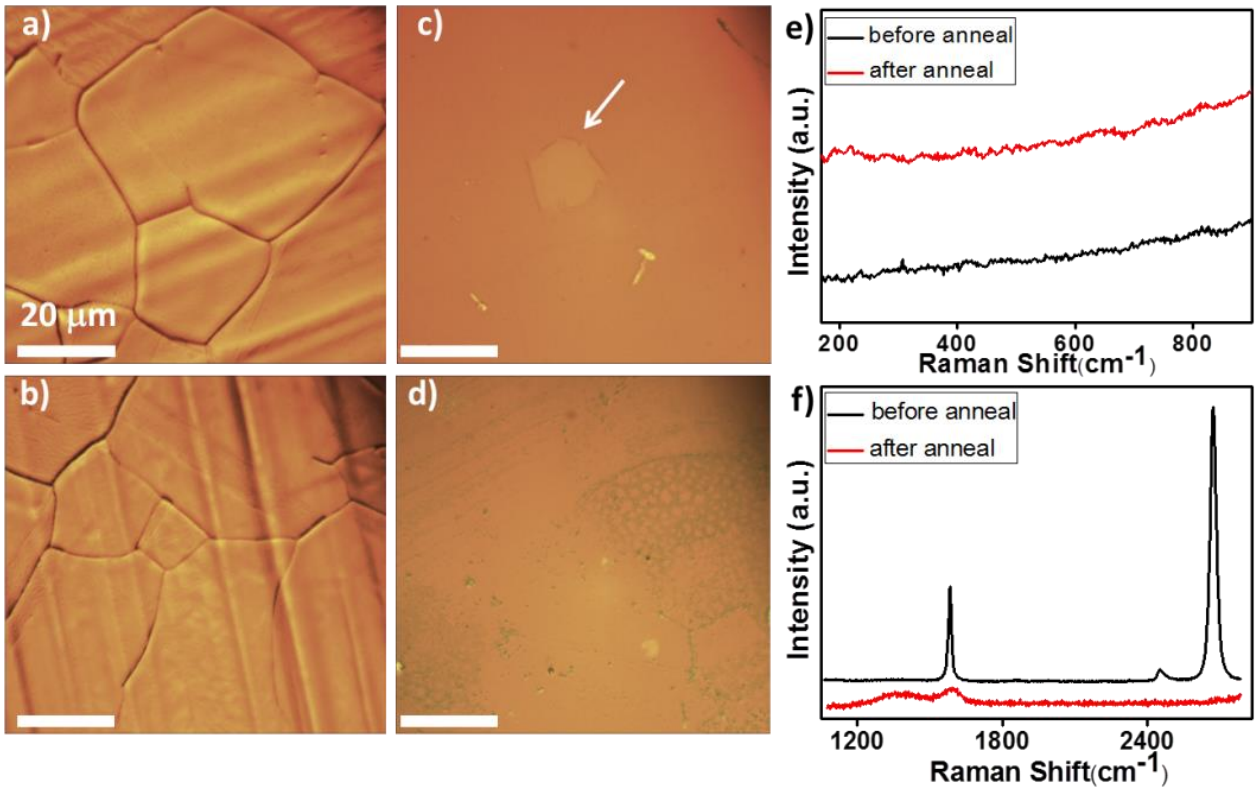

Figure 5-1 Optical micrographs of copper/graphene sample (a) before and (b) after thermal annealing in Ar under 600°C for 2 hours. (c) and (d) are optical images of graphene after it was transferred onto a SiO_2/Si substrate from (a) and (b), respectively. The arrow indicates a pinhole. (e) and (f) are typical Raman spectra taken on copper/graphene before (black) and after (red) thermal annealing.

5.4.1 Oxidation of copper-supported graphene

We firstly demonstrated that in the presence of trace amount of O_2, copper can act as an extremely active catalyst during the graphene-oxygen reaction above 600°C. In a typical experiment, we exposed a freshly prepared copper/graphene sample to air at room temperature for several hours and then annealed it in an Ar (99.999% purity, O_2 < 3 ppm, H_2O < 5 ppm) atmosphere at 600°C for 2 hours.

Figure 5.1(a) and (b) show the optical images of the same piece of copper/graphene sample before and after the thermal annealing. Both surfaces appeared to be bright yellow without pronounced color variation to the naked eye, indicating no extensive oxidation occurred on the copper surface after thermal annealing. The absence of extensive copper oxidation is further supported by micro-Raman spectroscopy, which has a detection limit of a few tens of nanometers.[210-211] As shown in Figure 5.1(e), Raman spectra were collected on the copper/graphene sample surface before (black) and after (red) the annealing. Neither Cu_2O (214 and 613 cm^{-1}) nor CuO (300 cm^{-1}) peak could be observed after the annealing.[212-213] However, it should be noted that the Raman intensity of a native metallic oxide could be weakened due to surface selection rule.[199] In this regard, the formation of native Cu_2O or CuO cannot be excluded from Raman spectroscopy results (see below).

In contrast to the negligible oxidation on copper, graphene demonstrated severe damage after thermal annealing in Ar atmosphere with trace amount of oxygen (< 3 ppm). Because graphene grown on copper surface could not be directly visualized under optical microscope, we transferred graphene film onto silicon substrate after thermal annealing. Shown in Figure 5.1(c) and (d) are the optical images of transferred graphene film before and after annealing, respectively. An area of 1 cm x 1 cm has been surveyed to give an overall single layer graphene coverage of >

99% before thermal annealing. The surface coverage of graphene decreased to < 5% after 2 hours of annealing in the Ar atmosphere. Further inspection using micro-Raman spectroscopy is shown in Figure 5.1(f). Before the thermal annealing, the D peak (1360 cm^{-1}) was barely detectable, indicating the presence of high quality graphene with very low defect density. The ratio of 2D peak (2680 cm^{-1}) intensity to G peak (1580 cm^{-1}) intensity (I_{2D}/I_G) was 3.6, consistent with previously reported data for single layer graphene.[126] After 2 hours thermal annealing in Ar, all Raman peaks showed significant intensity decrease, reaffirming the oxidative removal of graphene. Additionally, the broadening of G peak width after annealing suggested that the sp^2 graphene structure degraded into more disordered amorphous C-C structure.[214-215] Overall, both the Raman spectra and the optical micrographs indicate that a copper-supported graphene was severely oxidized the presence of < 3 ppm of O_2 at 600°C.

It is noted that the room temperature air exposure before the high temperature treatment plays an important role in the oxidation of graphene. If the graphene/copper sample was subject to thermal annealing in Ar right after the synthesis and without any air exposure, it will take much longer time (> 4 hours) and higher temperature (> 700°C) to achieve a similar degree of oxidation (see below). This observation suggests that the residue oxygen (< 3 ppm) in the Ar contributes to the oxidation of graphene**.**

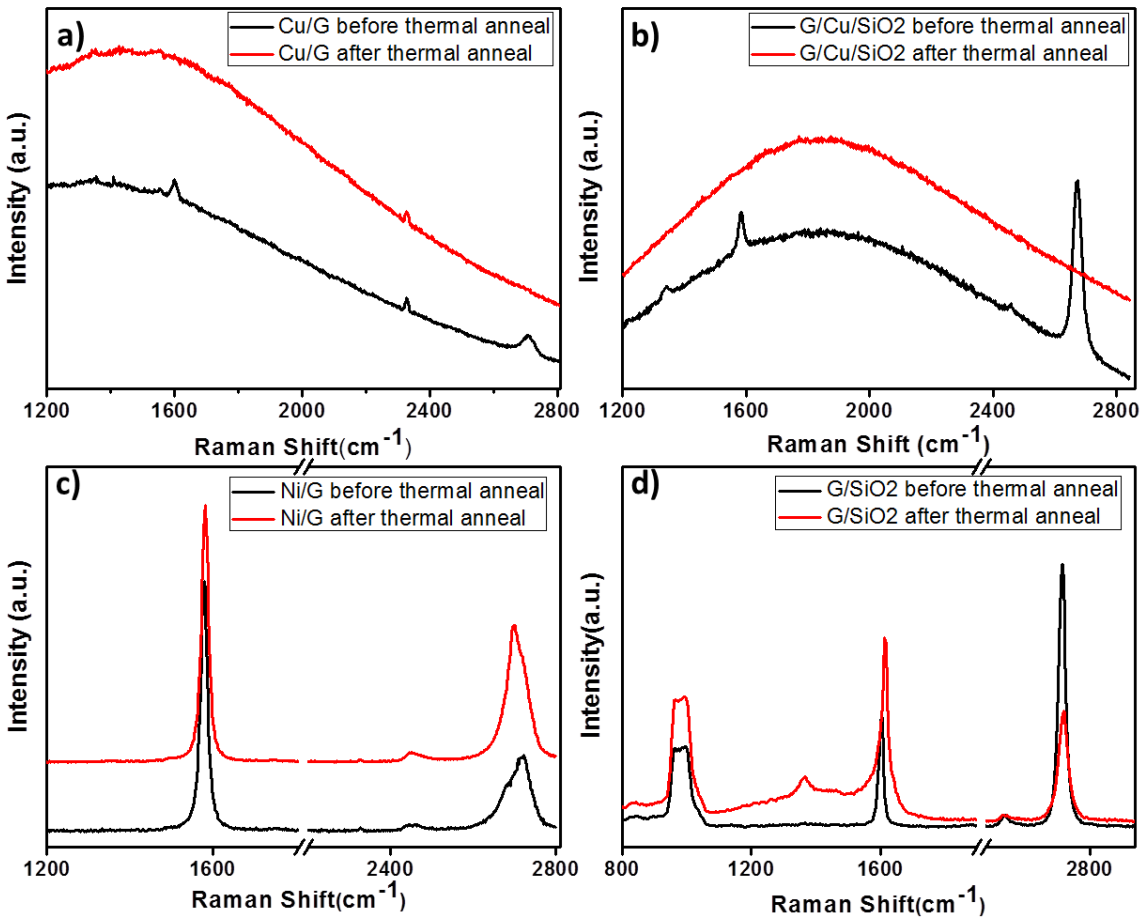

Figure 5-2 Raman spectra of graphene grown on (a) copper and (c) nickel, transferred onto (b) copper coated SiO_2/Si and (d) SiO_2/Si substrate before (black) and after (red) thermal annealing in Ar at 600°C for 2 hours, the integration time are 30 min for (a) and 1 min for (b), (c), and (d). Note: the small sharp peak around 2330 cm^{-1} in figure 2a is due to N_2 in air.

5.4.2 Catalytic effect of the copper substrate

Given that only a monolayer of graphene covered on copper surface, simply thermal annealing copper/graphene sample with oxygen gas in ppm level does not provide unambiguous conclusion that copper catalyzed the oxidation of graphene. In fact, during the 2 hours thermal annealing in Ar flow (1.5 L/min) at 600ºC, ~2.41 x 10^{-5} mol oxygen molecules will flow into the tube furnace compared to only ~1.72 x 10^{-9} mol carbon atoms located on 1 x 1 cm copper surface. Thus it is still possible that graphene has been directly reacted with ambient oxygen molecules in a non-catalytic process.

In order to confirm the catalytic behavior of copper in graphene-oxygen reaction above 600ºC, we conducted three additional control experiments to probe the role played by the substrate during the oxidation of graphene. We transferred CVD-grown single layer graphene onto silicon and copper coated silicon substrates, respectively. In addition, we prepared a multi-layer graphene sample grown on a Ni foil. All the three samples along with a copper/graphene sample were annealed in an Ar atmosphere at 600ºC for 2 hours. Raman spectra were taken on each sample before (black) and after (red) thermal annealing. As shown in Figure 5.2(a) and (b), both copper supported graphene samples showed a complete disappearance of G peak and 2D peak right after thermal annealing, indicating a drastic oxidative degradation of graphene on both copper surfaces. The small/sharp peak around 2350 cm^{-1} in Figure 5.2(a) attributed to N_2 molecule vibration in air. In contrast, graphene on Ni and silicon substrates still showed clear Raman characteristic peaks after annealing, with only slight blue shift of G peak position and decrease of 2D/G peak intensity ratio which we attribute to doping induced by the underlying substrates and/or adsorbed oxygen.[109, 216-219] The broadening of D peak and G peak region in Figure 5.2(d) is attributed to the

carbonization of airborne hydrocarbons during high temperature annealing.[220] Collectively, the substrate effect showed clear evidence that the underlying copper plays an active role in promoting the graphene-oxygen reactions in trace amount of oxygen at 600ºC.

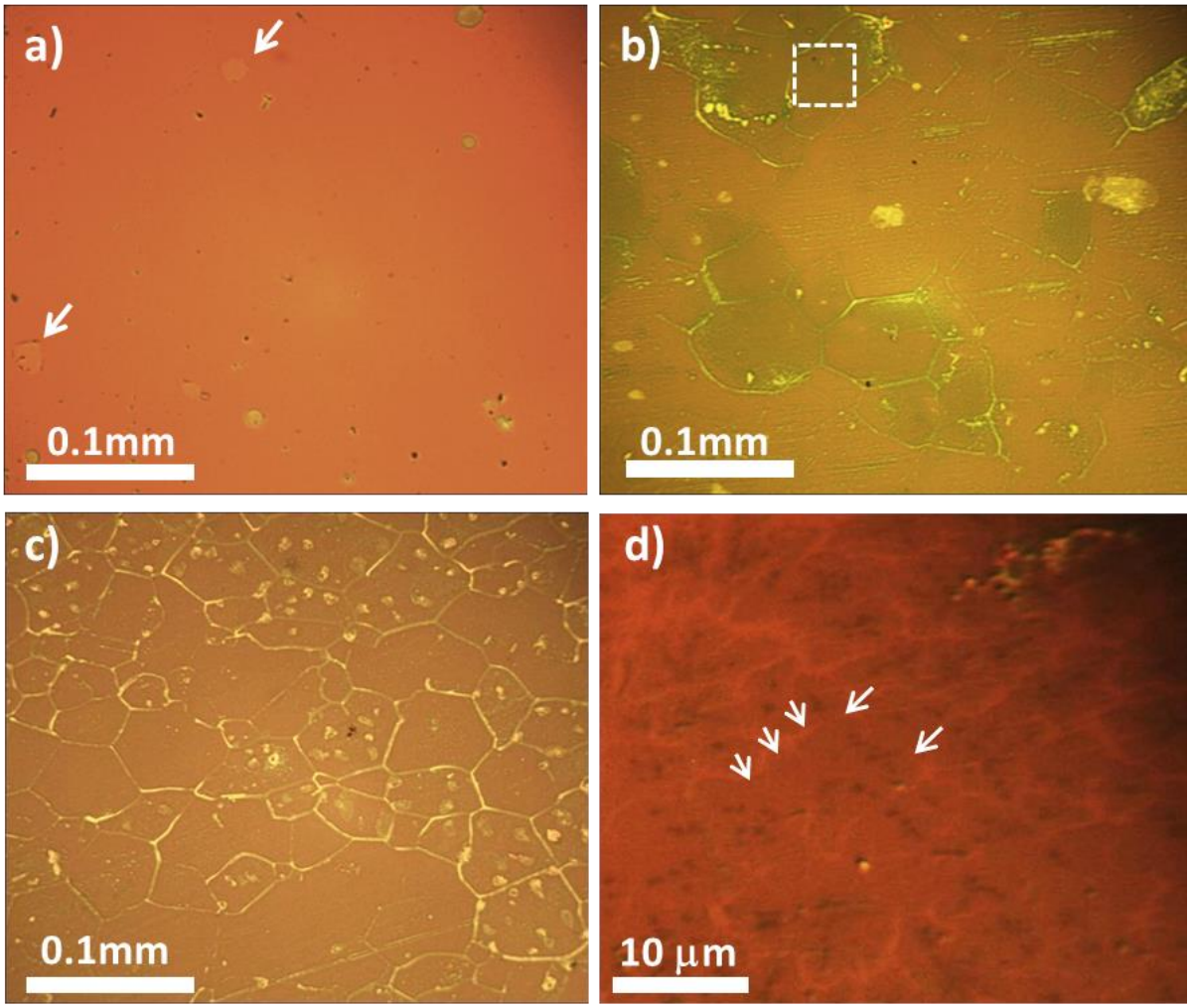

Figure 5-3 (a)-(c) Optical micrographs of graphene transferred onto SiO_2/Si substrate. Before transferring, copper/graphene sample has been thermal annealed for (a) 0 min, (b) 1 hour, (c) 2 hours in Ar at 600°C. The arrow in (a) indicates a pinhole. (d) is a magnified optical image of the dashed area in (b). The image contrast and color was adjusted to enhance the visibility of graphene and pin holes. The remaining graphene in (b) is in greenish-yellow color. The lines in (b) and (c) were due to PMMA residues.

5.4.3 Surface morphology of graphene during oxidation

To investigate the surface morphology evolution of graphene during the oxidation process, we performed the thermal annealing of copper/graphene samples over 0 min, 1 hour and 2 hours, respectively. After annealing, graphene was transferred onto a silicon substrate for optical microscopy characterization. As shown in Figure 5.3(a), before thermal annealing, the surface coverage of graphene was estimated to be over 95% with several micro-sized pinholes due to the physical damage during the transferring process. Annealing at 600°C for 1 hour resulted in the reduction of surface coverage of graphene film to < 40% (Figure 5.3(b)); after 2 hours of annealing, the graphene film completely disappeared leaving only PMMA residues (Figure 5.3(c)).

According to previous studies, cupric oxide (CuO) is the active compound that catalyzes the oxidation of graphite in the 400° - 700°C temperature range.[208] The catalytic cycle involves two reactions:

(i) O_2 molecules diffuse to copper surface to produce cupric oxide:

$$2Cu + O_2 \longrightarrow 2CuO$$

(ii) CuO is reduced to metallic copper at the copper-graphite interface:

$$CuO + C \longrightarrow Cu + CO$$

We noted that once the oxidative etching on graphene gets started as shown in Figure 5.3(d), the graphene film developed island-like structures whose boundaries coincide with that of the underlying copper grains. This is indicative of the preferential catalytic sites in the initial stage of graphene oxidation. As the thermal annealing time increased, the removal of graphene film was not uniform and instead occurred in patches (Figure 5.3(b)): while some areas enclosed by the PMMA residue lines are completely free of graphene, other areas are fully covered by it.

We attribute the formation of island-like structures on graphene surface shown in Figure 5.3(d) to its underlying copper grain boundaries. In our experiments, polycrystalline Cu foil with mixed crystalline facets was used for graphene growth. The grain boundaries can act as preferential nucleation sites for CuO growth due to much higher interfacial energy,[221] resulting in active catalytic sites in the initial stage of graphene oxidation. The inhomogeneous oxidative removal of graphene is probably due to the different oxidation rate on each copper facet.[221-223] It is known that oxidation rate on copper surface decreases in the order: (100) > (111) > (110).[223] Therefore, the area with higher surface density of CuO will result in faster oxidation of graphene.

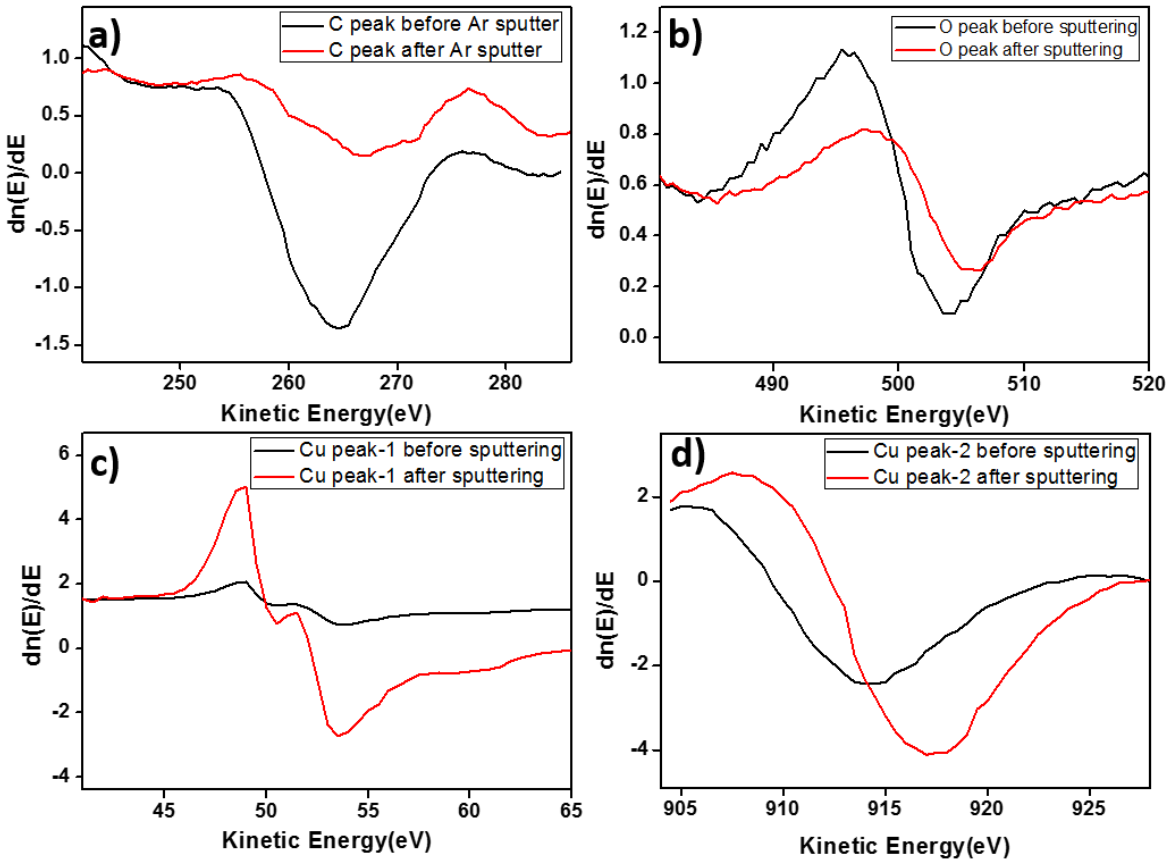

Figure 5-4 (a) – (d) Carbon (KLL), Oxygen (KLL), Copper (LMM) Auger spectra extracted from copper/graphene film before (black) and after (red) 2 hours Ar^+ ion sputter process.

5.4.4 Presence of oxygen underneath graphene after ambient air exposure

It is generally accepted that metal-catalyzed graphite oxidation can be divided two mechanisms,

that is, electron-transfer mechanism where π -electrons from graphite transfer to vacant orbitals of the metallic catalyst (like iron and cobalt) and oxygen-transfer mechanism where catalyst undergoes a red-ox reaction cycle.[224-225] Copper catalyzed graphene-oxidation fits the latter mechanism,[208] which raises an intriguing questions as how can the ambient oxygen directly react with copper. Indeed, graphene is considered as an effective physical barrier which prevents the further interaction between ambient oxygen and copper.

As we noted above, an interesting observation in our experiment is that prior air exposure at room temperature has a profound impact on the thermal stability of graphene. The experiment shown in Figure 5.1 was conducted on a copper/graphene sample that has been exposed to air at room temperature for 5 hours. In contrast, if the graphene sample was annealed in Ar right after synthesis and without any air exposure, such oxidative removal of graphene can only be observed at 700^{o}C over 4 hours of thermal annealing. To explain these observations, we hypothesized that upon the air exposure, oxygen molecules can diffuse into the space between copper and graphene and contribute to the oxidation of graphene at high temperature.

To confirm this hypothesis, we performed a 2-hour Ar^+ ion sputtering on copper/graphene surface in UHV and collected the electron excited Auger spectra (AES) during the sputtering process. The copper/graphene sample used in this experiment has been exposed in air for 18 hours before putting into the UHV chamber. Figure 5.4 showed the Auger spectra taken from copper/graphene surface before (black) and after (red) 2-hour Ar^+ ion sputtering. Among all four spectra, the C (KLL) Auger signal taken after 2-hour Ar^+ sputtering showed ~77% decrease of peak height. This is expected because AES is surface sensitive and graphene is at the top of the surface and will be the first material to be removed by Ar^+. Interestingly, only ~50% peak height decrease occurred at O (KLL) Auger signal, suggesting that the O species are located below

graphene. Finally, both Cu (LMM) Auger spectra showed sharp increase of peak intensity after sputtering. This increase is expected as removing graphene and oxygen should result in a higher yield of Auger electrons emitted from copper surface. It is also interesting to note that the kinetic energy of the Cu LMM transition shifted from 915.0 eV to 918.0 eV. Such spectroscopic change mimics those observed during the reduction of Cu_2O surface to Cu surface during H_2 thermal annealing, suggesting a similar transformation could have occurred on our sample.[188] Collectively, our AES results suggested that although copper surface is fully covered with monolayer graphene, oxygen can still diffuse between copper and graphene.

It should be noted that the Auger peak intensity is only intended to give a relative measurement of the surface concentration of elements. To quantify the surface coverage of the elements, the same copper/graphene sample was also characterized by XPS before and after the Ar^+ sputtering. As is shown in Figure 5.5(a) and (b), carbon 1s peak showed a drastic intensity decrease compared to a slight decrease of oxygen 1s peak during the 2 hours Ar^+ sputtering process.

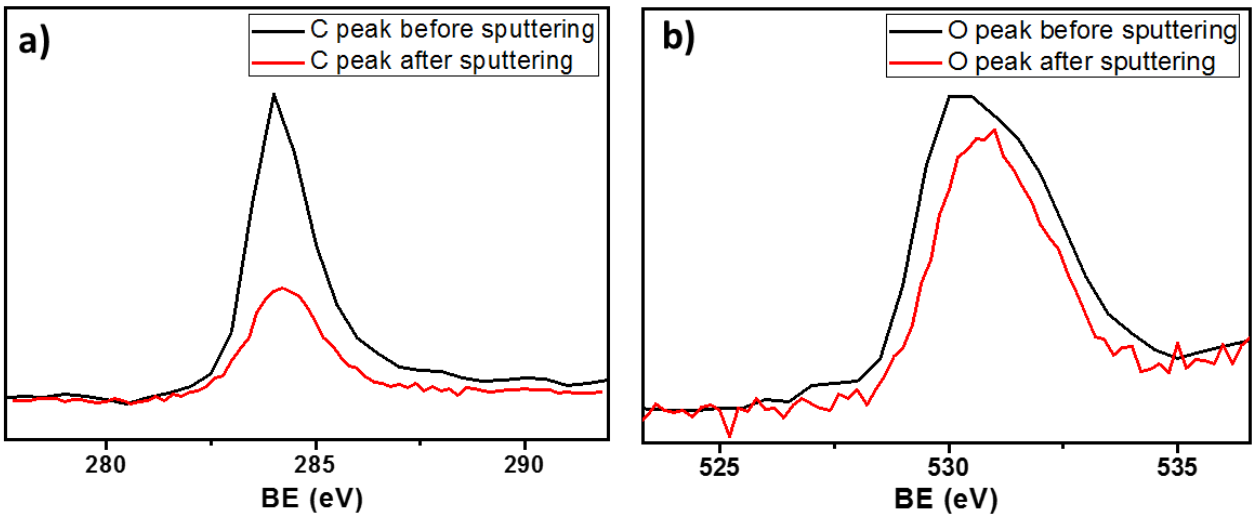

Figure 5-5 (a) Carbon 1s and (b) Oxygen 1s XPS peak of the same copper/graphene sample before (black) and after (red) 2 hours Ar^+ sputtering.

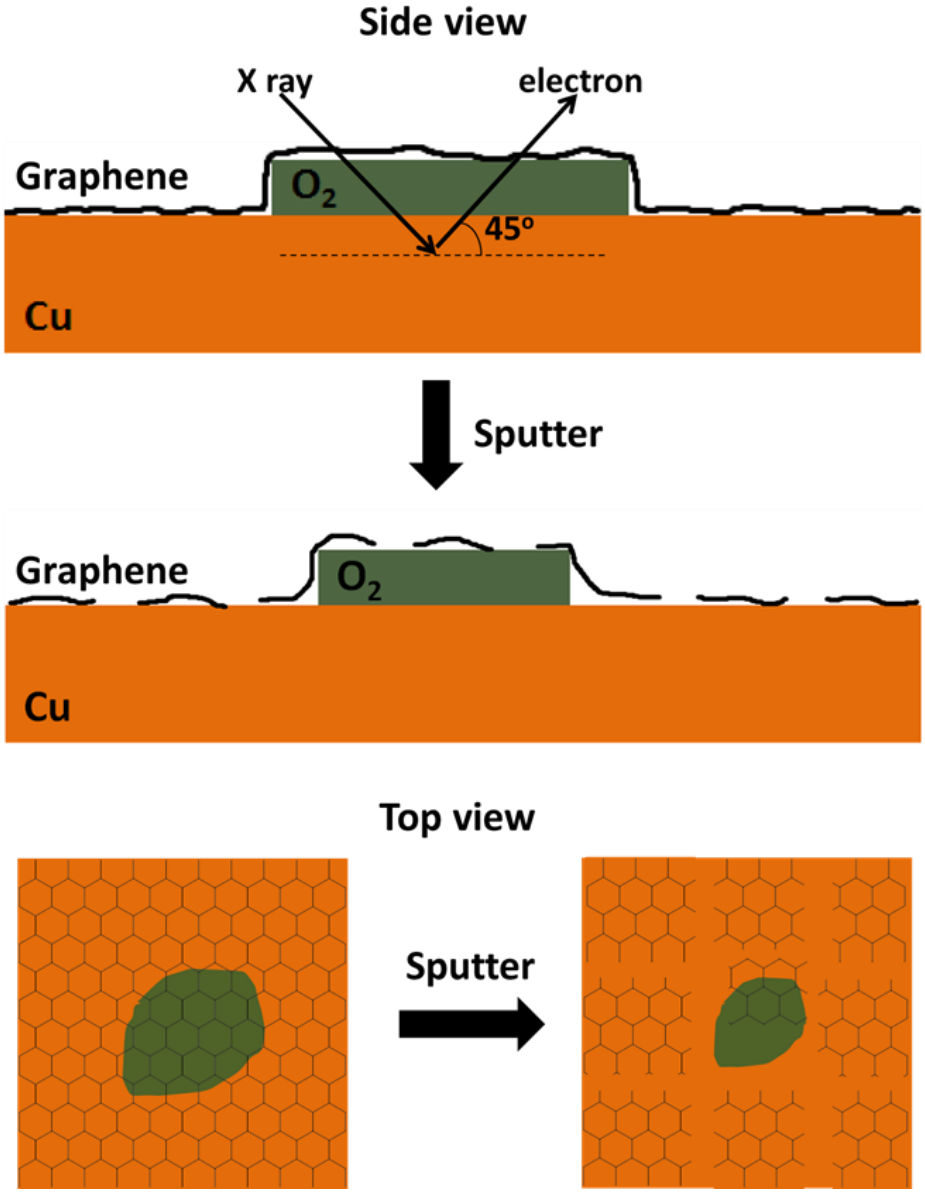

Figure 5-6 the schematic of Ar^+ sputtering process on copper/graphene surface. Note that the spatial distribution of oxygen underneath graphene is for illustration purpose only; the actual spatial distribution of oxygen on the surface is unknown.

Quantitative analysis of the XPS data will require modeling because the oxygen species are believed to be located below graphene and its XPS signal will be attenuated by graphene. Shown in Figure 5.6 is the model of the copper/graphene surface we used. The model assumes that (i) oxygen species with certain average surface density existed between copper and graphene; and (ii) after 2 hours of Ar^+ sputtering, the average surface density of oxygen species remained unchanged underneath remaining graphene while decreased to a constant value where the graphene was removed. With these assumptions, the unattenuated oxygen 1s peak intensity after escape depth correction is given by (5).

$I_o = I / \exp(-d / \lambda)$ (5)

Where I_o is the peak intensity of oxygen in the absence of graphene layer, I is the intensity of oxygen 1s peak collected by XPS, d is the travelling distance in the graphene monolayer film with $d = d_G / \cos\theta$, where $d_G = 3.5$ Å is the thickness of graphene layer and θ is the escape angle (45°), λ is the Inelastic Mean Free Path (IMFP) and equals 17.6 Å for photoelectrons emitted from oxygen (953.7 eV).[173]

Considering that graphene is the top layer, $I_o(C)$ should be equal to $I(C)$. Using the actual peak intensity of both carbon 1s peak and oxygen 1s peaks, we calculated the surface coverage of oxygen on graphene surface before and after Ar^+ ion sputtering by equation (5).

$$n(o)/n(c) = \frac{I_o(O)/R(O)}{I_o(C)/R(C)} \quad (6)$$

Where (i) n is number of atoms; (ii) I_o is the actual peak intensity derived from equation (1); (iii) R is the relative sensitivity factor (R.S.F.): $R(O) = 0.66$ for oxygen 1s peak and $R(C) = 0.25$ for carbon 1s peak.[64]

Our calculation results showed that 58% of the carbon species have been removed during

the 2 hours of Ar^+ sputtering process while oxygen species showed a moderate decrease of 26%. Due to the preferential removal of carbon species, the atom ratio of O : C, as calculated from equation (6), increased from 0.42 to 0.74 after sputtering. Both results are in agreement with the conclusions we drew from the AES studies.

On the basis of all the results shown above, we tentatively propose the following three steps in the catalytic oxidation process:

(1) Ambient oxygen diffuses into the interlayer of copper/graphene within hours of air exposure. The O : C atom ratio reached 0.42 : 1 after 18 hours of air exposure. Partial oxidation of copper surface to Cu_2O was indicated by the AES.

(2) Graphene-oxygen reaction initiates around the grain boundary above 600^{o}C. The reaction is likely due to the presence of Cu oxide near grain boundary; the reaction results in fissures formed on graphene surface which allow more oxygen diffuse into the interlayer space between graphene and copper.

(3) The intercalated oxygen reacts with graphene, likely through the formation of copper oxide at the interface. The kinetics of this process appears to depend on the crystalline facet of copper, as suggested by the optical microscopy results.

5.5. CONCLUSION

In this work, we revealed the catalytic behavior of copper substrate upon graphene-oxygen reaction above 600ºC. Both AES and XPS results showed that ambient oxygen molecules can diffuse into the interlayer space between graphene and copper after several hours air exposure, promoting the formation of copper oxide as the preferential catalytic sites during the annealing process. In this regards, the copper foil should not be considered as an inert substrate in the post-synthesis processing of graphene, especially when high temperature treatment is involved.

6.0 SUMMARY

My research aims at revealing the intrinsic surface property of graphene, understanding how such properties are affected by the environment (*e.g.*, airborne hydrocarbons, ambient oxygen). In addition, my thesis also includes substantial studies on controlling the surface properties of graphene, which is critical for many applications since it determines the interaction between graphene and its environments, effecting its adhesion, electrical properties, and electrochemical activities. Below I summarized the key observations and main conclusions in this dissertation.

1. Intrinsic wettability of graphene.

It is generally accepted that graphitic materials are hydrophobic with water contact angle (WCA) of *ca.* 90^{o}; this view has persisted for the past 70 years or so. Surprisingly, in my research, we occasionally observed much smaller WCAs on graphene surfaces. I suspected that graphitic surfaces could be contaminated by air exposure leading to a change of their wettability. In order to test this hypothesis, we conducted extensive wetting and surface characterization of various graphitic samples as a function of their air exposure. These results show that a clean graphitic surface is much hydrophilic than previously thought. Upon exposure to ambient atmosphere, graphitic surface absorbs hydrocarbons in air, resulting in a much more hydrophobic surface and a significant increase in its WCA as shown in Figure 6.1(a). Wettability is a fundamental property of a surface and is key to understand many other interfacial phenomena, such as adhesion and heat transfer. As such, this work could have a profound impact on the research of graphitic materials in

general, potentially changing the way people model and manipulate graphitic materials and developing new applications.

Accordingly, an effective method to minimize the hydrocarbon contamination is urgently needed due to the rapid kinetics of hydrocarbon adsorption on graphitic surface and the enormous effect on surface wettability. In the follow-up research, I found that by storing a freshly prepared graphitic surface at low temperature, the surface hydrocarbon contamination can be greatly minimized and thus its intrinsic surface wetting behavior can be well preserved as shown in Figure 6.1 (b). This new method potentially offers new fabrication approaches that can effectively minimize hydrocarbon contaminants, further promoting the device applications for all graphitic materials in the future.

2. Effect of ambient oxygen on copper/graphene surface.

Given that graphene grown on a copper substrate is mostly defect-free, it is generally expected that graphene could resist atmospheric oxidation by itself and also serve as an anti-corrosion barrier to protect the underlying metals from short-term thermal, wet, electrochemical corrosion. To evaluate the effect of ambient exposure on copper/graphene surface, we conducted both long-term corrosion at room temperature and thermal annealing in Ar atmosphere (O_2 < 3 ppm) at high temperature, respectively. Graphene-coated copper foil showed a higher degree of oxidation than uncoated one after 6 months of ambient exposure and conversely, copper-supported graphene underwent more severe oxidative removal at 600^{o}C than that deposited on other substrate. The corrosion of copper enhanced by graphene and breakage of graphene on copper can be clearly observed in Figure 6.1 (c-d). Our experimental results indicate an underestimated interaction between ambient oxygen and copper/graphene surface, which needs to be seriously considered in its practical applications.

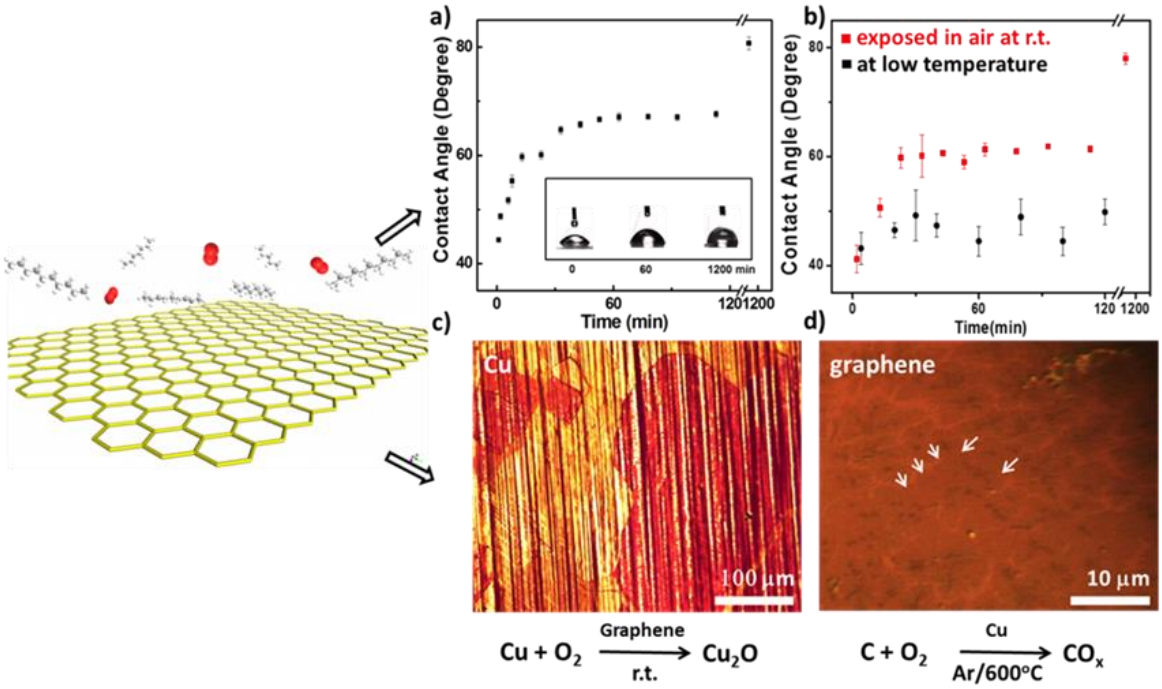

Figure 6-1 Summary of research. (a) Temporal evolution of the WCA measured on freshly synthesized copper/graphene sample. The data shows that a clean graphene is intrinsically hydrophilic. (b) WCA evolution of fresh copper/graphene samples stored at r.t. (red) and low temperature (black), respectively. This comparison indicates that low temperature storage retards the WCA increase and associated airborne hydrocarbon adsorption rate on graphitic surface. (c-d) Optical images of copper/graphene samples after (c) exposure in ambient atmosphere for 6 months and (d) thermal annealing in Ar (O_2 < 3ppm) for 2h. The data shows that graphene (copper) promotes the oxidation of copper (graphene) after ambient air exposure.

In summary, my research provided new insight into the interaction between graphitic surface and its environment. These results could have significant implications to the understanding of fundamental properties of graphene and to its application as a coating material, field effect transistor, gas sensor, etc.

APPENDIX

PUBLICATIONS

Kozbial, A.; Li, Z.; *et al*. *Langmuir*, **2014**, 30, 8598-8606

Kozbial, A.; Li, Z.; *et al*. *Carbon* **2014**, 74, 218-225

Li, Z.; Zhou, F.; *et al*. *Journal of Solid State Chemistry* **2014**, 224, 14-20

Li, Z.; Wang, Y.; *et al*. *Nature Materials.* **2013**, 12, 925-931

Zhou, F.; Li, Z.; *et al*. *ACS Nano* **2013**, 7, 6939-6947

LIST OF ABBREVIATIONS

Table 1. List of abbreviations

Abbreviation		Abbreviation	
Cu/G	Copper/graphene	AFM	Atomic force microscopy
PMMA	Poly-methyl methacrylate	OM	Optical microscopy
CVD	Chemical vapor deposition	WCA	Water contact angle
HOPG	Highly ordered pyrolytic graphite	XPS	X-ray photoelectron spectroscopy
UHV	Ultrahigh vacuum	CV	Cyclic voltammetry
AHC	Airborne hydrocarbon contaminants	FTIR	Fourier-transform infrared spectroscopy
ppt	Parts-per-trillion	ATR	Attenuated total reflectance
ppm	Parts-per-million	EDX	Energy-dispersive X-ray spectroscopy
SCCM	Standard cubic centimeters per minute	AES	Auger electron spectroscopy
BN	Boron nitride	IMFP	Inelastic mean free path
VOC	Volatile organic compounds	RH	Relative humidity
FWHM	Full width at half maximum	TOC	Total organic carbon

PET	Polyethylene terephthalate	vdW	Van der waals
FET	Filed effect transistor	iTO	in-plane transverse optical

BIBLIOGRAPHY

1. Geim, A. K.; Novoselov, K. S., The rise of graphene. *Nat. Mater.* **2007,** *6* (3), 183-191.

2. Novoselov, K. S.; Geim, A. K.; Morozov, S. V.; Jiang, D.; Zhang, Y.; Dubonos, S. V.; Grigorieva, I. V.; Firsov, A. A., Electric Field Effect in Atomically Thin Carbon Films. *Science (Washington, DC, United States)* **2004,** *306* (5696), 666-669.

3. Gupta, A.; Chen, G.; Joshi, P.; Tadigadapa, S.; Eklund, P. C., Raman Scattering from High-Frequency Phonons in Supported n-Graphene Layer Films. *Nano Letters* **2006,** *6* (12), 2667-2673.

4. Novoselov, K. S.; Jiang, Z.; Zhang, Y.; Morozov, S. V.; Stormer, H. L.; Zeitler, U.; Maan, J. C.; Boebinger, G. S.; Kim, P.; Geim, A. K., Room-Temperature Quantum Hall Effect in Graphene. *Science (Washington, DC, United States)* **2007,** *315* (5817), 1379.

5. Bolotin, K. I.; Sikes, K. J.; Hone, J.; Stormer, H. L.; Kim, P., Temperature-dependent transport in suspended graphene. *Physical review letters* **2008,** *101* (9), 096802.

6. Balandin, A. A.; Ghosh, S.; Bao, W.; Calizo, I.; Teweldebrhan, D.; Miao, F.; Lau, C. N., Superior Thermal Conductivity of Single-Layer Graphene. *Nano Lett.* **2008,** *8* (3), 902-907.

7. Frank, I. W.; Tanenbaum, D. M.; van der Zande, A. M.; McEuen, P. L., Mechanical properties of suspended graphene sheets. *J. Vac. Sci. Technol., B Microelectron. Nanometer Struct.--Process., Meas., Phenom.* **2007,** *25* (6), 2558-2561.

8. Sorkin, V.; Zhang, Y. W., Graphene-based pressure nano-sensors. *Journal of Molecular Modeling* **2011,** *17* (11), 2825-2830.

9. Bunch, J. S.; van der Zande, A. M.; Verbridge, S. S.; Frank, I. W.; Tanenbaum, D. M.; Parpia, J. M.; Craighead, H. G.; McEuen, P. L., Electromechanical Resonators from Graphene Sheets. *Science (Washington, DC, United States)* **2007,** *315* (5811), 490-493.

10. Chen, C.; Rosenblatt, S.; Bolotin, K. I.; Kalb, W.; Kim, P.; Kymissis, I.; Stormer, H. L.; Heinz, T. F.; Hone, J., Performance of monolayer graphene nanomechanical resonators with electrical readout. *Nature Nanotechnology* **2009,** *4* (12), 861-867.

11. Zhu, S.-E.; Krishna Ghatkesar, M.; Zhang, C.; Janssen, G. C. A. M., Graphene based

piezoresistive pressure sensor. *Applied Physics Letters* **2013,** *102* (16), 161904.

12. Ma, J.; Jin, W.; Ho, H. L.; Dai, J. Y., High-sensitivity fiber-tip pressure sensor with graphene diaphragm. *Opt. Lett.* **2012,** *37* (13), 2493-2495.

13. Stankovich, S.; Piner, R. D.; Chen, X.; Wu, N.; Nguyen, S. T.; Ruoff, R. S., Stable aqueous dispersions of graphitic nanoplatelets via the reduction of exfoliated graphite oxide in the presence of poly(sodium 4-styrenesulfonate). *J. Mater. Chem.* **2006,** *16* (2), 155-158.

14. Berger, C.; Song, Z.; Li, X.; Wu, X.; Brown, N.; Naud, C.; Mayou, D.; Li, T.; Hass, J.; Marchenkov, A. N.; Conrad, E. H.; First, P. N.; de Heer, W. A., Electronic Confinement and Coherence in Patterned Epitaxial Graphene. *Science (Washington, DC, United States)* **2006,** *312* (5777), 1191-1196.

15. Li, X.; Cai, W.; An, J.; Kim, S.; Nah, J.; Yang, D.; Piner, R.; Velamakanni, A.; Jung, I.; Tutuc, E.; Banerjee, S. K.; Colombo, L.; Ruoff, R. S., Large-Area Synthesis of High-Quality and Uniform Graphene Films on Copper Foils. *Science (Washington, DC, United States)* **2009,** *324* (5932), 1312-1314.

16. Kim, K. S.; Zhao, Y.; Jang, H.; Lee, S. Y.; Kim, J. M.; Kim, K. S.; Ahn, J.-H.; Kim, P.; Choi, J.-Y.; Hong, B. H., Large-scale pattern growth of graphene films for stretchable transparent electrodes. *Nature (London, U. K.)* **2009,** *457* (7230), 706-710.

17. Jiao, L.; Zhang, L.; Wang, X.; Diankov, G.; Dai, H., Narrow graphene nanoribbons from carbon nanotubes. *Nature (London, U. K.)* **2009,** *458* (7240), 877-880.

18. Cano-Marquez, A. G.; Rodriguez-Macias, F. J.; Campos-Delgado, J.; Espinosa-Gonzalez, C. G.; Tristan-Lopez, F.; Ramirez-Gonzalez, D.; Cullen, D. A.; Smith, D. J.; Terrones, M.; Vega-Cantu, Y. I., Ex-MWNTs: Graphene Sheets and Ribbons Produced by Lithium Intercalation and Exfoliation of Carbon Nanotubes. *Nano Letters* **2009,** *9* (4), 1527-1533.

19. Kosynkin, D. V.; Higginbotham, A. L.; Sinitskii, A.; Lomeda, J. R.; Dimiev, A.; Price, B. K.; Tour, J. M., Longitudinal unzipping of carbon nanotubes to form graphene nanoribbons. *Nature (London, U. K.)* **2009,** *458* (7240), 872-876.

20. de Heer, W. A.; Berger, C.; Wu, X.; First, P. N.; Conrad, E. H.; Li, X.; Li, T.; Sprinkle, M.; Hass, J.; Sadowski, M. L.; Potemski, M.; Martinez, G., Epitaxial graphene. *Solid State Communications* **2007,** *143* (1-2), 92-100.

21. Lyakhovich, A. M.; Shakov, A. A.; Lyalina, N. V., Effect of ambient humidity to wetting angles of various hydrophilic surfaces. *Prot Met Phys Chem Surf* **2010,** *46* (5), 534-539.

22. Banerjee, B. C.; Hirt, T. J.; Walker, P. L., Jr., Pyrolytic carbon formation from carbon suboxide. *Nature (London, U. K.)* **1961,** *192*, 450-1.

23. Mattevi, C.; Kim, H.; Chhowalla, M., A review of chemical vapour deposition of graphene on copper. *J. Mater. Chem.* **2011,** *21* (10), 3324-3334.

24. Wofford, J. M.; Nie, S.; McCarty, K. F.; Bartelt, N. C.; Dubon, O. D., Graphene islands on Cu foils. The interplay between shape, orientation, and defects. *Nano Letters* **2010,** *10* (12), 4890-4896.

25. Li, X.; Zhu, Y.; Cai, W.; Borysiak, M.; Han, B.; Chen, D.; Piner, R. D.; Colombo, L.; Ruoff, R. S., Transfer of Large-Area Graphene Films for High-Performance Transparent Conductive Electrodes. *Nano Letters* **2009,** *9* (12), 4359-4363.

26. Li, X. S.; Cai, W. W.; An, J. H.; Kim, S.; Nah, J.; Yang, D. X.; Piner, R.; Velamakanni, A.; Jung, I.; Tutuc, E.; Banerjee, S. K.; Colombo, L.; Ruoff, R. S., Large-Area Synthesis of High-Quality and Uniform Graphene Films on Copper Foils. *Science* **2009,** *324* (5932), 1312-1314.

27. Raman spectroscopy in graphene. *Physics Reports 473* (5b).

28. Saito, R.; Hofmann, M.; Dresselhaus, G.; Jorio, A.; Dresselhaus, M. S., Raman spectroscopy of graphene and carbon nanotubes. *Advances in Physics* **2011,** *60* (3), 413-550.

29. Ferrari, A. C., Raman spectroscopy of graphene and graphite: Disorder, electron-phonon coupling, doping and nonadiabatic effects. *Solid State Communications* **2007,** *143* (1-2), 47-57.

30. Malard, L. M.; Pimenta, M. A.; Dresselhaus, G.; Dresselhaus, M. S., Raman spectroscopy in graphene. *Phys. Rep.* **2009,** *473* (5-6), 51-87.

31. R. Saito, G. D., M.S. Dresselhaus, *Physical Properties of Carbon Nanotubes*. Imperial College Press: London, 1998.

32. Yan, J.; Zhang, Y.; Kim, P.; Pinczuk, A., Electric Field Effect Tuning of Electron-Phonon Coupling in Graphene. *Phys. Rev. Lett.* **2007,** *98* (16), 166802/1-166802/4.

33. Mohiuddin, T. M. G.; Lombardo, A.; Nair, R. R.; Bonetti, A.; Savini, G.; Jalil, R.; Bonini, N.; Basko, D. M.; Galiotis, C.; Marzari, N.; Novoselov, K. S.; Geim, A. K.; Ferrari, A. C., Uniaxial strain in graphene by Raman spectroscopy: G peak splitting, Gruneisen parameters, and sample orientation. *Physical Review B: Condensed Matter and Materials Physics* **2009,** *79* (20), 205433/1-205433/8.

34. Elias, D. C.; Nair, R. R.; Mohiuddin, T. M. G.; Morozov, S. V.; Blake, P.; Halsall, M. P.; Ferrari, A. C.; Boukhvalov, D. W.; Katsnelson, M. I.; Geim, A. K.; Novoselov, K. S., Control of

Graphene's Properties by Reversible Hydrogenation: Evidence for Graphane. *Science (Washington, DC, United States)* **2009,** *323* (5914), 610-613.

35. Ryu, S.; Han, M. Y.; Maultzsch, J.; Heinz, T. F.; Kim, P.; Steigerwald, M. L.; Brus, L. E., Reversible Basal Plane Hydrogenation of Graphene. *Nano Letters* **2008,** *8* (12), 4597-4602.

36. Fujiwara, H., *Spectroscopic Ellipsometry: Principle and Applications*. John Wiley & Sons: 2007.

37. Kattner, J.; Hoffmann, H., Simultaneous Determination of Thicknesses and Refractive Indices of Ultrathin Films by Multiple Incidence Medium Ellipsometry. *The Journal of Physical Chemistry B* **2002,** *106* (38), 9723-9729.

38. Kozbial, A.; Li, Z.; Sun, J.; Gong, X.; Zhou, F.; Wang, Y.; Xu, H.; Liu, H.; Li, L., Understanding the intrinsic water wettability of graphite. *Carbon* **2014,** *74* (0), 218-225.

39. Fowkes, F. M.; Harkins, W. D., The state of monolayers adsorbed at the interface solid—aqueous solution. *J. Am. Chem. Soc.* **1940,** *62* (12), 3377-3386.

40. Mao, Y.; Chen, C.-L.; Zhang, Y., Molecular dynamic study on contact angle of water droplet on a single-wall carbon nanotube (SWCNT) plate. *Appl. Phys. A* **2013,** *111* (3), 747-754.

41. Lau, K. K. S.; Bico, J.; Teo, K. B. K.; Chhowalla, M.; Amaratunga, G. A. J.; Milne, W. I.; McKinley, G. H.; Gleason, K. K., Superhydrophobic carbon nanotube forests. *Nano Lett.* **2003,** *3* (12), 1701-1705.

42. Taherian, F.; Marcon, V.; van der Vegt, N. F. A.; Leroy, F., What is the contact angle of water on graphene? *Langmuir* **2013,** *29* (5), 1457-1465.

43. Wang, S.; Zhang, Y.; Abidi, N.; Cabrales, L., Wettability and surface free energy of graphene films. *Langmuir* **2009,** *25* (18), 11078-11081.

44. Morcos, I., On contact angle and dispersion energy of the cleavage graphite/water system. *J. Colloid Interface Sci.* **1970,** *34* (3), 469-471.

45. Morcos, I., Surface tension of stress-annealed pyrolytic graphite. *J. Chem. Phys.* **1972,** *57* (4), 1801-1802.

46. Ou, J.; Wang, J.; Liu, S.; Mu, B.; Ren, J.; Wang, H.; Yang, S., Tribology study of reduced graphene oxide sheets on silicon substrate synthesized via covalent assembly. *Langmuir* **2010,** *26* (20), 15830-15836.

47. Raj, R.; Maroo, S. C.; Wang, E. N., Wettability of Graphene. *Nano Letters* **2013,** *13* (4), 1509-1515.

48. Shin, Y. J.; Wang, Y.; Huang, H.; Kalon, G.; Wee, A. T. S.; Shen, Z.; Bhatia, C. S.; Yang, H., Surface-Energy Engineering of Graphene. *Langmuir* **2010,** *26* (6), 3798-3802.

49. Adamson, A. W.; Gast, A. P., *Physical Chemistry of Surfaces*. 6 ed.; John Wiley & Sons, Inc.: New York, 1997.

50. Kogan, M. J.; Dalcol, I.; Gorostiza, P.; Lopez-Iglesias, C.; Pons, R.; Pons, M.; Sanz, F.; Giralt, E., Supramolecular properties of the proline-rich γ-zein N-terminal domain. *Biophys. J.* **2002,** *83* (2), 1194-1204.

51. Westreich, P.; Fortier, H.; Flynn, S.; Foster, S.; Dahn, J. R., Exclusion of salt solutions from activated carbon pores and the relationship to contact angle on graphite. *J. Phys. Chem. C* **2007,** *111* (9), 3680-3684.

52. Li, S.; Li, H.; Wang, X.; Song, Y.; Liu, Y.; Jiang, L.; Zhu, D., Super-hydrophobicity of large-area honeycomb-like aligned carbon nanotubes. *J. Phys. Chem. B* **2002,** *106* (36), 9274-9276.

53. Li, H.; Wang, X.; Song, Y.; Liu, Y.; Li, Q.; Jiang, L.; Zhu, D., Super-"amphiphobic" aligned carbon nanotube films. *Angew. Chem. Int. Ed.* **2001,** *40* (9), 1743-1746.

54. Li, Z.; Wang, Y.; Kozbial, A.; Shenoy, G.; Zhou, F.; McGinley, R.; Ireland, P.; Morganstein, B.; Kunkel, A.; Surwade, S. P.; Li, L.; Liu, H., Effect of airborne contaminants on the wettability of supported graphene and graphite. *Nature Mater.* **2013,** *12* (10), 925-931.

55. Schrader, M. E., Ultrahigh vacuum techniques in the measurement of contact angles. IV. water on graphite (0001). *J. Phys. Chem.* **1975,** *79* (23), 2508-2515.

56. Schrader, M. E., Ultrahigh-vacuum techniques in the measurement of contact angles. 5. LEED study of the effect of structure on the wettability of graphite. *J. Phys. Chem.* **1980,** *84* (21), 2774-2779.

57. Tadros, M. E.; Hu, P.; Adamson, A. W., Adsorption and contact angle studies: I. water on smooth carbon, linear polyethylene, and stearic acid-coated copper. *J. Colloid Interface Sci.* **1974,** *49* (2), 184-195.

58. Cao, P.; Xu, K.; Varghese, J. O.; Heath, J. R., The Microscopic Structure of Adsorbed Water on Hydrophobic Surfaces under Ambient Conditions. *Nano Letters* **2011,** *11* (12), 5581-5586.

59. Luna, M.; Colchero, J.; Baró, A. M., Study of water droplets and films on graphite by noncontact scanning force microscopy. *J. Phys. Chem. B* **1999,** *103* (44), 9576-9581.

60. Schrader, M. E., Ultrahigh vacuum techniques in the measurement of contact angles. IV. Water on graphite (0001). *The Journal of Physical Chemistry* **1975,** *79* (23), 2508-2515.

61. Garcia, R.; Osborne, K.; Subashi, E., Validity of the "sharp-kink approximation" for water and other fluids. *J. Phys. Chem. B* **2008,** *112* (27), 8114-8119.

62. Bourges-Monnier, C.; Shanahan, M. E. R., Influence of evaporation on contact angle. *Langmuir* **1995,** *11* (7), 2820-2829.

63. Hu, H.; Larson, R. G., Evaporation of a sessile droplet on a substrate. *J. Phys. Chem. B* **2002,** *106* (6), 1334-1344.

64. Webb, M. J.; Palmgren, P.; Pal, P.; Karis, O.; Grennberg, H., A simple method to produce almost perfect graphene on highly oriented pyrolytic graphite. *Carbon* **2011,** *49* (10), 3242-3249.

65. Characterization of amorphous and nanocrystalline carbon films. *Materials Chemistry and Physics 96* (2b).

66. Larciprete, R.; Fabris, S.; Sun, T.; Lacovig, P.; Baraldi, A.; Lizzit, S., Dual Path Mechanism in the Thermal Reduction of Graphene Oxide. *Journal of the American Chemical Society* **2011,** *133* (43), 17315-17321.

67. Sun, T.; Fabris, S.; Baroni, S., Surface Precursors and Reaction Mechanisms for the Thermal Reduction of Graphene Basal Surfaces Oxidized by Atomic Oxygen. *The Journal of Physical Chemistry C* **2011,** *115* (11), 4730-4737.

68. Jia, C.; Jiang, J.; Gan, L.; Guo, X., Direct Optical Characterization of Graphene Growth and Domains on Growth Substrates. *Sci. Rep.* **2012,** *2*, 707.

69. Nayak, P. K.; Hsu, C.-J.; Wang, S.-C.; Sung, J. C.; Huang, J.-L., Graphene Coated Ni Films: A Protective Coating. *Thin Solid Films* **2013,** *529*, 312-316.

70. Kousalya, A. S.; Kumar, A.; Paul, R.; Zemlyanov, D.; Fisher, T. S., Graphene: An Effective Oxidation Barrier Coating for Liquid and Two-phase Cooling Systems. *Corros. Sci.* **2013,** *69*, 5-10.

71. Chen, S. S.; Brown, L.; Levendorf, M.; Cai, W. W.; Ju, S. Y.; Edgeworth, J.; Li, X. S.; Magnuson, C. W.; Velamakanni, A.; Piner, R. D.; Kang, J. Y.; Park, J.; Ruoff, R. S., Oxidation Resistance of Graphene-Coated Cu and Cu/Ni Alloy. *Acs Nano* **2011,** *5* (2), 1321-1327.

72. Schedin, F.; Geim, A. K.; Morozov, S. V.; Hill, E. W.; Blake, P.; Katsnelson, M. I.; Novoselov, K. S., Detection of individual gas molecules adsorbed on graphene. *Nat Mater* **2007,** *6* (9), 652-655.

73. Qi, Y.; Eskelsen, J. R.; Mazur, U.; Hipps, K. W., Fabrication of Graphene with CuO Islands by Chemical Vapor Deposition. *Langmuir* **2012,** *28* (7), 3489-93.

74. Nilsson, L.; Andersen, M.; Balog, R.; Laegsgaard, E.; Hofmann, P.; Besenbacher, F.; Hammer, B.; Stensgaard, I.; Hornekaer, L., Graphene Coatings: Probing the Limits of the One Atom Thick Protection Layer. *Acs Nano* **2012,** *6* (11), 10258-66.

75. Luechinger, N. A.; Athanassiou, E. K.; Stark, W. J., Graphene-Stabilized Copper Nanoparticles as An Air-Stable Substitute for Silver and Gold in Low-Cost Ink-Jet Printable Electronics. *Nanotechnology* **2008,** *19*, 445201.

76. Ahn, Y.; Jeong, Y.; Lee, Y., Improved Thermal Oxidation Stability of Solution-Processable Silver Nanowire Transparent Electrode by Reduced Graphene Oxide. *ACS Appl. Mater. Interfaces* **2012,** *4* (12), 6410-6414.

77. Roy, S. S.; Arnold, M. S., Improving Graphene Diffusion Barriers via Stacking Multiple Layers and Grain Size Engineering. *Adv. Funct. Mater.* **2013**, ASAP online; DOI: 10.1002/adfm.201203179.

78. Kang, D.; Kwon, J. Y.; Cho, H.; Sim, J. H.; Hwang, H. S.; Kim, C. S.; Kim, Y. J.; Ruoff, R. S.; Shin, H. S., Oxidation Resistance of Iron and Copper Foils Coated with Reduced Graphene Oxide Multilayers. *Acs Nano* **2012,** *6* (9), 7763-9.

79. Preston, D. J.; Mafra, D. L.; Miljkovic, N.; Kong, J.; Wang, E. N., Scalable Graphene Coatings for Enhanced Condensation Heat Transfer. *Nano Letters* **2015,** *15* (5), 2902-2909.

80. Velicky, M.; Bissett, M. A.; Toth, P. S.; Patten, H. V.; Worrall, S. D.; Rodgers, A. N. J.; Hill, E. W.; Kinloch, I. A.; Novoselov, K. S.; Georgiou, T.; Britnell, L.; Dryfe, R. A. W., Electron transfer kinetics on natural crystals of MoS2 and graphite. *Physical Chemistry Chemical Physics* **2015,** *17* (27), 17844-17853.

81. Velický, M.; Bradley, D. F.; Cooper, A. J.; Hill, E. W.; Kinloch, I. A.; Mishchenko, A.; Novoselov, K. S.; Patten, H. V.; Toth, P. S.; Valota, A. T.; Worrall, S. D.; Dryfe, R. A. W., Electron Transfer Kinetics on Mono- and Multilayer Graphene. *ACS Nano* **2014,** *8* (10), 10089-10100.

82. Patel, A. N.; Collignon, M. G.; O'Connell, M. A.; Hung, W. O. Y.; McKelvey, K.; Macpherson, J. V.; Unwin, P. R., A New View of Electrochemistry at Highly Oriented Pyrolytic Graphite. *Journal of the American Chemical Society* **2012,** *134* (49), 20117-20130.

83. Nioradze, N.; Chen, R.; Kurapati, N.; Khvataeva-Domanov, A.; Mabic, S.; Amemiya, S., Organic Contamination of Highly Oriented Pyrolytic Graphite As Studied by Scanning Electrochemical Microscopy. *Analytical Chemistry* **2015,** *87* (9), 4836-4843.

84. Sharkey, T. D., Emission of low molecular mass hydrocarbons from plants. *Trends in Plant*

Science **1996,** *1* (3), 78-82.

85. Sharkey, T. D.; Wiberley, A. E.; Donohue, A. R., Isoprene Emission from Plants: Why and How. *Annals of Botany* **2008,** *101* (1), 5-18.

86. Fraser, M. P.; Cass, G. R.; Simoneit, B. R. T., Gas-Phase and Particle-Phase Organic Compounds Emitted from Motor Vehicle Traffic in a Los Angeles Roadway Tunnel. *Environmental Science & Technology* **1998,** *32* (14), 2051-2060.

87. Goldan, P. D.; Kuster, W. C.; Fehsenfeld, F. C.; Montzka, S. A., Hydrocarbon measurements in the southeastern United States: The Rural Oxidants in the Southern Environment (ROSE) Program 1990. *Journal of Geophysical Research: Atmospheres* **1995,** *100* (D12), 25945-25963.

88. Goldan, P. D.; Trainer, M.; Kuster, W. C.; Parrish, D. D.; Carpenter, J.; Roberts, J. M.; Yee, J. E.; Fehsenfeld, F. C., Measurements of hydrocarbons, oxygenated hydrocarbons, carbon monoxide, and nitrogen oxides in an urban basin in Colorado: Implications for emission inventories. *Journal of Geophysical Research: Atmospheres* **1995,** *100* (D11), 22771-22783.

89. Millet, D. B.; Donahue, N. M.; Pandis, S. N.; Polidori, A.; Stanier, C. O.; Turpin, B. J.; Goldstein, A. H., Atmospheric volatile organic compound measurements during the Pittsburgh Air Quality Study: Results, interpretation, and quantification of primary and secondary contributions. *Journal of Geophysical Research: Atmospheres* **2005,** *110* (D7), D07S07.

90. Rafiee, J.; Mi, X.; Gullapalli, H.; Thomas, A. V.; Yavari, F.; Shi, Y.; Ajayan, P. M.; Koratkar, N. A., Wetting transparency of graphene. *Nat Mater* **2012,** *11* (3), 217-222.

91. Shih, C.-J.; Wang, Q. H.; Lin, S.; Park, K.-C.; Jin, Z.; Strano, M. S.; Blankschtein, D., Breakdown in the Wetting Transparency of Graphene. *Physical Review Letters* **2012,** *109* (17), 176101.

92. Holt, J. K.; Park, H. G.; Wang, Y.; Stadermann, M.; Artyukhin, A. B.; Grigoropoulos, C. P.; Noy, A.; Bakajin, O., Fast Mass Transport Through Sub-2-Nanometer Carbon Nanotubes. *Science* **2006,** *312* (5776), 1034-1037.

93. Lee, C. Y.; Choi, W.; Han, J.-H.; Strano, M. S., Coherence Resonance in a Single-Walled Carbon Nanotube Ion Channel. *Science* **2010,** *329* (5997), 1320-1324.

94. Liu, H.; He, J.; Tang, J.; Liu, H.; Pang, P.; Cao, D.; Krstic, P.; Joseph, S.; Lindsay, S.; Nuckolls, C., Translocation of Single-Stranded DNA Through Single-Walled Carbon Nanotubes. *Science* **2010,** *327* (5961), 64-67.

95. Bowling, R. J.; Packard, R. T.; McCreery, R. L., Activation of highly ordered pyrolytic graphite for heterogeneous electron transfer: relationship between electrochemical performance and carbon microstructure. *Journal of the American Chemical Society* **1989,** *111* (4), 1217-1223.

96. Verdaguer, A.; Sacha, G. M.; Bluhm, H.; Salmeron, M., Molecular Structure of Water at Interfaces: Wetting at the Nanometer Scale. *Chemical Reviews* **2006,** *106* (4), 1478-1510.

97. Koumoutsakos, A.; Avramidis, S., Enthalpy-entropy compensation in water sorption by various wood species. *Holz als Roh- und Werkstoff* **1999,** *57* (5), 379-382.

98. Chakarov, D. V.; Österlund, L.; Kasemo, B., Water adsorption on graphite (0001). *Vacuum* **1995,** *46* (8–10), 1109-1112.

99. Algara-Siller, G.; Lehtinen, O.; Wang, F. C.; Nair, R. R.; Kaiser, U.; Wu, H. A.; Geim, A. K.; Grigorieva, I. V., Square ice in graphene nanocapillaries. *Nature* **2015,** *519* (7544), 443-445.

100. Liu, L.; Ryu, S. M.; Tomasik, M. R.; Stolyarova, E.; Jung, N.; Hybertsen, M. S.; Steigerwald, M. L.; Brus, L. E.; Flynn, G. W., Graphene oxidation: Thickness-dependent etching and strong chemical doping. *Nano Lett* **2008,** *8* (7), 1965-1970.

101. Surwade, S. P.; Li, Z. T.; Liu, H. T., Thermal Oxidation and Unwrinkling of Chemical Vapor Deposition-Grown Graphene. *J Phys Chem C* **2012,** *116* (38), 20600-20606.

102. Yang, R. T.; Wong, C., Kinetics and Mechanism of Oxidation of Basal-Plane on Graphite. *J Chem Phys* **1981,** *75* (9), 4471-4476.

103. Radovic, L. R., Active Sites in Graphene and the Mechanism of CO2 Formation in Carbon Oxidation. *J Am Chem Soc* **2009,** *131* (47), 17166-17175.

104. Yan, J.-A.; Chou, M. Y., Oxidation functional groups on graphene: Structural and electronic properties. *Physical Review B: Condensed Matter and Materials Physics* **2010,** *82* (12), 125403/1-125403/10.

105. Ishigami, M.; Choi, H. J.; Aloni, S.; Louie, S. G.; Cohen, M. L.; Zettl, A., Identifying defects in nanoscale materials. *Phys. Rev. Lett.* **2004,** *93* (19), 196803/1-196803/4.

106. Barinov, A.; Ustunel, H.; Fabris, S.; Gregoratti, L.; Aballe, L.; Dudin, P.; Baroni, S.; Kiskinova, M., Defect-controlled transport properties of metallic atoms along carbon nanotube surfaces. *Phys Rev Lett* **2007,** *99* (4), 046803.

107. Brukh, R.; Mitra, S., Kinetics of carbon nanotube oxidation. *J. Mater. Chem.* **2007,** *17* (7), 619-623.

108. Wang, Y.; Chen, X.; Zhong, Y.; Zhu, F.; Loh, K. P., Large area, continuous, few-layered

graphene as anodes in organic photovoltaic devices. *Appl. Phys. Lett.* **2009,** *95* (6), 063302/1-063302/3.

109. Ryu, S.; Liu, L.; Berciaud, S.; Yu, Y.-J.; Liu, H.; Kim, P.; Flynn, G. W.; Brus, L. E., Atmospheric Oxygen Binding and Hole Doping in Deformed Graphene on a SiO2 Substrate. *Nano Letters* **2010,** *10* (12), 4944-4951.

110. Ishigami, M.; Chen, J. H.; Cullen, W. G.; Fuhrer, M. S.; Williams, E. D., Atomic Structure of Graphene on SiO2. *Nano Letters* **2007,** *7* (6), 1643-1648.

111. Chen, K.; Wang, X.; Xu, J.-B.; Pan, L.; Wang, X.; Shi, Y., Electronic Properties of Graphene Altered by Substrate Surface Chemistry and Externally Applied Electric Field. *The Journal of Physical Chemistry C* **2012,** *116* (10), 6259-6267.

112. Tsukamoto, T.; Yamazaki, K.; Komurasaki, H.; Ogino, T., Effects of Surface Chemistry of Substrates on Raman Spectra in Graphene. *The Journal of Physical Chemistry C* **2012,** *116* (7), 4732-4737.

113. Shemella, P.; Nayak, S. K., Electronic structure and band-gap modulation of graphene via substrate surface chemistry. *Applied Physics Letters* **2009,** *94* (3), 032101.

114. Kang, Y.-J.; Kang, J.; Chang, K. J., Electronic structure of graphene and doping effect on ${\text{SiO}}_{2}$. *Physical Review B* **2008,** *78* (11), 115404.

115. Seol, J. H.; Jo, I.; Moore, A. L.; Lindsay, L.; Aitken, Z. H.; Pettes, M. T.; Li, X.; Yao, Z.; Huang, R.; Broido, D.; Mingo, N.; Ruoff, R. S.; Shi, L., Two-Dimensional Phonon Transport in Supported Graphene. *Science (Washington, DC, United States)* **2010,** *328* (5975), 213-216.

116. Wang, R.; Wang, S.-N.; Zhang, D.-D.; Li, Z.-J.; Fang, Y.; Qiu, X.-H., Control of Carrier Type and Density in Exfoliated Graphene by Interface Engineering. *ACS Nano* **2011,** *5* (1), 408-412.

117. Lafkioti, M.; Krauss, B.; Lohmann, T.; Zschieschang, U.; Klauk, H.; von Klitzing, K.; Smet, J. H., Graphene on a Hydrophobic Substrate: Doping Reduction and Hysteresis Suppression under Ambient Conditions. *Nano Letters* **2010,** *10* (4), 1149-1153.

118. Du, X.; Skachko, I.; Barker, A.; Andrei, E. Y., Approaching ballistic transport in suspended graphene. *Nature Nanotechnology* **2008,** *3* (8), 491-495.

119. Lin, Y.-M.; Avouris, P., Strong Suppression of Electrical Noise in Bilayer Graphene Nanodevices. *Nano Letters* **2008,** *8* (8), 2119-2125.

120. Morozov, S. V.; Novoselov, K. S.; Katsnelson, M. I.; Schedin, F.; Ponomarenko, L. A.;

Jiang, D.; Geim, A. K., Strong Suppression of Weak Localization in Graphene. *Phys. Rev. Lett.* **2006,** *97* (1), 016801/1-016801/4.

121. Hwang, E. H.; Adam, S.; Das Sarma, S., Transport in chemically doped graphene in the presence of adsorbed molecules. *Physical Review B: Condensed Matter and Materials Physics* **2007,** *76* (19), 195421/1-195421/6.

122. Ishigami, M.; Chen, J. H.; Cullen, W. G.; Fuhrer, M. S.; Williams, E. D., Atomic Structure of Graphene on SiO2. *Nano Letters* **2007,** *7* (6), 1643-1648.

123. Lui, C. H.; Liu, L.; Mak, K. F.; Flynn, G. W.; Heinz, T. F., Ultraflat graphene. *Nature (London, U. K.)* **2009,** *462* (7271), 339-341.

124. Tsukamoto, T.; Yamazaki, K.; Komurasaki, H.; Ogino, T., Effects of Surface Chemistry of Substrates on Raman Spectra in Graphene. *J. Phys. Chem. C* **2012,** *116* (7), 4732-4737.

125. Yan, Z.; Lin, J.; Peng, Z.; Sun, Z.; Zhu, Y.; Li, L.; Xiang, C.; Samuel, E. L.; Kittrell, C.; Tour, J. M., Toward the Synthesis of Wafer-Scale Single-Crystal Graphene on Copper Foils. *ACS Nano* **2012,** *6* (10), 9110-9117.

126. Li, X.; Cai, W.; An, J.; Kim, S.; Nah, J.; Yang, D.; Piner, R.; Velamakanni, A.; Jung, I.; Tutuc, E.; Banerjee, S. K.; Colombo, L.; Ruoff, R. S., Large-Area Synthesis of High-Quality and Uniform Graphene Films on Copper Foils. *Science* **2009,** *324* (5932), 1312-1314.

127. Li, X.; Magnuson, C. W.; Venugopal, A.; Tromp, R. M.; Hannon, J. B.; Vogel, E. M.; Colombo, L.; Ruoff, R. S., Large-Area Graphene Single Crystals Grown by Low-Pressure Chemical Vapor Deposition of Methane on Copper. *Journal of the American Chemical Society* **2011,** *133* (9), 2816-2819.

128. Bae, S.; Kim, H.; Lee, Y.; Xu, X.; Park, J.-S.; Zheng, Y.; Balakrishnan, J.; Lei, T.; Kim, H. R.; Song, Y. I.; Kim, Y.-J.; Kim, K. S.; Oezyilmaz, B.; Ahn, J.-H.; Hong, B. H.; Iijima, S., Roll-to-roll production of 30-inch graphene films for transparent electrodes. *Nat. Nanotechnol.* **2010,** *5* (8), 574-578.

129. Wood, J. D.; Schmucker, S. W.; Lyons, A. S.; Pop, E.; Lyding, J. W., Effects of Polycrystalline Cu Substrate on Graphene Growth by Chemical Vapor Deposition. *Nano Lett.* **2011,** *11* (11), 4547-4554.

130. Hao, Y.; Bharathi, M. S.; Wang, L.; Liu, Y.; Chen, H.; Nie, S.; Wang, X.; Chou, H.; Tan, C.; Fallahazad, B.; Ramanarayan, H.; Magnuson, C. W.; Tutuc, E.; Yakobson, B. I.; McCarty, K. F.; Zhang, Y.-W.; Kim, P.; Hone, J.; Colombo, L.; Ruoff, R. S., The Role of Surface Oxygen in the

Growth of Large Single-Crystal Graphene on Copper. *Science (Washington, DC, U. S.)* **2013,** *342* (6159), 720-723.

131. Shin, Y. J.; Wang, Y. Y.; Huang, H.; Kalon, G.; Wee, A. T. S.; Shen, Z. X.; Bhatia, C. S.; Yang, H., Surface-Energy Engineering of Graphene. *Langmuir* **2010,** *26* (6), 3798-3802.

132. Kim, K. S.; Lee, H. J.; Lee, C.; Lee, S. K.; Jang, H.; Ahn, J. H.; Kim, J. H.; Lee, H. J., Chemical Vapor Deposition-Grown Graphene: The Thinnest Solid Lubricant. *Acs Nano* **2011,** *5* (6), 5107-5114.

133. Wu, Y.; Aluru, N. R., Graphitic Carbon–Water Nonbonded Interaction Parameters. *The Journal of Physical Chemistry B* **2013,** *117* (29), 8802-8813.

134. Liu, H. T.; He, J.; Tang, J. Y.; Liu, H.; Pang, P.; Cao, D.; Krstic, P.; Joseph, S.; Lindsay, S.; Nuckolls, C., Translocation of Single-Stranded DNA Through Single-Walled Carbon Nanotubes. *Science* **2010,** *327* (5961), 64-67.

135. Lee, C. Y.; Choi, W.; Han, J. H.; Strano, M. S., Coherence Resonance in a Single-Walled Carbon Nanotube Ion Channel. *Science* **2010,** *329* (5997), 1320-1324.

136. Holt, J. K.; Park, H. G.; Wang, Y. M.; Stadermann, M.; Artyukhin, A. B.; Grigoropoulos, C. P.; Noy, A.; Bakajin, O., Fast mass transport through sub-2-nanometer carbon nanotubes. *Science* **2006,** *312* (5776), 1034-1037.

137. Koenig, S. P.; Boddeti, N. G.; Dunn, M. L.; Bunch, J. S., Ultrastrong adhesion of graphene membranes. *Nat. Nanotechnol.* **2011,** *6* (9), 543-546.

138. Schedin, F.; Geim, A. K.; Morozov, S. V.; Hill, E. W.; Blake, P.; Katsnelson, M. I.; Novoselov, K. S., Detection of individual gas molecules adsorbed on graphene. *Nature Mater.* **2007,** *6* (9), 652-655.

139. Ponomarenko, L. A.; Yang, R.; Mohiuddin, T. M.; Katsnelson, M. I.; Novoselov, K. S.; Morozov, S. V.; Zhukov, A. A.; Schedin, F.; Hill, E. W.; Geim, A. K., Effect of a High-kappa Environment on Charge Carrier Mobility in Graphene. *Phys. Rev. Lett.* **2009,** *102* (20), 206603.

140. Shim, J.; Lui, C. H.; Ko, T. Y.; Yu, Y.-J.; Kim, P.; Heinz, T. F.; Ryu, S., Water-Gated Charge Doping of Graphene Induced by Mica Substrates. *Nano Letters* **2012,** *12* (2), 648-654.

141. Bernett, M. K.; Zisman, W. A., Confirmation of Spontaneous Spreading by Water on Pure Gold. *J Phys Chem-Us* **1970,** *74* (11), 2309-&.

142. Zubkov, T.; Stahl, D.; Thompson, T. L.; Panayotov, D.; Diwald, O.; Yates, J. T., Ultraviolet light-induced hydrophilicity effect on TiO2(110)(1x1). Dominant role of the photooxidation of

adsorbed hydrocarbons causing wetting by water droplets. *J Phys Chem B* **2005,** *109* (32), 15454-15462.

143. Shinozaki, A.; Arima, K.; Morita, M.; Kojima, I.; Azuma, Y., FTIR-ATR evaluation of organic contaminant cleaning methods for SiO2 surfaces. *Anal Sci* **2003,** *19* (11), 1557-1559.

144. Choi, K.; Eom, T. J.; Lee, C., Comparison of the removal efficiency for organic contaminants on silicon wafers stored in plastic boxes between UV/O-3 and ECR oxygen plasma cleaning methods. *Thin Solid Films* **2003,** *435* (1-2), 227-231.

145. Boinovich, L. B.; Emelyanenko, A. M.; Pashinin, A. S.; Lee, C. H.; Drelich, J.; Yap, Y. K., Origins of Thermodynamically Stable Superhydrophobicity of Boron Nitride Nanotubes Coatings. *Langmuir* **2012,** *28* (2), 1206-1216.

146. Fox, H. W.; Hare, E. F.; Zisman, W. A., Wetting Properties of Organic Liquids on High Energy Surfaces. *J Phys Chem-Us* **1955,** *59* (10), 1097-1106.

147. Li, X.; Zhu, Y.; Cai, W.; Borysiak, M.; Han, B.; Chen, D.; Piner, R. D.; Colombo, L.; Ruoff, R. S., Transfer of Large-Area Graphene Films for High-Performance Transparent Conductive Electrodes. *Nano Letters* **2009,** *9* (12), 4359-4363.

148. Rafiee, J.; Mi, X.; Gullapalli, H.; Thomas, A. V.; Yavari, F.; Shi, Y. F.; Ajayan, P. M.; Koratkar, N. A., Wetting transparency of graphene. *Nat Mater* **2012,** *11* (3), 217-222.

149. Shih, C. J.; Wang, Q. H.; Lin, S. C.; Park, K. C.; Jin, Z.; Strano, M. S.; Blankschtein, D., Breakdown in the Wetting Transparency of Graphene. *Physical Review Letters* **2012,** *109* (17).

150. Smith, T., The Hydrophilic Nature of a Clean Gold Surface. *Journal of Colloid and Interface Science* **1980,** *75* (1), 51-55.

151. Afshari, A.; Gunnarsen, L.; Clausen, P. A.; Hansen, V., Emission of phthalates from PVC and other materials. *Indoor Air* **2004,** *14* (2), 120-128.

152. Smith, P. J.; Lindley, P. M., Analysis of organic contamination in semiconductor processing. *AIP Conference Proceedings* **1998,** *449* (1), 133-139.

153. Millet, D. B.; Donahue, N. M.; Pandis, S. N.; Polidori, A.; Stanier, C. O.; Turpin, B. J.; Goldstein, A. H., Atmospheric volatile organic compound measurements during the Pittsburgh Air Quality Study: Results, interpretation, and quantification of primary and secondary contributions. *J Geophys Res-Atmos* **2005,** *110* (D7).

154. Kumar, K.; Kim, Y.-S.; Yang, E.-H., The influence of thermal annealing to remove polymeric residue on the electronic doping and morphological characteristics of graphene. *Carbon*

2013, *65*, 35-45.

155. Werder, T.; Walther, J. H.; Jaffe, R. L.; Halicioglu, T.; Koumoutsakos, P., On the water-carbon interaction for use in molecular dynamics simulations of graphite and carbon nanotubes. *J Phys Chem B* **2003,** *107* (6), 1345-1352.

156. Rubes, M.; Kysilka, J.; Nachtigall, P.; Bludsky, O., DFT/CC investigation of physical adsorption on a graphite (0001) surface. *Phys Chem Chem Phys* **2010,** *12* (24), 6438-6444.

157. Li, Z.; Wang, Y.; Kozbial, A.; Shenoy, G.; Zhou, F.; McGinley, R.; Ireland, P.; Morganstein, B.; Kunkel, A.; Surwade, S. P.; Li, L.; Liu, H., Effect of airborne contaminants on the wettability of supported graphene and graphite. *Nat Mater* **2013,** *12* (10), 925-931.

158. Kozbial, A.; Li, Z.; Conaway, C.; McGinley, R.; Dhingra, S.; Vahdat, V.; Zhou, F.; D'Urso, B.; Liu, H.; Li, L., Study on the Surface Energy of Graphene by Contact Angle Measurements. *Langmuir* **2014,** *30* (28), 8598-8606.

159. Ashraf, A.; Wu, Y.; Wang, M. C.; Aluru, N. R.; Dastgheib, S. A.; Nam, S., Spectroscopic Investigation of the Wettability of Multilayer Graphene Using Highly Ordered Pyrolytic Graphite as a Model Material. *Langmuir* **2014,** *30* (43), 12827-12836.

160. Wei, Y.; Jia, C. Q., Intrinsic wettability of graphitic carbon. *Carbon* **2015,** *87* (0), 10-17.

161. Amadei, C. A.; Lai, C.-Y.; Heskes, D.; Chiesa, M., Time dependent wettability of graphite upon ambient exposure: The role of water adsorption. *The Journal of Chemical Physics* **2014,** *141* (8), 084709.

162. Mücksch, C.; Rösch, C.; Müller−Renno, C.; Ziegler, C.; Urbassek, H. M., Consequences of Hydrocarbon Contamination for Wettability and Protein Adsorption on Graphite Surfaces. *The Journal of Physical Chemistry C* **2015,** *119* (22), 12496-12501.

163. Dwivedi, P.; Gaur, V.; Sharma, A.; Verma, N., Comparative study of removal of volatile organic compounds by cryogenic condensation and adsorption by activated carbon fiber. *Separation and Purification Technology* **2004,** *39* (1–2), 23-37.

164. Taketoshi Fujimoto, K. T., Tatsuo Nonaka, *Developments in Surface Contamination and Cleaning Fundamentals and Applied Aspects*. William Andrew Inc.: NY, 2007; p 329-456.

165. Xia, Z. Y.; Pezzini, S.; Treossi, E.; Giambastiani, G.; Corticelli, F.; Morandi, V.; Zanelli, A.; Bellani, V.; Palermo, V., The Exfoliation of Graphene in Liquids by Electrochemical, Chemical, and Sonication-Assisted Techniques: A Nanoscale Study. *Advanced Functional Materials* **2013,** *23* (37), 4684-4693.

166. Kibanova, D.; Cervini-Silva, J.; Destaillats, H., Efficiency of Clay−TiO2 Nanocomposites on the Photocatalytic Elimination of a Model Hydrophobic Air Pollutant. *Environmental Science & Technology* **2009,** *43* (5), 1500-1506.

167. Williams, G.; Seger, B.; Kamat, P. V., TiO2-Graphene Nanocomposites. UV-Assisted Photocatalytic Reduction of Graphene Oxide. *ACS Nano* **2008,** *2* (7), 1487-1491.

168. Gotoh, K., *Development in Surface Contamination and Cleaning*. NY, 2007; p 889-916.

169. Koenig, S. P.; Boddeti, N. G.; Dunn, M. L.; Bunch, J. S., Ultrastrong adhesion of graphene membranes. *Nat Nano* **2011,** *6* (9), 543-546.

170. Novoselov, K. S.; Geim, A. K.; Morozov, S. V.; Jiang, D.; Zhang, Y.; Dubonos, S. V.; Grigorieva, I. V.; Firsov, A. A., Electric Field Effect in Atomically Thin Carbon Films. *Science* **2004,** *306* (5696), 666-669.

171. McDermott, M. T.; Kneten, K.; McCreery, R. L., Anthraquinonedisulfonate adsorption, electron-transfer kinetics, and capacitance on ordered graphite electrodes: the important role of surface defects. *The Journal of Physical Chemistry* **1992,** *96* (7), 3124-3130.

172. Bard, A. J. F., L.R., *Electrochemical methods: fundamentals and applications, 2nd ed.* John Wiley & Sons: New York, 2001.

173. G. E. Ewing, M. F., W. Cantrell, V. Sadtchenko, *Thin film water on insulator surfaces, in Water in Confining Geometries*. Springer-Verlag: Berlin, 2003; p 179-211.

174. Teschke, O., Imaging Ice-Like Structures Formed on HOPG at Room Temperature. *Langmuir* **2010,** *26* (22), 16986-16990.

175. Wang, Y.; Bowman, J. M., IR Spectra of the Water Hexamer: Theory, with Inclusion of the Monomer Bend Overtone, and Experiment Are in Agreement. *The Journal of Physical Chemistry Letters* **2013,** *4* (7), 1104-1108.

176. Gledhill, R. A.; Kinloch, A. J.; Shaw, S. J., Effect of Relative Humidity on the Wettability of Steel Surfaces. *The Journal of Adhesion* **1977,** *9* (1), 81-85.

177. Luna, M.; Colchero, J.; Gil, A.; Gómez-Herrero, J.; Baró, A. M., Application of non-contact scanning force microscopy to the study of water adsorption on graphite, gold and mica. *Applied Surface Science* **2000,** *157* (4), 393-397.

178. Gil, A.; Colchero, J.; Luna, M.; Gómez-Herrero, J.; Baró, A. M., Adsorption of Water on Solid Surfaces Studied by Scanning Force Microscopy. *Langmuir* **2000,** *16* (11), 5086-5092.

179. Abbatt, J. P. D., Interactions of Atmospheric Trace Gases with Ice Surfaces: Adsorption

and Reaction. *Chemical Reviews* **2003,** *103* (12), 4783-4800.

180. Sokolov, O.; Abbatt, J. P. D., Adsorption to Ice of n-Alcohols (Ethanol to 1-Hexanol), Acetic Acid, and Hexanal. *The Journal of Physical Chemistry A* **2002,** *106* (5), 775-782.

181. Winkler, A. K.; Holmes, N. S.; Crowley, J. N., Interaction of methanol, acetone and formaldehyde with ice surfaces between 198 and 223 K. *Physical Chemistry Chemical Physics* **2002,** *4* (21), 5270-5275.

182. Fries, E.; Haunold, W.; Jaeschke, W.; Hoog, I.; Mitra, S. K.; Borrmann, S., Uptake of gaseous aromatic hydrocarbons by non-growing ice crystals. *Atmospheric Environment* **2006,** *40* (28), 5476-5485.

183. Fries, E.; Starokozhev, E.; Haunold, W.; Jaeschke, W.; Mitra, S. K.; Borrmann, S.; Schmidt, M. U., Laboratory studies on the uptake of aromatic hydrocarbons by ice crystals during vapor depositional crystal growth. *Atmospheric Environment* **2007,** *41* (29), 6156-6166.

184. Habuka, H.; Shimada, M.; Okuyama, K., Adsorption and Desorption Rate of Multicomponent Organic Species on Silicon Wafer Surface. *Journal of The Electrochemical Society* **2001,** *148* (7), G365-G369.

185. Hihara, L. H.; Latanision, R. M., Corrosion of Metal-Matrix Composites. *Int. Mater. Rev.* **1994,** *39* (6), 245-264.

186. Bobić, B.; Mitrović, S.; Babić, M.; Bobić, I., Corrosion of Metal-Matrix Composites with Aluminium Alloy Substrate. *Tribology in Industry* **2010,** *32* (1), 3-11.

187. Hihara, L. H.; Latansion, R. M., Localized Corrosion Induced in Graphite/Aluminum Metal-Matrix Composites by Residual Microstructural Chloride. *Corrosion* **1991,** *47* (5), 335-340.

188. Poulston, S.; Parlett, P. M.; Stone, P.; Bowker, M., Surface Oxidation and Reduction of CuO and Cu2O Studied Using XPS and XAES. *Surface and Interface Analysis* **1996,** *24* (12), 811-820.

189. Dube, C. E.; Workie, B.; Kounaves, S. P.; Robbat, A.; Aksu, M. L.; Davies, G., Electrodeposition of Metal Alloy and Mixed-Oxide Films Using a Single-Precursor Tetranuclear Copper-Nickel Complex. *J. Electrochem. Soc.* **1995,** *142* (10), 3357-3365.

190. Yoon, C.; Cocke, D. L., Evidence for Electron-Transfer Control of Oxygen Incorporation into Bulk Copper. *J. Electrochem. Soc.* **1987,** *134* (3), 643-644.

191. Espinos, J. P.; Morales, J.; Barranco, A.; Caballero, A.; Holgado, J. P.; Gonzalez-Elipe, A. R., Interface Effects for Cu, CuO, and Cu2O Deposited on SiO2 and ZrO2. XPS Determination of

the Valence State of Copper in Cu/SiO2 and Cu/ZrO2 Catalysts. *J. Phys. Chem. B* **2002,** *106* (27), 6921-6929.

192. Gan, Z. H.; Yu, G. Q.; Tay, B. K.; Tan, C. M.; Zhao, Z. W.; Fu, Y. Q., Preparation and Characterization of Copper Oxide Thin Films Deposited by Filtered Cathodic Vacuum Arc. *J. Phys. D: Appl. Phys.* **2004,** *37* (1), 81-85.

193. Biesinger, M. C.; Lau, L. W. M.; Gerson, A. R.; Smart, R. S. C., Resolving Surface Chemical States in XPS Analysis of First Row Transition Metals, Oxides and Hydroxides: Sc, Ti, V, Cu and Zn. *Appl. Surf. Sci.* **2010,** *257* (3), 887-898.

194. Keil, P.; LC.

195. Goldstein, J. I., *Electron Beam-Specimen Interaction*. Springer: 1975; p 49-94.

196. Chou, M. H.; Liu, S. B.; Huang, C. Y.; Wu, S. Y.; Cheng, C. L., Confocal Raman Spectroscopic Mapping Studies on A Single CuO Nanowire. *Appl. Surf. Sci.* **2008,** *254* (23), 7539-7543.

197. Irwin, J. C.; Chrzanowski, J.; Wei, T.; Lockwood, D. J.; Wold, A., Raman-Scattering from Single-Crystals of Cupric Oxide. *Phys. C* **1990,** *166* (5-6), 456-464.

198. Niaura, G., Surface-Enhanced Raman Spectroscopic Observation of Two Kinds of Adsorbed OH- ions at Copper Electrode. *Electrochim. Acta* **2000,** *45* (21), 3507-3519.

199. Greenler, R. G.; Slager, T. L., Method for Obtaining the Roman Spectrum of A Thin Film on A Metal Surface. *Spectrochim. Acta, Part A* **1973,** *29* (1), 193-201.

200. Dante, J. F.; Kelly, R. G., The Evolution of the Adsorbed Solution Layer during Atmospheric Corrosion and Its Effects on the Corrosion Rate of Copper. *J. Electrochem. Soc.* **1993,** *140* (7), 1890-1897.

201. Kear, G.; Barker, B. D.; Walsh, F. C., Electrochemical Corrosion of Unalloyed Copper in Chloride Media - A Critical Review. *Corros. Sci.* **2004,** *46* (1), 109-135.

202. Hara, M.; Kondo, T.; Komoda, M.; Ikeda, S.; Shinohara, K.; Tanaka, A.; Kondo, J. N.; Domen, K., Cu2O as A Photocatalyst for Overall Water Splitting under Visible Light Irradiation. *Chem. Commun.* **1998,** (3), 357-358.

203. Tapiero, M.; Zielinger, J. P.; Noguet, C., Electrical Conductivity and Thermal Activation Energies in Cu2O Single Crystals. *Phys. Status Solidi A* **1972,** *12* (2), 517-520.

204. Li, Z.; Zhou, F.; Parobek, D.; Shenoy, G. J.; Muldoon, P.; Liu, H., Copper substrate as a catalyst for the oxidation of chemical vapor deposition-grown graphene. *Journal of Solid State*

Chemistry **2015,** *224*, 14-20.

205. Zhou, F.; Li, Z.; Shenoy, G. J.; Li, L.; Liu, H., Enhanced Room-Temperature Corrosion of Copper in the Presence of Graphene. *ACS Nano* **2013,** *7* (8), 6939-6947.

206. Baker, R. T. K.; Chludzinski Jr, J. J., Catalytic gasification of graphite by chromium and copper in oxygen, steam and hydrogen. *Carbon* **1981,** *19* (2), 75-82.

207. McKee, D. W., Metal oxides as catalysts for the oxidation of graphite. *Carbon* **1970,** *8* (5), 623-635.

208. McKee, D. W., The copper-catalyzed oxidation of graphite. *Carbon* **1970,** *8* (2), 131-139.

209. McKee, D. W., Mechanisms of catalyzed gasification of carbon. *AIP Conference Proceedings* **1981,** *70* (1), 236-255.

210. Colomban, P.; Schreiber, H. D., Raman signature modification induced by copper nanoparticles in silicate glass. *Journal of Raman Spectroscopy* **2005,** *36* (9), 884-890.

211. Colomban, P.; March, G.; Mazerolles, L.; Karmous, T.; Ayed, N.; Ennabli, A.; Slim, H., Raman identification of materials used for jewellery and mosaics in Ifriqiya. *Journal of Raman Spectroscopy* **2003,** *34* (3), 205-213.

212. Hurley, B. L.; McCreery, R. L., Raman Spectroscopy of Monolayers Formed from Chromate Corrosion Inhibitor on Copper Surfaces. *J. Electrochem. Soc.* **2003,** *150* (8), B367-B373.

213. Texier, F.; Servant, L.; Bruneel, J. L.; Argoul, F., In situ probing of interfacial processes in the electrodeposition of copper by confocal Raman microspectroscopy. *J. Electroanal. Chem.* **1998,** *446* (1-2), 189-203.

214. Ferrari, A. C.; Robertson, J., Interpretation of Raman spectra of disordered and amorphous carbon. *Phys. Rev. B: Condens. Matter Mater. Phys.* **2000,** *61* (20), 14095-14107.

215. Teweldebrhan, D.; Balandin, A. A., Modification of graphene properties due to electron-beam irradiation [Appl. Phys. Lett.95, 246101(2009)]. Response to Comment. *Appl. Phys. Lett.* **2009,** *95* (24), 246102/1-246102/2.

216. Berciaud, S.; Ryu, S.; Brus, L. E.; Heinz, T. F., Probing the Intrinsic Properties of Exfoliated Graphene: Raman Spectroscopy of Free-Standing Monolayers. *Nano Lett.* **2009,** *9* (1), 346-352.

217. Chen, C.-C.; Bao, W.; Theiss, J.; Dames, C.; Lau, C. N.; Cronin, S. B., Raman Spectroscopy of Ripple Formation in Suspended Graphene. *Nano Lett.* **2009,** *9* (12), 4172-4176.

218. Liu, L.; Ryu, S.; Tomasik, M. R.; Stolyarova, E.; Jung, N.; Hybertsen, M. S.; Steigerwald,

M. L.; Brus, L. E.; Flynn, G. W., Graphene Oxidation: Thickness-Dependent Etching and Strong Chemical Doping. *Nano Letters* **2008,** *8* (7), 1965-1970.

219. Lee, J. E.; Ahn, G.; Shim, J.; Lee, Y. S.; Ryu, S., Optical separation of mechanical strain from charge doping in graphene. *Nat Commun* **2012,** *3*, 1024.

220. Hong, J.; Park, M. K.; Lee, E. J.; Lee, D.; Hwang, D. S.; Ryu, S., Origin of New Broad Raman D and G Peaks in Annealed Graphene. *Sci. Rep.* **2013,** *3*.

221. Zhou, G.; Wang, L.; Yang, J. C., Effects of surface topology on the formation of oxide islands on Cu surfaces. *J. Appl. Phys.* **2005,** *97* (6), 063509/1-063509/6.

222. Yang, J. C.; Yeadon, M.; Kolasa, B.; Gibson, J. M., The Limited Role of Surface Defects as Nucleation Sites for Cu2 O on Cu(001). *Journal of The Electrochemical Society* **1999,** *146* (6), 2103-2106.

223. Swanson, A. W.; Uhlig, H. H., Initial oxidation rates of single-crystal copper and the effect of gaseous pretreatment. *J. Electrochem. Soc.* **1971,** *118* (8), 1325-31.

224. Long, F. J.; Sykes, K. W., The effect of specific catalysts on the reactions of the steam-carbon system. *Proc. R. Soc. London, Ser. A* **1952,** *215*, 100-10.

225. Walker, P. L., Jr.; Shelef, M.; Anderson, R. A., Catalysis of carbon gasification. *Chem. Phys. Carbon, Ser. Advan.* **1968,** *4*, 287-383.